ABSTRACT

Title of Document: EQUILIBRIUM AND NON-EQUILIBRIUM PROPERTIES OF FINITE-VOLUME CRYSTALLITES

Masashi Degawa, Doctor of Philosophy, 2006

Directed By: Professor Ellen D. Williams
Department of Physics

Finite volume effects on equilibrium and non-equilibrium properties of nano-crystallites are studied theoretically and compared to both experiment and simulation.

When a system is isolated or its size is small compared to the correlation length, all equilibrium and close-to-equilibrium properties will depend on the system boundary condition. Specifically for solid nano-crystallites, their finite size introduces global curvature to the system, which alters its equilibrium properties compared to the thermodynamic limit. Also such global curvature leads to capillary-induced morphology changes of the surface. Interesting dynamics can arise when the crystallite is supported on a substrate, with crossovers of the dominant driving force from the capillary force and crystallite-substrate interactions.

To address these questions, we introduce thermodynamic functions for the boundary conditions, which can be derived from microscopic models. For nano-crystallites, the boundary is the surface (including interfaces), the thermodynamic description is based on the steps that define the shape of the surface, and the underlying microscopic model includes kinks.

The global curvature of the surface introduces metastable states with different shapes governed by a constant of integration of the extra boundary condition, which we call the shape parameter c. The discrete height of the steps introduces transition states in between the metastable states, and the lowest energy accessible structure (energy barrier less $10k_BT$) as a function of the volume has been determined. The dynamics of nano-crystallites as they relax from a non-equilibrium structure is described quantitatively in terms of the motion of steps in both capillary-induced and interface-boundary-induced regimes. The step-edge fluctuations of the top facet are also influenced by global curvature and volume conservation and the effect yields different dynamic scaling exponents from a pure 1D system.

Theoretical results are compared with experimental results for Pb crystallites supported on a Ru substrate. The thermodynamic and kinetic parameters are obtained from the observations of equilibrium structures and rates of structure evolution. The predicted dynamic scaling exponents of facet-edge fluctuations are also obtained and compared to an isolated step. Facet-edge fluctuations are also tested with Monte Carlo Simulations (MCS) using the Terrace-Step-Kink (TSK) model with thermally exited kink formations and conserved microscopic processes.

EQUILIBRIUM AND NON-EQUILIBRIUM PROPERTIES OF FINITE-VOLUME CRYSTALLITES

By

Masashi Degawa

Dissertation submitted to the Faculty of the Graduate School of the
University of Maryland, College Park, in partial fulfillment
of the requirements for the degree of
Doctor of Philosophy
2006

Advisory Committee:
Professor Ellen D. Williams, Chair
Professor Theodore L. Einstein
Professor Janice E. Reutt-Robey
Professor John D. Weeks
Professor Chris Lobb
Professor Alberto Pimpinelli

Dedication

Dedicated to my beloved wife

Tomoko Degawa

Acknowledgements

I would like to acknowledge all of the members in Ellen Williams group for their support throughout the years. Graduate students, Mihaela Breban, Chenggang Tao, Jianhao Chen, Tracy Moore and Brad Conrad. Special thanks to senior graduates, Ruchi Yongsonthun and Daniel Dougherty with who I spent most of the time during my stay here. PostDocs, Bo Xu, Masahiro Ishigami, Elba Gomar-Nadal. Special thanks to senior postdocs, Konrad Thurmer, Christoph Tegenkamp, Igor Lyubinetsky and Olexander Bondarchuk for advising me through the early years. Also thanks to people outside the group, graduate student Hailu Gebremariam and Tim Stasevich and postdoc Ferenc Szalma with who I had extensive discussions about the this work and physics in general. Lastly a special thanks to William Cullen the micrscopy facility manager who I could not have done any of the experiments in this work without.

I would also like to acknowledge all of the MRSEC staff for all their non-technical support. Donna Hammer, Shirley Winter, Julie Callis and Carolyn Gravey.

I would like to acknowledge all of the members of my committee. Prof. Chris Lobb, Prof. Janice E. Reutt-Robey, Prof. John D. Weeks, Prof. Alberto Pimpinelli, Prof. Theodore L. Einstein. Special thanks to Prof. Alberto Pimpinelli, Prof. John D. Weeks and Prof. Makio Uwaha with who I had tremendously useful discussions in the work of facet fluctuations, ECS and step dynamics, respectively. A special thanks to Prof. Theodore L. Einstein who gave up quite amount of his time to discuss most of the theory part of this work.

Last but not least, a great thank you to my advisor Ellen D. Williams who was so generous from the beginning on deciding to invite me into her group during my short stay as a visitor from T.I.T. Also for her guidance throughout this work and her great great patience with me to carry on with it.

Table of Contents

List of Tables

curvature, Crv-fr = an isolated curved step such as boundary of an island, Str-cfn = straight steps confined by the presence of neighboring steps as in a step bunch, and Crv-cfn = curved steps confined by the presence of neighboring steps as at the edge of a finite-volume crystal. Following ref. [29], we characterize the relevant growth equations by 3 letters and a number. The first (L or N) indicates whether the equation is linear or non-linear (i.e. has a KPZ term). The second and the third (both C or N) indicate whether the deterministic part or the noise, respectively, is conservative or non-conservative. The number, 2 or 4, indicates the power of ∇ in the linear conservative term. We also indicate the dimensionality of the independent variable. Note that the universality classes associated with LCN2 and NNN2 are EW (Edwards-Wilkinson) and KPZ..... 115

List of Figures

Chapter 1: Introduction

The definitions of equilibrium and the 2D continuum model are introduced to relate the properties of the surface of a solid to the calculation the equilibrium crystal shape (ECS). The concept of monatomic steps on surfaces is introduced using the continuum step model, and their thermodynamic properties and dynamics are reviewed. An analytic treatment of stochastic behavior is introduced by the means of the Langevin theory, and the statistical characterization of fluctuating steps, which reveal the kinetic properties of the steps. To provide a larger context of the work, dynamical scaling and the universality classes of interface fluctuation are introduced. Finally, discrete models of steps are introduced and their thermodynamic properties are calculated by statistical methods.

1.1 Motivation

The creation of smaller and faster devices has been the main driving force of the computer industry for the past few decades. As a result it has opened up a field in basic research of modern condensed matter physics called nanoscience and associated nanotechnology. In more recent years the possibility of quantum computing has further accelerated the field due to the demand of creating quantum bits or quantum dots[1-6]. An important research goal is the fabrication and control of such nanostructures using their natural properties and dynamics to the maximum capability, practical enough for mass production. The main difficulty in such research is the *scale* on which materials control must occur, the so-called *mesoscopic* length scale. At the longer end of this scale, thermodynamic (or continuum) descriptions in the thermodynamic limit break down, and the stochastic behavior of the discrete nature of the atoms start to arise. However, the structure size is still too large to allow practical computation based solely on atomic-scale descriptions (e.g. 1st principles, molecular dynamics).

The first approach is to evaluate the thermodynamic concepts and descriptions. Obviously the thermodynamic limit (infinite size system) must be abandoned, extensive variables should be strictly kept fixed and the new fundamental considerations will become the boundary condition. For the nanostructures of interest here, this is the *surface* as shown in Figure 1-1. The next approach is to introduce discrete features, which will lead to energy barriers and specific physical origin of stochastic behavior. For surfaces, the most relevant nano-scale defects are *steps*, resulting from an incomplete crystal plane as shown Figure 1-1. Next are *kinks*, an

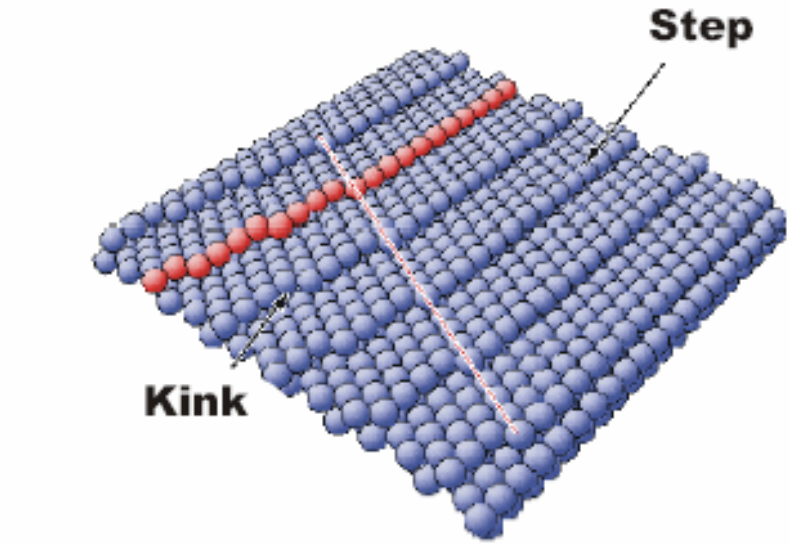

Figure 1-1 Schematic drawing of a crystal surface, adapted from ref. [7]. Spheres represent the atoms and also steps and kinks are shown.

equivalent defect to a step in one lower dimension, which makes statistical methods a lot easier. Atomic notion involving kinks and steps provides the introduction of *noise* to thermodynamic equations, which in the Langevin formalism provides a powerful tool to mimic stochastic behavior and make use of statistical methods.

In the remainder of this chapter all the ingredients needed to attack the problem of nanostructures, namely finite volume crystallites will be introduced. The continuum model and the issues with boundary conditions (section 1.2), the continuum step model and dynamics (section 1.3), the Langevin theory and dynamical universality (section 1.4), discrete models and Monte Carlo Simulations (MCS) (section 1.5) will all be introduced, and finally we will close the chapter with an overview of the whole study (section 1.6).

1.2 Equilibrium crystal shape and the continuum model

Equilibrium is defined as the absolute minimum of the total free energy of the system. For a crystallite with fixed volume this corresponds to lowering the surface free energy F_S, which is obtained from the surface morphology and project surface free energy per area $f(z_x, z_y)$, where $z_n=\partial z/\partial n$. When the surface is rough, meaning there is no cusp in the surface free energy density, the surface of a crystallite can be expressed by a coarse-grained 2D continuous interface model, the *continuum model* [8-11]. Examples of surface morphologies described in the continuum model are given in Figure 1-2. In this case, one thermodynamic function is enough to express the surface free energy and all microscopic information is stored in this one function, the *surface tension* γ. Assuming the *thermodynamic limit* of infinite volume V, we use Cartesian

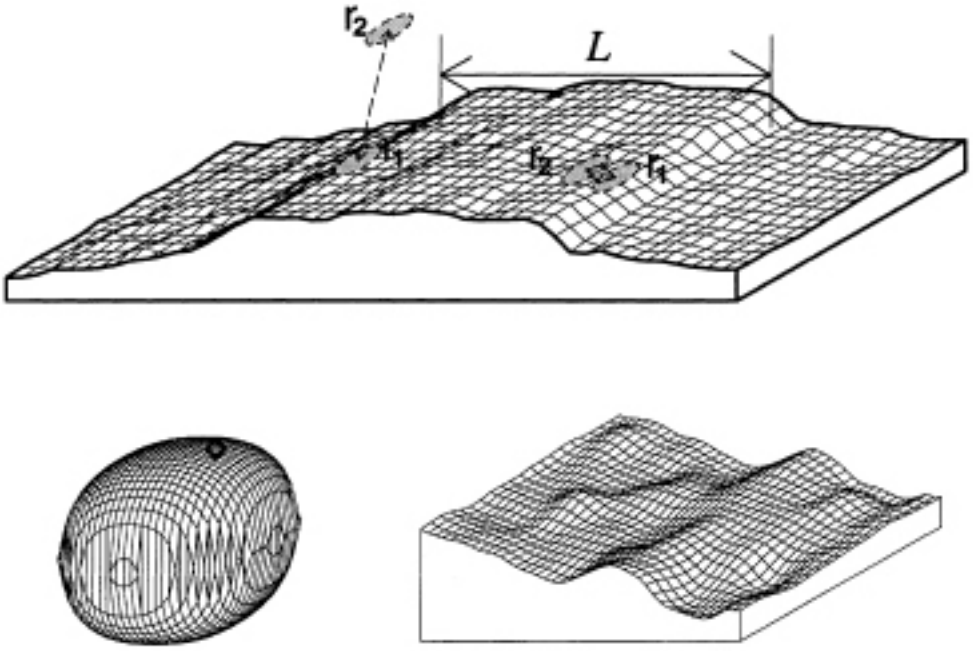

Figure 1-2 Schematic drawing of the continuum model [10]. The continuum model is a coarse-grained 2D continuous interface, used frequently in the thermodynamic description of the surface.

coordinates (Monge gauge) with the average surface position at z=0. The surface free energy is given as

$$F_S = \iint f\, dx\, dy = \iint \gamma(z_x, z_y)\sqrt{1 + z_x^2 + z_y^2}\, dx\, dy = \iint \gamma(z_x, z_y) dA\,, \qquad (1\text{-}1)$$

where A is the surface area and the integral is over the entire (infinite) surface. To obtain the absolute minimum of the total free energy $\delta F_S/\delta z$=0 we calculate

$$\delta F_S = -\iint \left[\frac{\partial}{\partial x}\frac{\partial f}{\partial z_x} + \frac{\partial}{\partial y}\frac{\partial f}{\partial z_y} \right] \delta z\, dx\, dy = \iint \frac{\mu}{v}\delta z\, dx\, dy\,, \qquad (1\text{-}2)$$

which gives the definition of the surface chemical potential μ ($\delta F_S/\delta N$) where v is the volume of an atom. The solution to the above equation is obtained when μ=μ_0, where μ_0 is the constant surface chemical potential given by the *boundary condition*, which ultimately is defined by the crystallite volume $V\rightarrow\infty$ so $\mu_0\rightarrow 0$ satisfying $\delta F_S/\delta z$=0 (this will be discussed shortly). If the surface tension has no radial dependence and the surface fluctuations are small, the surface free energy density and surface chemical potential become

$$f(z_x, z_y) = \frac{\tilde{\gamma}}{2}(z_x^2 + z_y^2) \qquad \text{and} \qquad \mu(z_{xx}, z_{yy}) = -v\tilde{\gamma}(z_{xx} + z_{yy})\,, \quad (1\text{-}3)$$

where v is the atomic volume and $\tilde{\gamma}$=γ+$\partial^2\gamma/\partial z_n^2$ is the (isotropic) *surface stiffness* (or rigidity). This results in the standard equilibrium crystal shape (ECS) of the infinite-volume isotropic crystal. The relation between the curvature of the shape and surface chemical potential is often referred to as the *Gibbs-Thomson relation* [9, 11-13] and is frequently used as the local equilibrium assumption in dynamical studies of surfaces and interfaces.

Below the roughening temperature, where the crystallite expresses a perfectly flat facet (Figure 1-3), there is a cusp in the surface free energy and the continuum

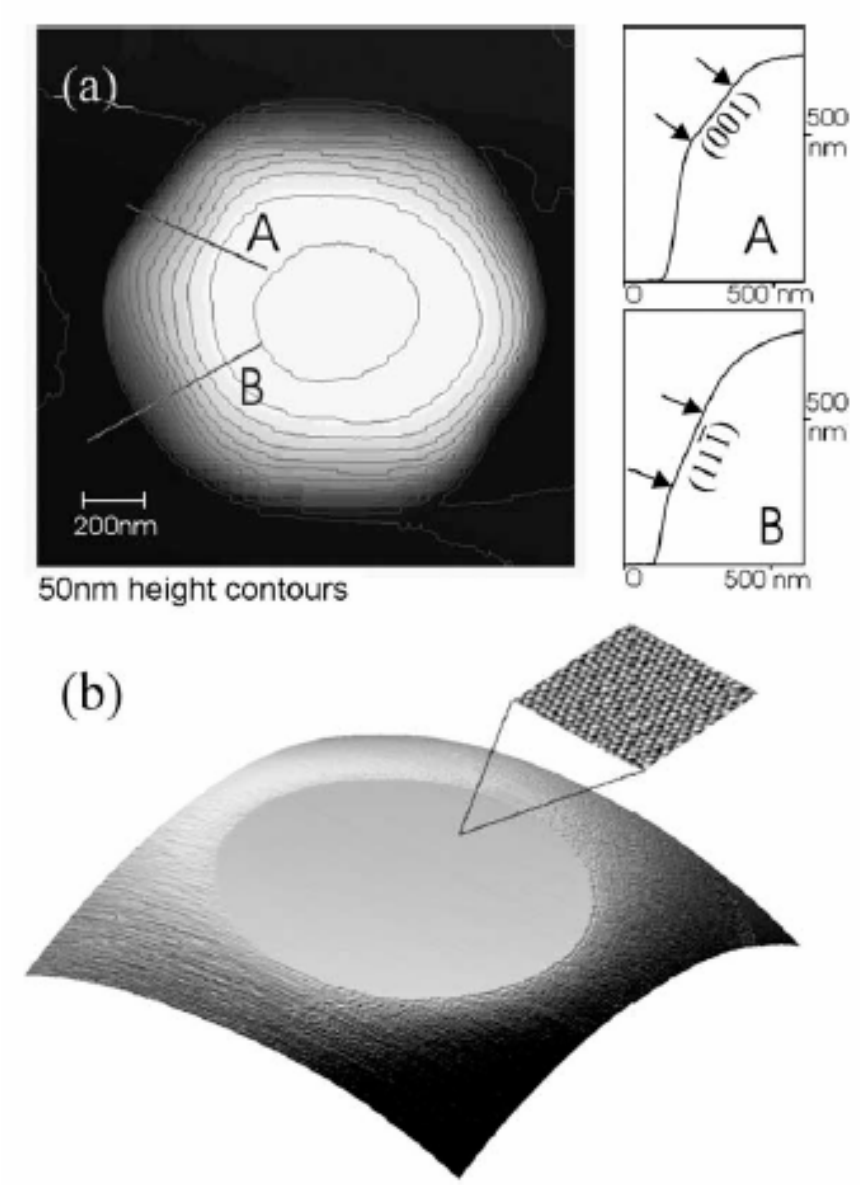

Figure 1-3 STM image of a Pb crystallite [14]. A vicinal surface smoothly attaches to a facet with a high symmetry plane, e.g. (001), (111)

model breaks down at this cusp. The structural anisotropy of the solid must be introduced. Fortunately, within the vicinity of the cusp, e.g. on the vicinal part of the surface, the surface can still be considered "rough" and the continuum model can be applied with an appropriate surface free energy density. The broadly applicable from of such surface free energy density is the *Gruber-Mullins-Pokrovsky-Talapov surface free energy density*, [8, 15, 16] in 1D

$$f(z_x) = \gamma_0 + \frac{\beta}{h} z_x + g z_x^3 \tag{1-4}$$

where h is the step height. Now there are three thermodynamic parameters, γ_0 the surface tension of a high symmetry plane, and two terms that introduce the orientational dependence β the step free energy and g the step-step interaction coefficient (all will be discussed in the next section with the definition of the step). Notice that there is no cusp in this formula so that the continuum model can be applied. Following eq. (2) the surface chemical potential and ECS are obtained as

$$\mu(z_x, z_{xx}) = 6vg\left|\frac{dz(x)}{dx}\frac{d^2z(x)}{dx^2}\right| \tag{1-5a}$$

$$z(x) = z_0 - \frac{2}{3}\sqrt{\frac{\mu_0}{3gv}}(x - x_0)^{3/2} \tag{1-5b}$$

where again μ_0, the facet radius x_0, and the crystal height z_0 are obtained from the *boundary condition*. This is the well known *Pokrovsky-Talapov equilibrium crystal shape* [8, 16, 17] (PTECS) with the characteristic $x^{3/2}$ shape approaching the facet.

Up to this point no specific relation between $\mu_0, x_0,$ and z_0 has been provided, since they come from the boundary condition at the facet edge, thus from the cusp of

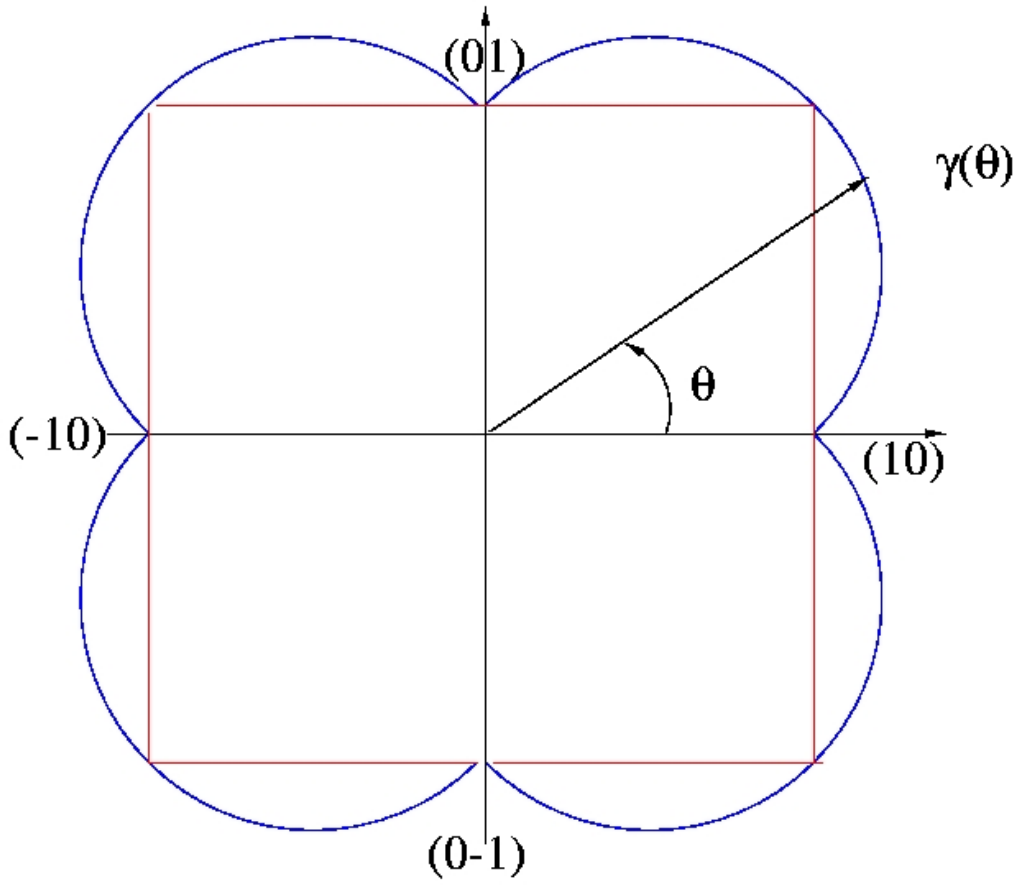

Figure 1-4 Geometric description of a 2D Wulff construction. Blue line is the surface tension as a function of rotational angle and red line is its Legendre transform, the ECS.

the surface free energy density, which can not be addressed within the continuum model. However in fact, they are physically related through the volume constraint of the crystallite, which has not been addressed so far. The relevant equilibrium relationship is often referred as the *Wulff relationship*. Here we introduce the elegant *Wulff construction* [8, 18, 19](Figure 1-4), which takes the volume constraint into account and leads to this Wulff relation along with the PTECS

$$\gamma(z_x, z_y) = \lambda \frac{z - xz_x - yz_y}{\sqrt{1 + z_x^2 + z_y^2}}. \qquad (1\text{-}6)$$

Mathematically, this is a *Legendre transform* from the surface free energy density (eq. (1)) to the ECS where λ is the Legendre multiplier. Since the Legendre multiplier is the conjugate field of the constrained volume in the total free energy λ=-μ_0/v. With eq. (4), the Wulff construction in 1D gives

$$z(r) = z_0 - \frac{2}{3}\sqrt{\frac{\beta}{3ghx_0}}(x - x_0)^{3/2} \quad \text{and} \quad \frac{\gamma_0}{z} = \frac{\beta}{hx_0}\left(= \frac{\mu_0}{v}\right). \qquad (1\text{-}7)$$

Although resulting from different surface free energy densities, the similarity between the Wulff relation for the facet and the Gibbs-Thomson relation for a rough surface is very interesting.

Here are a few remarks before closing the section. Since V and μ_0 are conjugate variables of one another, in principal knowledge of one must fix the other. Since we are considering the thermodynamic limit of $V\rightarrow\infty$, this results in $\mu_0\rightarrow 0$ and of course $x_0\rightarrow\infty$ and $z_0\rightarrow\infty$, leading to a flat surface. Thus a question arises of what a facet radius or crystallite height of an infinite volume means? Furthermore, what would happen if the volume is finite? Would the ECS change? Would the Wulff relationship still hold? (Note that the Wulff relationship originates from the volume

constraint not the volume itself.) These are the questions that will be answered in this study.

1.3 Steps on surfaces and the continuum step model

Below the roughening transition temperature, a crystallite forms a facet with a smoothly connecting vicinal surface as mentioned above. Within the continuum model this vicinal region can be considered as a "rough" surface, however, physically it is not. It is constructed by monatomic height defects on surfaces called *steps* separated by terraces with the same high symmetry orientation of the facet. Figure 1-5 a) shows an STM image of such steps on surfaces. These steps are the most important features of the surface at moderate temperatures since most dynamical activities e.g. crystal growth, surface reconstruction, start from the step-edges where motions of *adatoms* (diffusing atoms on the surface) are taking place. Thus it is natural to construct a model based on steps as fundamental building blocks, the *continuum step model* [10, 19-21] shown in Figure 1-5 b). The continuum step model is an array of 1D continuous non-crossing interfaces, representing the steps, which can interact with each other as we will see.

For an isolated step we can proceed exactly the same way as in the continuum model in 1D. As mentioned above since the step is rough

$$F_S = \iint \beta(x_y)\sqrt{1+x_y^2}\,dy \approx \iint \frac{\widetilde{\beta}(x_y)}{2} x_y^2\,dy \qquad \text{(1-8a)}$$

$$\mu = \frac{-\Omega\widetilde{\beta}(x_y)x_{yy}}{\sqrt{(1+x_y^2)^3}} \approx -\Omega\widetilde{\beta}(x_y)x_{yy} \qquad \text{(1-8b)}$$

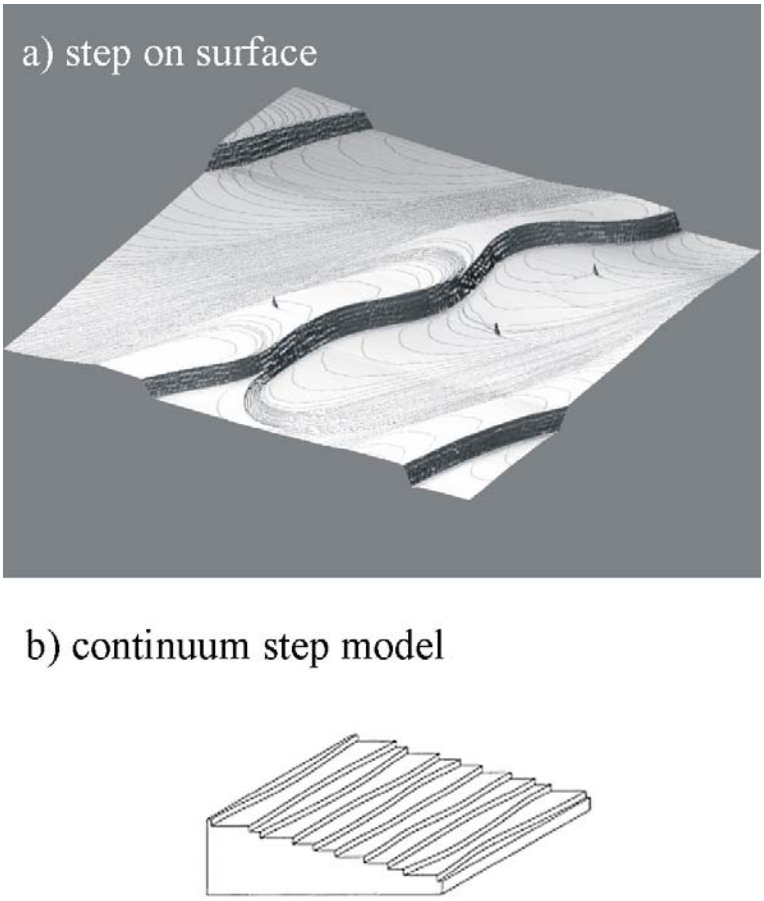

Figure 1-5 a) STM image of steps on surfaces on Si(111) [10] (step bands and anti-bands are also present). b) schematic drawing of the continuum step model [10]. The continuum step model is an array of coarse-grained 1D continuous interfaces representing the steps, forming the vicinal surface.

where β and $\tilde{\beta}=\beta+\partial^2\beta/\partial x_y^2$ are the *step free energy* and *step stiffness*, analogous to the surface tension and surface stiffness in 2D. (Note: "Maryland notation" of the coordinate system with the x axis perpendicular to the average step edge direction.) Here we introduce an experimentally accessible quantity, the *spatial correlation function* $G(y)$ [10, 22, 23] defined as

$$G(y) = \left\langle \left[x(y + y_0) - x(y_0) \right]^2 \right\rangle_{y_0}, \tag{1-9}$$

and compute this for an isolated step of eq. (8). With the use of Fourier transforms, it is straightforward to obtain for short distances

$$G(y) = \frac{k_B T}{\tilde{\beta}} |y|. \tag{1-10}$$

$k_B T/\tilde{\beta}$ is the *capillary length*, which is the minimum unit of the correlation length. The linear behavior in $G(y)$ is characteristic of a *random walk*.

The greatest advantage of the continuum step model arises when the step-step interactions are included [10]. Since crossings of the steps are highly prohibited due to overhangs there is a step-step interaction which follows $\sim l^{-2}$ where l is the distance between steps or terrace width (in more detail in section 1.5). For simplicity we consider straight steps (1D), then the analogous forms of the Gruber-Mullins-Pokrovsky-Talapov projected surface free energy per area (eq. (4)) and step chemical potential ((eq. (5a))) are

$$f(l_i) = \gamma_0 + \frac{\beta}{l_i} + g\left(\frac{h}{l_i}\right)^3 \quad \text{and} \quad \mu(x_i) = 2g\Omega\left[\left(\frac{h}{l_{i-1}}\right)^3 - \left(\frac{h}{l_i}\right)^3\right], \tag{1-11}$$

where x_i is the position of the ith step, $l_i=x_{i+1}-x_i$ and g is the *interaction coefficient*. This step chemical potential has been used well in the past for research in surface

dynamics and morphology evolution. Here we give a brief outline of the approach [16, 21, 24-26].

The numerical calculation is based on the concentration of adatoms $c_i(x)$ on the ith terrace between the i+1 and ith step and the adatom flux $j_i(x_i)$ from the ith terrace to the ith step, which obey

$$\frac{\partial c_i(x)}{\partial t} = D_S \frac{\partial^2 c_i(x)}{\partial x^2} - \frac{c_i(x)}{\tau} + f\,, \tag{1-12a}$$

$$\mp j_i(x_i) = D_S \left.\frac{\partial c(x)}{\partial x}\right|_{x_i} = \pm\kappa(c_i(x_i \pm 0) - c_{eq}^i)\,, \tag{1-12b}$$

$$c_{eq}^i = c_{eq}^0 \exp(\frac{\mu(l_i)}{k_B T}) \approx c_{eq}^0\left(1 + \frac{\mu(l_i)}{k_B T}\right), \tag{1-12c}$$

where D_S, κ, τ and f are the *kinetic parameters*, the diffusion constant of adatoms on the terrace, linear coefficient of attachment/detachment at the step-edge, life-time of an adatom and impinging atom flux from the vapor, respectively. $c_{eq}^0 = f\tau$ is satisfied at equilibrium. To apply these equations, first the step chemical potential, eq.(1-11), is calculated from the step positions and related to the terrace concentration with eq. (1-12c). Eq. (1-12a) is then solved for all terraces (in many cases using the static approximation $\partial c(x)/\partial t = 0$) with boundary conditions eq. (1-12b) at the i+1 and ith step-edge. The steps move with velocity $v_i = \Omega[j_i(x_i) - j_{i+1}(x_i)]$, and the step chemical potential is recalculated with the new positions. This kinetic model has been applied to many experimental observations e.g. MBE growth, electromigration with great success both qualitatively and quantitatively.

One remark is important before closing the section. The *boundary condition* of the bounding steps of the nano-structure has not been addressed so far and will

introduce new effects. In many cases, periodic boundary conditions have been used for $V\rightarrow\infty$, which strictly speaking does not give the PTECS. For a finite-volume crystallite, more serious consideration of boundary conditions is needed. In this case we will need to ask: How will the ECS compare with the PTECS in the continuum model? What is the role of the built in *steps* of the continuum step model? These are the questions that will be answered in this study.

1.4 Langevin theory and dynamical universality class

The Langevin theory is based on one essential hypothesis, *the hypothesis of linear regression*, which says that the deterministic relaxation process to *equilibrium* of any extensive density is linear in its thermodynamic force. This hypothesis leads to a relationship between this linear constant, the *dissipative transport coefficient*, and the magnitude of the *autocorrelation function* of the noise term (fluctuations), the so-called *fluctuation-dissipation theorem*, the heart and soul of the Langevin theory. The Langevin equation is given as (Maryland notation for step coordinates)

$$\frac{\partial x(y,t)}{\partial t} = f[x(y,t)] + \eta(y,t)\,. \qquad (1\text{-}13)$$

The function of the relaxation process $f[\bullet]$ is obtained from microscopic processes (discussed in the next section) or simply from symmetry properties of the model. It can be linear or non-linear, local or non-local. The fluctuations, which are in principle complicated atomic scale transport properties, are simply incorporated into the *noise term* $\eta(y,t)$ with property $\langle\eta(y,t)\rangle=0$, which can be conservative or non-conservative, white or colored depending on the nature of $f[\bullet]$.

For isolated steps on surfaces there are several well known functions $f[\bullet]$ for describing the relaxation process. Here we introduce the most important two examples of *attachment/detachment* (A/D)

$$\frac{\partial x(y,t)}{\partial t} = \frac{-\Gamma_{AD}}{k_B T}\mu + \eta(y,t) \tag{1-14a}$$

$$\langle \eta(y,t)\eta(y',t') \rangle = 2\Gamma_{AD}\delta(y-y')\delta(t-t') \tag{1-14b}$$

and *periphery diffusion* (PD)

$$\frac{\partial x(y,t)}{\partial t} = \frac{\Gamma_{PD}}{k_B T}\frac{\partial^2 \mu}{\partial y^2} + \eta_C(y,t) \tag{1-15a}$$

$$\langle \eta_C(y,t)\eta_C(y',t') \rangle = -2\Gamma_{PD}\nabla^2\delta(y-y')\delta(t-t') \tag{1-15b}$$

where Γ_{AD} and Γ_{PD} are the dissipative transport coefficients, attachment/detachment and edge-hopping mobility, respectively [21, 24]. A/D and PD are schematically shown in Figure 1-6. Obviously, the dissipative transport coefficients have direct connections to the equation of motions of steps, eq. (1-12), derived in the previous section, e.g. for A/D, $\Gamma_{AD}=\kappa\Omega c_{\mathrm{eq}}{}^0$. Eq. (1-14b) and (1-15b) are the *fluctuation-dissipation theorem* in mathematical presentation for non-conservative and conservative noise, respectively. For the step chemical potential we can use eq. (1-8b) for an isolated step. Here we introduce an experimentally accessible quantity, the *temporal correlation function* $G(t)$ [10, 22, 27], similar to the spatial correlation function, defined as

$$G(t) = \left\langle \left[x(t) - x(t_0)\right]^2 \right\rangle_{t_0}. \tag{1-16}$$

For A/D (eq. (1-14a)) and PD kinetics (eq. (1-15a)), with similar Fourier transforms we obtain analytical results of

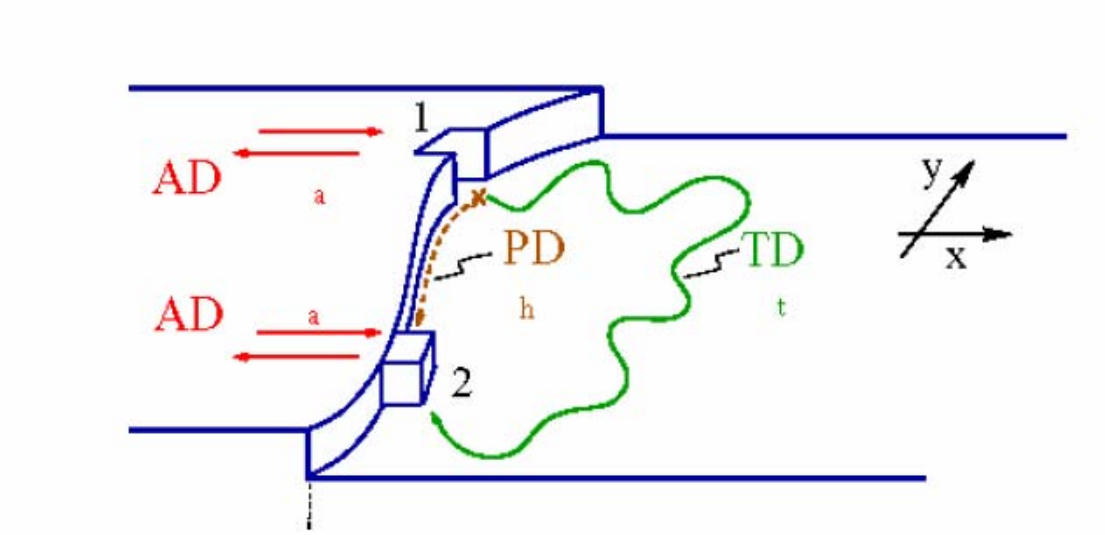

Figure 1-6 Schematic drawing of kinetic processes [28]. Attachment/detachment (A/D) shown as a red line, adjacent to a thermodynamic reservoir and periphery diffusion (PD) shown as a dotted brown line, diffusion along the step-edge. (Also shown is terrace diffusion (TD) not in text)

$$G(t) = \frac{2\Gamma((z-1)/z)}{\pi}\left(\frac{k_B T}{\Omega\tilde{\beta}}\right)^{\frac{z-1}{z}}\left(\Gamma_z t\right)^{\frac{1}{z}} \qquad (1\text{-}17)$$

where $\Gamma(x)$ is the gamma function and z = 2,4 for A/D and PD, respectively. Experimental results on metal surfaces show that A/D is observed mainly on (110) surfaces whereas PD is on (111) surfaces[10, 22].

All of the above is a part of a larger research field in statistical physics that of *dynamical scaling and universality classes*, mostly developed in the field of interface growth [29]. For all types of Langevin equations with any $f[\bullet]$ and $\eta(y,t)$ we can measure the *interface width* defined as

$$w(L_y, t) = \left\langle \left[x(y,t) - \bar{x}(t)\right]^2 \right\rangle_y^{1/2} \qquad (1\text{-}18)$$

The ansatsz for the universal scaling form is

$$w(L_y,t) \sim L_y^{\alpha} f\left(\frac{t}{L_y^z}\right) \qquad (1\text{-}19a)$$

$$f(u) \sim \begin{cases} u^{\beta}, (u << 1) \\ const, (u >> 1) \end{cases} \qquad (1\text{-}19b)$$

where α, β and z are the scaling exponents, *roughness*, *growth* and *dynamic exponent*, respectively, which define the dynamic universality class. The three exponents are not independent and are related by $z = \alpha/\beta$. The time when $u \sim 1$ or $t_x \sim L_y^z$ is called the crossover time t_x. The ansatsz also leads to a similar scaling for the correlation functions, spatial $G(y) \sim y^{2\alpha}$ and temporal $G(t) \sim t^{2\beta}$. Thus A/D kinetics for an isolated step gives α=1/2, β=1/4 and z=2 belonging to a class of linear, conservative dynamics and non-conservative noise (LCN2) and PD, which give α=1/2, β=1/8 and

z=4 to linear, conservative dynamics and conservative noise (LCC4) (Notation in ref.[29]).

The problem that has not been addressed in the formalism described above is the *isolation* conditions for the steps on a finite volume crystallite. For a flat surface it is not so hard to find an isolated step, however, for a facet with global curvature and neighboring steps, how will the function of deterministic relaxation process be the altered? Will the result lead to the same or another universality class of dynamical scaling? These are the questions that will be answered in this study.

1.5 Discrete models and microscopic processess

Discrete models are heavily used in statistical physics to extract thermodynamic properties from a *microscopic effective energy* ε used in the Hamiltonian of the model. This is a powerful tool since such effective energies can often be calculated by *ab initio* methods. Here we introduce some of the discrete models often used in surface studies and show results of calculated thermodynamic parameters introduced in section 1.1 and 1.2. To describe a surface with atoms on lattice sites, the *Kossel crystal* is often used. This model is just an array of cubes stacked on top of each other in a lattice shown in Figure 1-7. The most commonly used model for the Hamiltonian is the *solid-on-solid* (SOS) *model* [30, 31] illustrated in Figure 1-8 a).

$$H_{SOS} = \frac{\varepsilon_{SOS}}{a} \sum_{\langle i,j \rangle} \left| h_i - h_j \right| \qquad (1\text{-}20)$$

where a is the lattice constant and h_i is the height of the ith column. In 2D it represents a rough surface and in 1D it represents a step. For a surface below the roughening temperature, an array of 1D SOS models is used to describe the vicinal

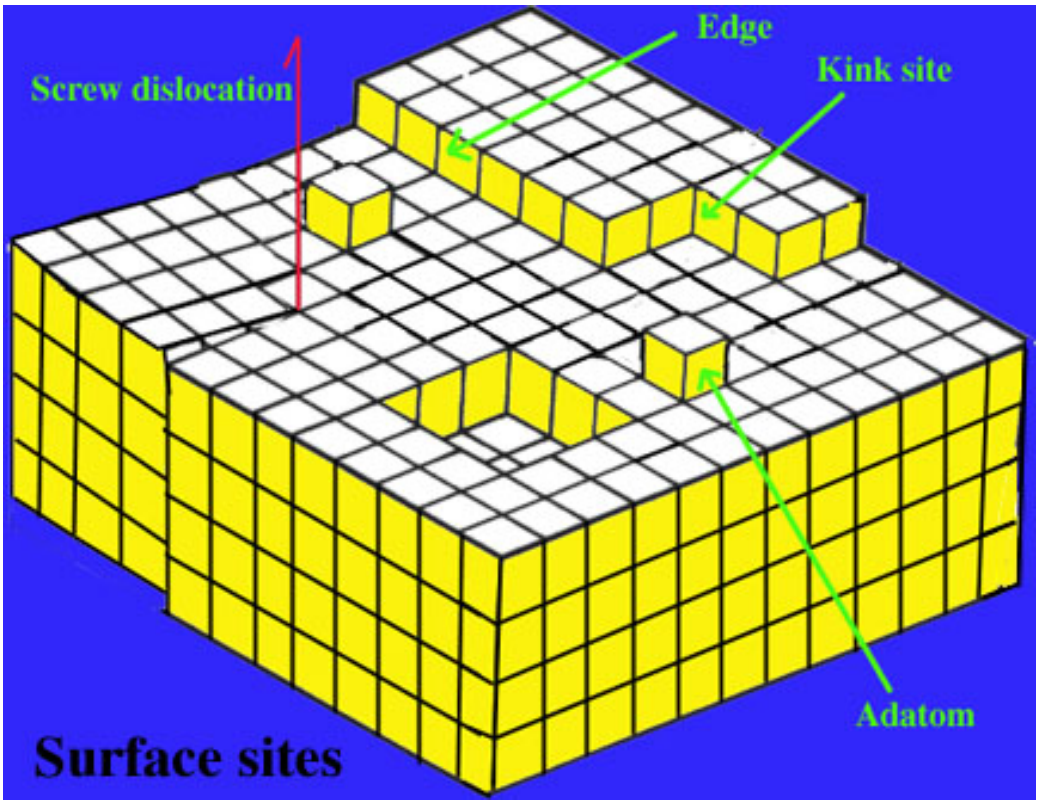

Figure 1-7 Schematic drawing of a Kossel crystal with an array of cubes stacked on top of each other. Adatom, kink site, step-edge and a screw dislocation is shown within the Kossel crystal description of the surface.

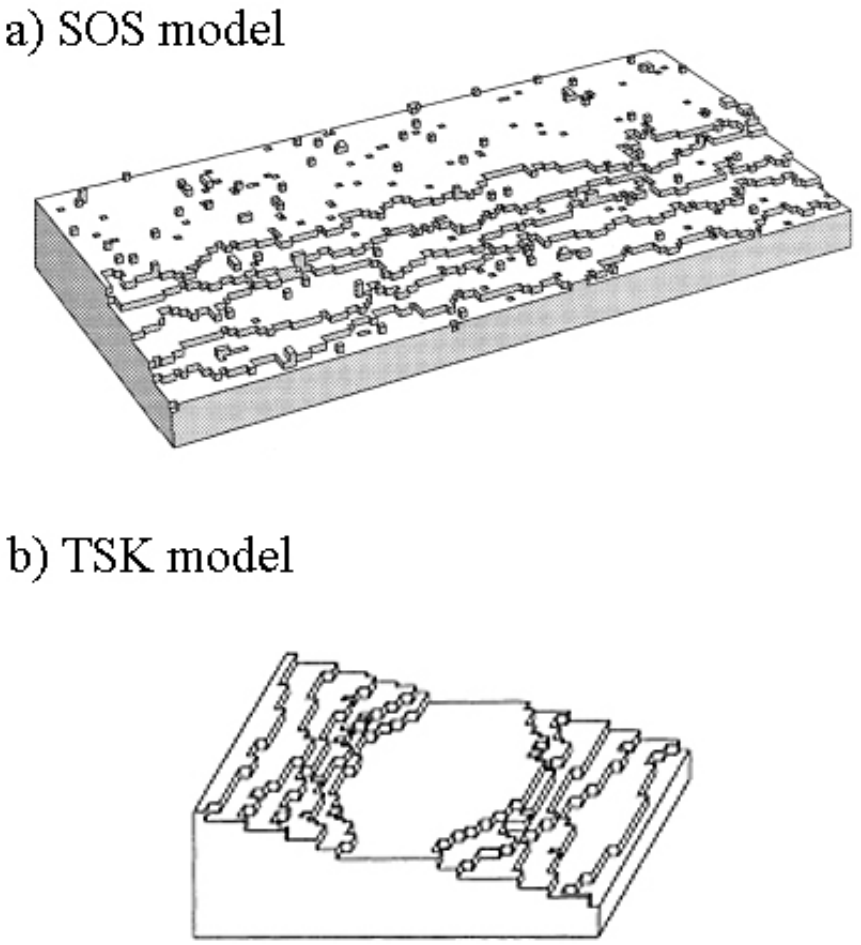

Figure 1-8 Schematic drawing [10] of a) the 2D SOS model, which include adatoms and vacancies and b) the TSK model, which is an array of 1D SOS models, with information of adatoms and vacancies integrated out.

surface. This is called the *terrace-step-kink* (TSK) *model*, and its relationship to the SOS model is similar to the relationship between the 1D continuum model and continuum step model. The TSK model is illustrated in Figure 1-8 b). The direction along the step is also discretized with thermally excited *kinks* where ε_{sos} is now the *kink energy*. The step free energy and step stiffness, as a function of temperature within the TSK model for an isolated step along the high symmetry [001] direction is given as

$$\beta(T) = \frac{\varepsilon_{SOS}}{a} + \frac{k_B T}{a} \log\left(\tanh\left(\frac{\varepsilon_{SOS}}{2k_B T} \right) \right), \tag{1-21a}$$

$$\widetilde{\beta}(T) = \frac{2k_B T}{a} \sinh^2\left(\frac{\varepsilon_{SOS}}{2k_B T} \right). \tag{1-21b}$$

However, the TSK model is not an ideal model at high temperatures since it does not allow overhangs. To include such overhangs we must consider the *Ising model* (lattice-gas model) [30, 32] with a Hamiltonian

$$H_{Ising} = \varepsilon_{Ising} \sum_{\langle i,j \rangle} \sigma_i \sigma_j \tag{1-22}$$

where $\sigma_i = 2n_i - 1$ is the Ising spin (n_i the occupation variable). The coupling constant ε_{Ising} is related to ε_{sos} by $\varepsilon_{Ising} = \varepsilon_{sos}/2$. The calculated step free energy for a step along the [001] direction in the Ising model is exactly the same as in the SOS model, however, the stiffness is different due to the allowed overhangs

$$\widetilde{\beta}(T) = \frac{k_B T}{a} \sinh\left(\cosh^{-1}\left(\frac{(W^2(T)+1)^2}{2W(T)(1-W^2(T))} \right) \right) \quad \text{and}$$

$$W(T) = \exp\left(\frac{-2\varepsilon_{Ising}}{k_B T} \right). \tag{1-23}$$

For the TSK model with multiple steps if there is a hard core repulsion between the steps restricting multiple height steps, then there is a reduction of available configurations due to this repulsion. This is known as an *entropic interaction*, and the thermodynamic step-step interaction coefficient can be calculated. The partition function can be calculated by mapping it onto a quantum mechanics problem of the time evolution of 1D fermion particles [10, 33], the result gives

$$g(T) = \frac{(\pi k_B T)^2}{6h^3 \widetilde{\beta}(\theta, T)}. \qquad (1\text{-}24)$$

Another great advantage of discrete models is the construction of *Monte Carlo* (MC) *simulations* since the only parameter is the effective energy J, which can be compared to the temperature $k_B T$ in the MC simulation. Such research has been done extensively in the field of interface growth, where dynamical scaling and universality classes were introduced as mentioned in the previous section. Many models of microscopic processes eg. random deposition with surface relaxation [34], Wolf-Villain model [35], Das Sarma-Tamborenea model [36] all fall into different universality classes although they are very similar in their microscopic processes. For steps on surfaces, with the use of the SOS model and random position deposition and evaporation, MC results give α=1/2, β=1/4 and z=2, the same class as A/D kinetics of the Langevin equation. Although kinetic MC, which includes energy barriers, is more favorable to compare with real systems, MC is still useful for quantitative discussions of the equilibrium configurations.

In the previous section we have talked about the effect of finite volume on the Langevin theory. The same questions can be applied here. With interacting steps, which reduces the number of available configurations, and with conserved

microscopic processes within steps and between them, will we see different universality classes of dynamical scaling from a pure 1D system? These are the questions that will be answered in this study.

1.6 Overview

In the following chapters, the questions presented in each section above will be answered theoretically and confirmed by experiments and simulations. We will start with the equilibrium properties of nano-structures using the continuum model and discuss how important the surface, including the interface, is for the nanostructures and how drastically the properties can be altered with respect to the thermodynamic limit. Next we move to the continuum step model and see how the introduction of steps will influence the continuum model results. Also non-equilibrium and close-to-equilibrium properties, dynamics and evolution of nano-structures will be discussed. The Langevin theory will be applied to facet-edge fluctuations at equilibrium to investigate how finite volume effects change the scaling behavior known for purely isolated 1D structures.

The theory will be simultaneously compared to experiments of Pb crystallites supported on a Ru substrate (see Figure 1-3). Pb crystallites are ideal model systems for such research since they have clean observable facets at moderate temperatures and have been used in experiments for over two decades. Experimental observation are done by scanning tunneling microscope (STM) techniques, which detects the tunnel current for imaging of the surface topography. Atomistic spatial resolution of the STM makes it possible to do fluctuation measurements of the steps in the nm

range, but it can also zoom out to take profiles of the crystallites and follow their evolution due to environment change in the μm range. Computational simulations will also be carried out for comparison with both theory and experiment. From numerical calculations of the step equations of motion within the continuum step model introduced in section 1.3 to MC simulations within the TSK model with restricted nearest neighbor hopping processes.

This work is the attempt to give an example of how different the properties at mesoscopic length scales can be from both macroscopic and microscopic lengths, where all properties are deterministic and stochastic, respectively. It is also an attempt to once again recognize the power of thermodynamics, which goes beyond the normally-considered thermodynamic limit. For fixed extensive variables, if the boundary conditions are well defined, thermodynamics can still capture the equilibrium and dynamical properties of the system extremely well. Finally, our ultimate goal in the present work is to give some insight to the difficulties and challenges we will probably face in the near future in the journey of research in nanofabrication and associated nanotechnologies.

Chapter 2: Nanoscale Equilibrium Crystal Shapes

The finite size and interface effects on equilibrium crystal shape (ECS) have been investigated for the case of a surface free energy density including the free energy of step formation and inverse-square step-step interactions. Explicitly including the curvature of a crystallite leads to an extra boundary condition in the solution of the crystal shape, yielding a family of crystal shapes, governed by a constant of integration, which we call the shape parameter c. The total crystallite free energy, including interface energy, is minimized for $c=0$, yielding in all cases the traditional Pakrovsky-Talapov shape. Solutions of the crystal shape for $c\neq 0$ are presented and discussed in the context of meta-stable states due to the energy barrier for nucleation. Explicit scaled relationships for the ECS and metastable states in terms of the measurable step parameters and the interfacial energy are presented.

2.1 Introduction

Technological demands for the fabrication of nano-structures and quantum dots [4, 6, 37] provides renewed motivation for understanding the atomistic properties that control the morphology of crystal shapes. With decreasing structure size, the issues of finite size and shape effects become non-negligible [2, 5] including issues of stability against decay and structural rearrangement [38-40]. Small structures are also increasing sensitive to external perturbations, such as the adhesion energy and stress caused by the substrate interface [1, 41-45]. In this work we will address the issues of nanoscale equilibrium crystal shape for the surface free energy of the continuum step model [10, 22], which allows experimentally determined thermodynamic parameters for step free energies to be connected rigorously to structural predictions.

The theory of equilibrium crystal shapes (ECS) has been extensively studied in the last half century [8, 9, 16, 17, 46-51]. The formation of facets below the roughening temperature, and the Pakrovsky-Talapov predictions [15] for the edge shape ($z(x)$) of crystals have been demonstrated in a number of clean systems [52-59]. In addition to studies on 3D crystals, there has been substantial work on the 2D ECS of islands [18, 22, 60-63] to obtain the edge free energy, equilibrium edge fluctuations and decay kinetics.

While 2D studies have intrinsically addressed the effects of finite size, most theoretical 3D studies have been performed in the limit of large crystal size, where curvature effects can be neglected. However, indications of size effects have been presented in theoretical work on nucleation barriers in crystal evolution [9, 64, 65] and shape [4, 66]. Furthermore, curvature effects are clearly important in the stability or

evolution on 3D crystallites [14, 67-69]. Moreover, interesting new fluctuation phenomena are possible in small crystallites, as shown theoretically by Ferrari et al.[70].

Here we explicitly consider the case of a "free standing" truncated crystal, as in Figure 2-1 a) or supported truncated crystallite, Figure 2-1 b). We address the nature of the equilibrium shape for these models, as a first step in describing the evolution of crystallites under external perturbation [71]. The effects of finite curvature and interfacial effects are presented quantitatively in terms of experimentally measurable parameters.

2.2 Background

The equilibrium crystal shape arises as the result of the minimization of the orientation-dependent surface free energy $\gamma(\hat{n})$ with the constraint of constant volume. This calculation is performed via the Wulff construction [17, 19], which mathematically is a Legendre transform from the surface tension to the ECS. Vice versa the ECS provides a direct measurement of the surface tension. Interface effects in ECS have been considered for T=0 crystal shapes by Muller and Kern [41]. They have considered a crystal shape truncated at a bottom surface (with surface free energy γ_A equal to that of the top facet) and brought into contact with a substrate surface of free energy γ_B. They use the Dupré relationship $\gamma_{AB} = \gamma_A + \gamma_B - E_A$ for the interface free energy γ_{AB}, where E_A is the adhesion energy. This yields a change in the substrate free energy per unit area due to formation of the interface of $\gamma_{AB} - \gamma_B = \gamma_A - E_A$. They show that when the substrate free energy change is zero, e.g. $\gamma_A - E_A = 0$, the crystal truncation occurs

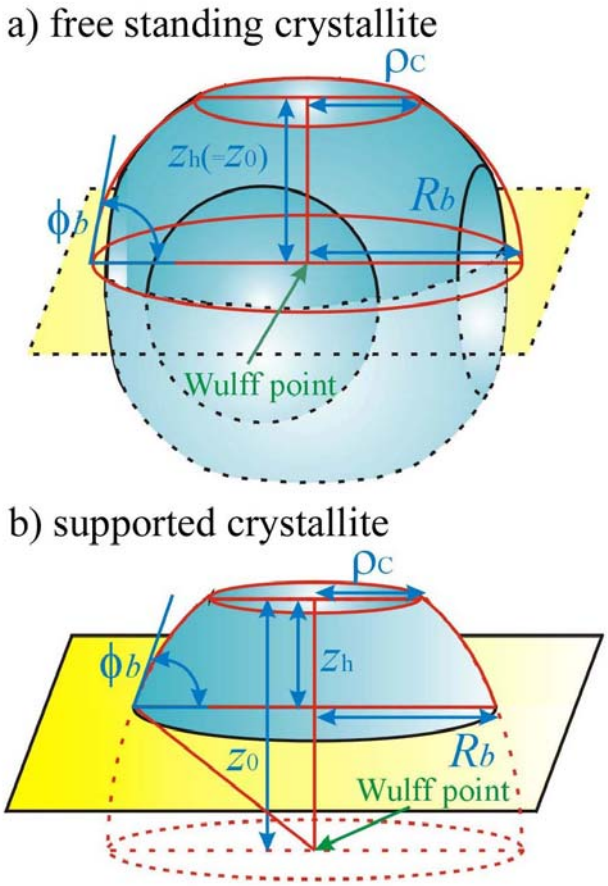

Figure 2-1 Illustration of a finite size crystallite with rounded regions between low index facets. A model for structure evolution is proposed in which the truncated shape, as illustrated by the dotted line, is treated as a constant volume crystal shape for purposes of modeling crystallite reshaping. Note here that the center of the crystallite (Wulff point) is in the interface plane of the modeled crystallite, a "free standing" boundary condition. b) Schematic drawing of a supported crystallite with a single flat facet bounded by rounded regions that terminate at the substrate. Here the Wulff point is not located in the interface plane and the height of the crystallite z_h is determined by the adhesion energy.

at the Wulff point, e.g. the configuration shown in Figure 2-1 a). For larger values of the binding energy, the truncation occurs as shown in Figure 2-1 b), with the crystallite height z_h proportional to $2\gamma_A - E_A$.

Most studies of the rounded edges of crystals have used the limit of infinite size, in which curvature effects are neglected, and thus yield an edge profile $z(x)$ independent of the third dimension [9]. For finite size crystallites, curvature effects of the steps become non-negligible, thus the full profile $z(x,y)$ must be considered. The full 3D Wulff construction can be presented in rectangular coordinates [11], however a more efficient way to take curvature effects into account is to work in cylindrical coordinates yielding $z(r,\theta)$. The 3D Wulff construction in cylindrical coordinates is [18]

$$\gamma(\hat{n}) = \left(\frac{\lambda}{2}\right) \frac{z - r\left(\frac{\partial z}{\partial r}\right)}{\left[1 + \left(\frac{\partial z}{\partial r}\right)^2 + \frac{1}{r^2}\left(\frac{\partial z}{\partial \theta}\right)^2\right]^{1/2}}, \qquad (2\text{-}1)$$

where λ is the Legendre multiplier, which turns out to be the *excess* chemical potential due to the surfaces. For the surface tension $\gamma(\varphi)$, or the surface free energy density $f(\varphi)$, let us consider the Pokrovsky-Talapov type surface free energy density [15], which is a good approximation for surfaces which make a low angle φ with respect to a neighboring low-index facet orientation:

$$\frac{\gamma(\hat{n})}{\cos\varphi} = f(\varphi) = \gamma_0(T) + \frac{\beta(\theta,T)}{h}\tan\varphi + g(\theta,T)\tan^3\varphi\,. \qquad (2\text{-}2)$$

Here h is the step height, β and g are the thermodynamic step free energy and step-step interaction coefficient, respectively, γ_0 is the surface tension of the low-index terrace and φ is the angle of the surface relative to that terrace, thus $\tan\varphi = \partial z/\partial r$

corresponds to the step density. With an isotropic step free energy (no θ dependence, $\beta=\tilde{\beta}$), this Wulff construction gives the same solution as the Pokrovsky-Talapov equilibrium crystal shape (PT-ECS) for an infinite volume in 1D. The only difference is the factor of 2 in the denominator of the Legendre multiplier in eq.(2-1) due to the dimensionality [18].

In addressing the evolution of crystal shapes, it is useful to address the ECS by defining a local excess chemical potential that must be the same everywhere on the crystal surface. The local surface chemical potential is obtained by calculating the change in total free energy when there is a small local deformation of the surface, e.g. one must take the functional derivative $\delta F / \delta N$. Here, we evaluate this derivative using the continuum model, where the surface is approximated as a 2D continuous interface. This is usually used for a crystal shape above the roughening temperature, however it is still valid for the rounded regions on a crystal with facets that are below their roughening temperature.

For a single-component incompressible ($V=vN$) crystallite, the Helmholtz free energy $F(T,N)$ is the most convenient ensemble to consider. For an arbitrary surface free energy density f, the total free energy of the crystallite in cylindrical coordinates is

$$F = \iint f(z_r, \frac{z_\theta}{r}) r dr d\theta + \frac{\mu_B}{v} \iint z(r,\theta) r dr d\theta + (\gamma_0 - E_A) \iint r dr d\theta , \quad (2\text{-}3)$$

where $z_r=\partial z/\partial r$ is the local slope of the surface, v the atomic volume and μ_B is the fixed chemical potential of the bulk. The first term is the surface free energy, the second term is a constant bulk free energy and the third term is the free energy of the truncated bottom surface including the adhesion energy at the interface if there is any.

The equilibrium configuration minimizes the total free energy at fixed N, and yields a uniform value of the excess chemical potential

$$\frac{\delta F}{\delta N} = -\mu_S(r,\theta) + \mu_B = \mu(V)\,. \tag{2-4}$$

From eq. (2-3) and (2-4), the local excess chemical potential can be defined as

$$\mu_S(r,\theta) = v\left[\frac{1}{r}\frac{\partial f}{\partial z_r} + \frac{d}{dr}\left(\frac{\partial f}{\partial z_r}\right) + \frac{d}{d\theta}\left(\frac{\partial f}{\partial z_\theta}\right)\right]. \tag{2-5}$$

Here let us use eq. (2-2) for the surface free energy density. We also neglect any variation along the step edge direction ($\beta=\tilde{\beta}$) by dropping the third term in eq. (5), e.g. assuming cylindrical symmetry as shown in Figure 2-1. This gives the dependence of $\mu_S(r)$ for an arbitrary crystallite shape:

$$\mu_S(r) = \frac{\Omega\beta(T)}{r} + \frac{3vg(T)}{r}\left(\frac{dz(r)}{dr}\right)^2 + 6vg(T)\left(\frac{dz(r)}{dr}\frac{d^2z(r)}{dr^2}\right). \tag{2-6}$$

The first term in eq. (2-6) is the 2D Gibbs-Thomson term originating from the curvature of the edge of the top facet and the corresponding curvature of the crystal edge. The second term is the change in step interaction energy due to the change of the circumference of the interacting step edge when a single atom is removed from the layer edge. The last term is a change in step interaction energy, which is obtained also in the limit of zero curvature (straight steps). The first two terms vanish as r$\rightarrow\infty$, as must be the case.

2.3 Results

The steady state crystallite shape (e.g. a shape where $\mu_S(V)$ is everywhere the same) can be obtained from eq. (2-6), where the excess chemical potential $\mu_S(V)= \mu_B$-

$\mu(V)$ will be determined by the volume of the crystallite. Setting $y(r)=(dz(r)/dr)^2$ and performing the integration once gives

$$\frac{dz(r)}{dr} = -\sqrt{\frac{\mu_S(V)r - 2\beta\Omega}{6gv} + \frac{c}{r}}, \tag{2-7}$$

where c is a constant of integration that appears due to including the third dimension (curvature) in the calculation. For brevity we will refer to c as the shape parameter hereafter. The minus sign is taken to conform with the coordinate system shown in Figure 2-1. It is possible to find the relationship between the facet radius ρ_c (see Figure 2-1) and the excess chemical potential $\mu_S(V)$ simply by setting $dz(r)/dr\,|_{\rho c}=0$. This yields:

$$\rho_c = \frac{\beta\Omega + \sqrt{\beta^2\Omega^2 - 6cgv\mu_S(V)}}{\mu_S(V)} \quad \text{or} \quad \mu_S(V) = \frac{2(\beta\rho_c\Omega - 3cgv)}{\rho_c^2} \tag{2-8}$$

2.3.1 Pokrovsky-Talapov shape

At this point, it is possible to reproduce the known results for the PT-ECS, which is a specific solution of eq.(2-7). In order to satisfy one component of the Wulff relation, $\rho_0=2\beta\Omega/\mu_S(V)$ the constant of integration c must equal 0. Integrating eq. (2-7) with $c = 0$ yields:

$$z(r) = z_0 - \sqrt{\frac{2\mu_s(V)}{27gv}}\left(r - \frac{2\Omega\beta}{\mu_S(V)}\right)^{3/2}, \tag{2-9}$$

where z_0 is taken to be the distance between the facet and the center of the crystallite (the Wulff point) to satisfy the other component of the Wulff relation $z_0=2\gamma_0 v/\mu_S(V)$. So

$$z(r) = z_0 - \frac{2}{3}\sqrt{\frac{\beta}{3gh\rho_0}}(r-\rho_0)^{3/2} \qquad \frac{\gamma_0}{z_0} = \frac{\beta}{h\rho_0}\left(=\frac{\mu_S(V)}{2v}\right). \qquad (2\text{-}10)$$

Thus the solution with the boundary conditions (z_h=z_0, c=0) that gives the Wulff relation, also gives the Pokrovsky-Talapov ECS[9, 16].

By defining the crystallite so that its truncated interface passes through the Wulff point as in Figure 2-1 a) (z_h=z_0), we are using the free standing boundary condition where the top (and bottom) facet surface tension is equal to the adhesion energy [41]. For this case, we can calculate the radius of the interface area R_b and also the contact angle to the interface plane φ_b analytically, from $z(R_b)$=0 and $\tan\varphi_b = dz(r)/dr\,\big|_{Rb}$:

$$R_b = \frac{2\beta\Omega + 3v\left(2g\gamma_0^2\right)^{1/3}}{\mu_S(V)} \qquad \text{and} \qquad \tan\varphi_b = \left(\frac{\gamma_0}{2g}\right)^{1/3} \qquad (2\text{-}11)$$

An explicit expression for the excess chemical potential can now be precisely determined by the volume constraint:

$$\pi\rho_0^2 z_0 + \int_0^{2\pi}\int_{\rho_0}^{Rb} z(r)\,r\,dr\,d\theta = V = const.$$

yielding:

$$\mu_S(V) = \Omega\left(\frac{2\pi h\gamma_0(140\beta^2 + 252\beta h(2g\gamma_0^2)^{1/3} + 135h^2(2g\gamma_0^2)^{2/3})}{35V}\right)^{1/3}. \qquad (2\text{-}12)$$

A similar set of expressions can be obtained for a supported truncated crystallite as shown in Figure 2-1 b). This is the case where the adhesion energy is not equal to the facet surface free energy $E_A \neq \gamma_0$, and thus the Wulff point is *not* located in the truncation plane of the crystallite, $z_h \neq z_0$. Following Muller's arguments [41], the second Wulff relationship is replaced by the Wulff-Kaishew relation

$$\frac{\mu_S(E_A,V)}{2v} = \frac{2\gamma_0 - E_A}{z_h} = \frac{\beta}{h\rho_0}. \qquad (2\text{-}13)$$

This fixes the contact angle to the substrate φ_b and also the excess chemical potential is obtained as a function of adhesion energy and volume.

$$\tan\varphi_b = \left.\frac{dz}{dr}\right|_{R_b(z_0-z_h)} = \left(\frac{2\gamma_0 - E_A}{2g}\right)^{1/3} \rightarrow \qquad z_h(E_A) = \frac{2gh\rho_0 \tan^3\varphi_b}{\beta},$$

$$\mu_S(E_A,V) = 2\Omega\tan\varphi_b\left(\frac{2\pi gh(35\beta^2 + 126\beta gh\tan^2\varphi_b + 135g^2h^2\tan^4\varphi_b)}{35V}\right)^{1/3}. \qquad (2\text{-}14)$$

The phase space of parameters governing the ECS can be reduced by noting a common dependence on $2\gamma_0$-E_A, as shown in Appendix A, eqs. (A-1) and (A-2). This reduces eqs. (2-12) and (2-14) to a common form

$$\tilde{\mu}_S = \left(\frac{2\pi(140 + 252\sqrt[3]{2}\tilde{E}_A + 135\sqrt[3]{2^2}\tilde{E}_A^2)}{35\tilde{V}}\right)^{1/3} \qquad \text{where}$$

$$\tilde{E}_A = \frac{(g(2\gamma_0 - E_A)^2)^{1/3}}{\beta/h}. \qquad (2\text{-}15)$$

Figure 2-2 a) shows the dimensionless excess chemical potential $\tilde{\mu}_S$ as a function of the dimensionless volume $\tilde{V}=V/h\Omega$ with different physically reasonable values of $\tilde{E}_A$. The range of $\tilde{E}_A$ from1.0~2.0 was chosen to illustrate the estimated variations expected for Pb(111) for a temperature range from approximately room temperature to the melting temperature [57, 58]. Figure 2-2 b) gives the dimensionless facet radius $\tilde{\rho}_0$ (or height $\tilde{z}_h$), contact slope tan $\tilde{\varphi}_b$, and interface radius $\tilde{R}_b$ of the crystallite as a function of the ratio $\tilde{E}_A$ at constant volume $\tilde{V}$. The scaled facet radius and crystal height reduces to the same function, however the physical (unscaled) facet radius and

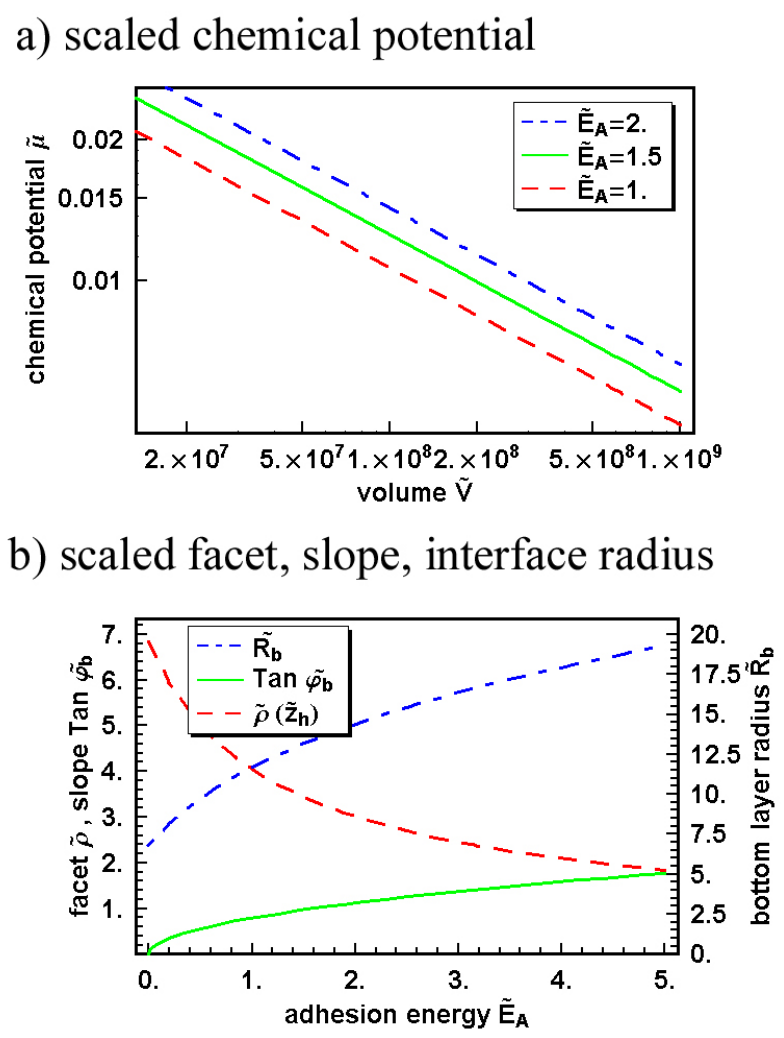

Figure 2-2 Dimensionless chemical potential $\tilde{\mu}_S$ as a function of dimensionless volume $\tilde{V}$ with different ratios of dimensionless adhesion energy $\tilde{E}_A$ =1., 1.5 and 2. at $\tilde{c}$=0. The parameter $\tilde{E}_A$ contains the temperature dependence through the temperature dependence of parameters β, g, E_A and γ_0. As an example $\tilde{E}_A$≈1.04 for Pb at 27 ˚C. b) Dimensionless facet radius $\tilde{\rho}$ (or height $\tilde{z}_h$), contact slope tan$\tilde{\varphi}_b$ and interface radius $\tilde{R}_b$ as a function of $\tilde{E}_A$ at constant volume at $\tilde{c}$=0. The dimensionless variables are given as eq. (A-1) and eq.(A-2)

height vary with temperature (or adhesion energy) quite differently. Specially, with all other parameters held constant the height decreases with increasing adhesion energy, where the facet radius increases.

2.3.2 Non- Pokrovsky-Talapov shapes

The results above have all been obtained with the shape parameter c of eq. (2-7) equal to zero. In the case of infinite (zero curvature) crystallites, this is the only solution, and it yields the ECS. However, in this case, there is an entire family of solutions, only one of which corresponds to the ECS. (E.g. it is possible for the whole surface to have a constant surface chemical potential and yet not be the minimum total free energy configuration that corresponds to the ECS.) Before discussing the physical meaning of the solutions with $c \neq 0$, we note from eq. (2-8) that there is a maximum possible value of c. This is simply obtained by setting the term in the root equal to 0.

$$c_{\max} = \frac{\beta^2 \Omega}{6gh\mu_S(c_{\max}, V)} = \frac{\beta \rho_{c\max}}{6gh} \tag{2-16}$$

At this maximum value of c, $\mu_S(c_{max}, V) = \beta\Omega/\rho_{cmax}$. With this value of $c_{\max}$, eq. (2-7) can be easily solved and gives a crystallite shape of

$$z(r) = z_h - \frac{2\beta\Omega}{3\mu_S(c_{\max}, V)}\sqrt{\frac{2\beta}{3gh}} - \frac{1}{3}\sqrt{\frac{2\mu_S(c_{\max}, V)r}{3gv}}\left(r - \frac{3\beta\Omega}{\mu_S(c_{\max}, V)}\right)$$

$$= z_h - \frac{2\rho_{c\max}}{3}\sqrt{\frac{2\beta}{3gh}} - \frac{1}{3}\sqrt{\frac{2\beta r}{3gh\rho_{c\max}}}(r - 3\rho_{c\max}) \qquad (r > \rho_{c\max})$$

$$\cong z_h - \frac{1}{3}\sqrt{\frac{2\beta}{3gh}}\left(\frac{3(r-\rho_{c\max})^2}{4\rho_{c\max}} - \frac{(r-\rho_{c\max})^3}{12\rho_{c\max}^2} + O^4\right) \tag{2-17}$$

As previously noted by Uwaha [16], $c=c_{max}$ at the vicinal surface leading to the facet has a parabolic shape $z \sim x^2$ in contrast to the PT-ECS where it has an $x^{3/2}$ dependence. At other values of the shape parameter, the crystallite shape must be determined numerically. Taking the free standing boundary condition ($E_A=\gamma_0$), Figure 2-3 shows size scaled cross sections $\tilde{z}(\tilde{r})$ of the crystallites with the same volume but different ratios of the scaled shape parameter (scaling given in the Appendix eq. (A-3) and (A-4) yields $\tilde{c}_{max}=1/6$). The shape changes from the parabolic shape for $\tilde{c}$ close to $\tilde{c}_{max}$ to the 3/2 exponent as the shape parameter decreases to zero. For arbitrary values for c and E_A, the crystal shapes can be obtained numerically. The results can be compiled using scaling so that they can be used for any chosen set of parameters, as shown in Figure 2-4. Figure 2-4 a) gives scaled (eq. (A-3), (A-5) and (A-6)) crystallite height $\tilde{z}_h$, b) interface radius $\tilde{R}_b$, c) contact slope tan $\tilde{\varphi}_b$ and d) crystallite volume $\tilde{V}$ as a function of the shape parameter $\tilde{c}$ up to 1/6 with constant volume. The scaling works perfectly in all cases when $\tilde{c}=0$. However, such parameters as $\tilde{R}_b$ and $\tilde{V}$ do not scale perfectly when $\tilde{c}\neq 0$. The ratios of the crystallite height, interface radius and volume to the facet radius are increasing functions of the shape parameter. The slope on the other hand decreases with shape parameter independent of the volume. Given the expression for the shape of the crystallite, it is possible once again to calculate the constraint of the volume to obtain the excess chemical potential in terms of the other physical parameters. The results for $\tilde{\mu}_S$ is shown also as a function of the scaled shape parameter in Figure 2-4 e). At constant volume, it is a decreasing function of the shape parameter.

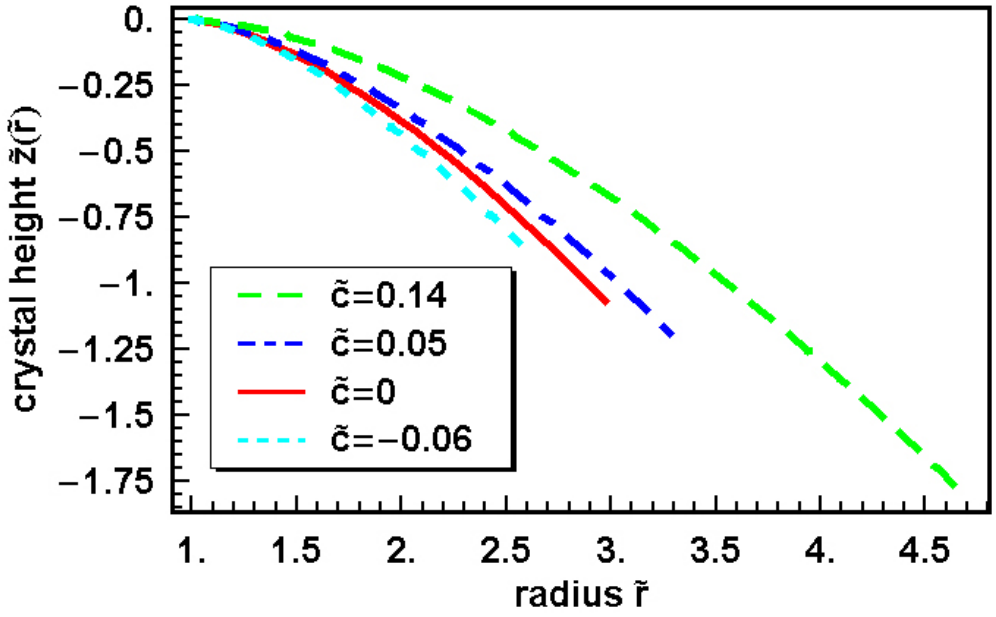

Figure 2-3 Size scaled cross sections of the crystallites $\tilde{z}(\tilde{r})$ with same volume but different scaled $\tilde{c}$. The boundary condition is the "free standing" boundary condition ($E_A=\gamma_0$). The size scaling is given as eq. (A-3) and results in eq. (A-4). Note that these curzes are scaled by the facet radius and not by the crystallite volume itself. The maximum scaled $\tilde{c}$ shown is below the limiting value $\tilde{c}$ =1/6.

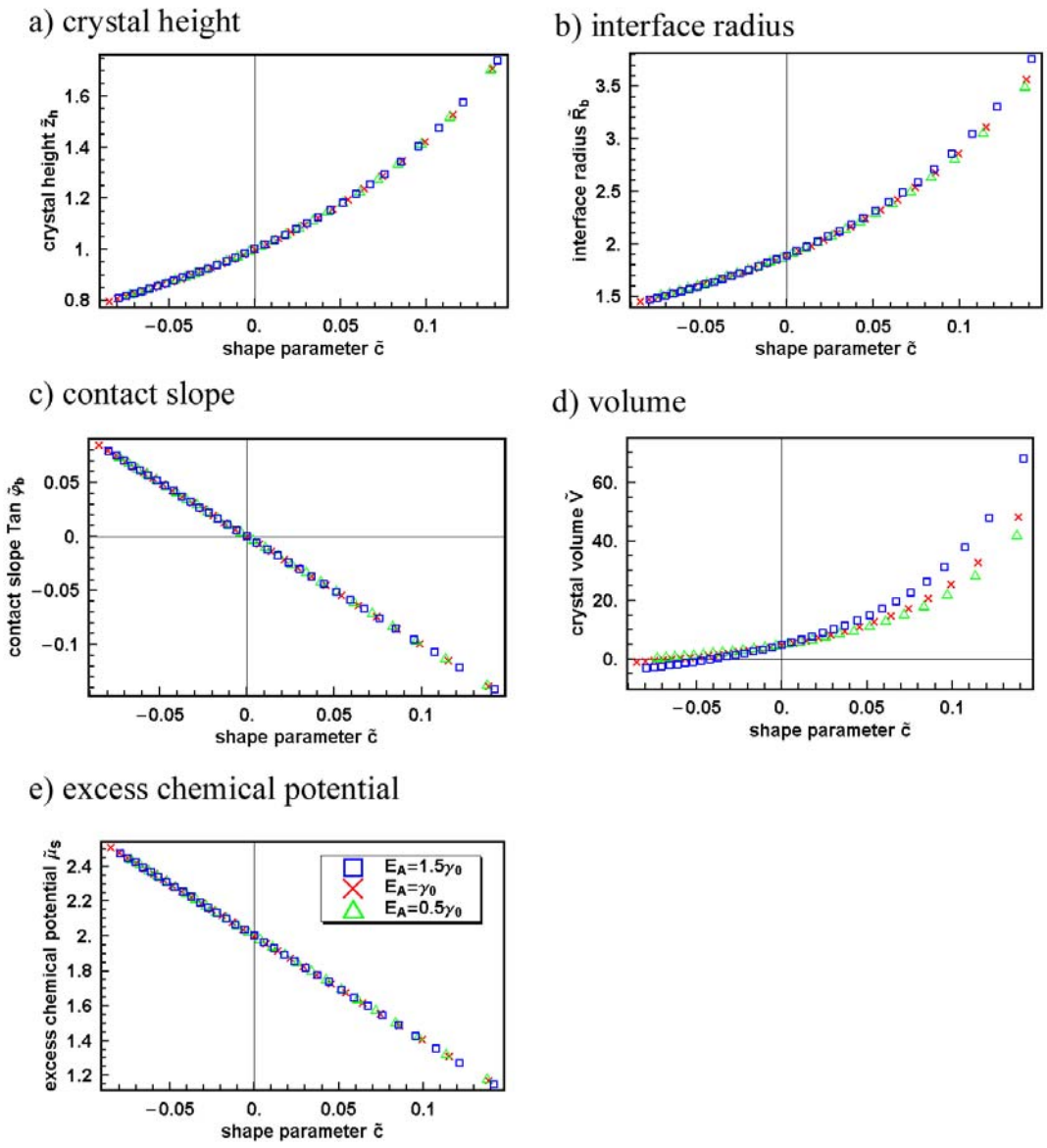

Figure 2-4 a) scaled crystallite height $\tilde{z}_h$, b) scaled interface radius $\tilde{R}_b$, c) contact slope tan $\tilde{\varphi}_b$ d) scaled crystallite volume and e) scaled excess chemical potential $\tilde{\mu}_S$ are shown as a function of scaled $\tilde{c}$ with constant volume. Size and adhesion energy (temperature) scaling is given as eq. (A-3) and (A-6) and results in eq. (A-5). The precise values of the universal scaled values at c=0 are given in Table 1.

2.3.3 Equilibrium shape and Metastable shape

Given the solutions above, we are now in a position to determine which value of c yields the minimum free energy for any value of the adhesion energy and thus the ECS. We begin with the crystallite free energy eq. (2-3)

$$F_S(c,V) = 2\pi \int_0^{Rb} f(r,c,\mu_S(c,V))rdr + \pi(\gamma_0 - E_A)R_b^2 + const.$$

$$= \pi\gamma_0\rho_c^2(c,\mu_S(c,V))$$
$$+ 2\pi \int_{\rho c}^{Rb} \left(\gamma_0 + \frac{\beta}{h}\sqrt{\frac{\mu_S(c,V)r - 2\beta\Omega}{6gv}} + \frac{c}{r} + g\left(\frac{\mu_S(c,V)r - 2\beta\Omega}{6gv} + \frac{c}{r}\right)^{3/2} \right) rdr$$
$$+ \pi(\gamma_0 - E_A)R_b^2 + const. \qquad (2\text{-}18)$$

Figure 2-5 a) gives the surface free energy (the first two terms in eq. (2-18)) as a function of c up to c_{max} with constant V for the free standing boundary condition ($E_A=\gamma_0$). The thermodynamic parameters where calculated using parameters for Pb at 27 ˚C, γ_0=1.7 eV/nm[272], β=0.34 eV/nm and g=0.65 eV/nm^2 [57, 58]. The value c=0 clearly gives the absolute minimum of the surface free energy and thus also of the total crystallite free energy, thus yielding the ECS. The solutions with $c\neq0$ are not absolute minima in the free energy, and thus since they have a constant surface chemical potential, they may represent meta-stable physical configurations.

Finally, let us consider the physically significant case of a heterogeneous crystallite-substrate system ($E_A\neq\gamma_0$) with $c\neq0$. Combining eqs. (2-8) and (2-13), the boundary condition is now

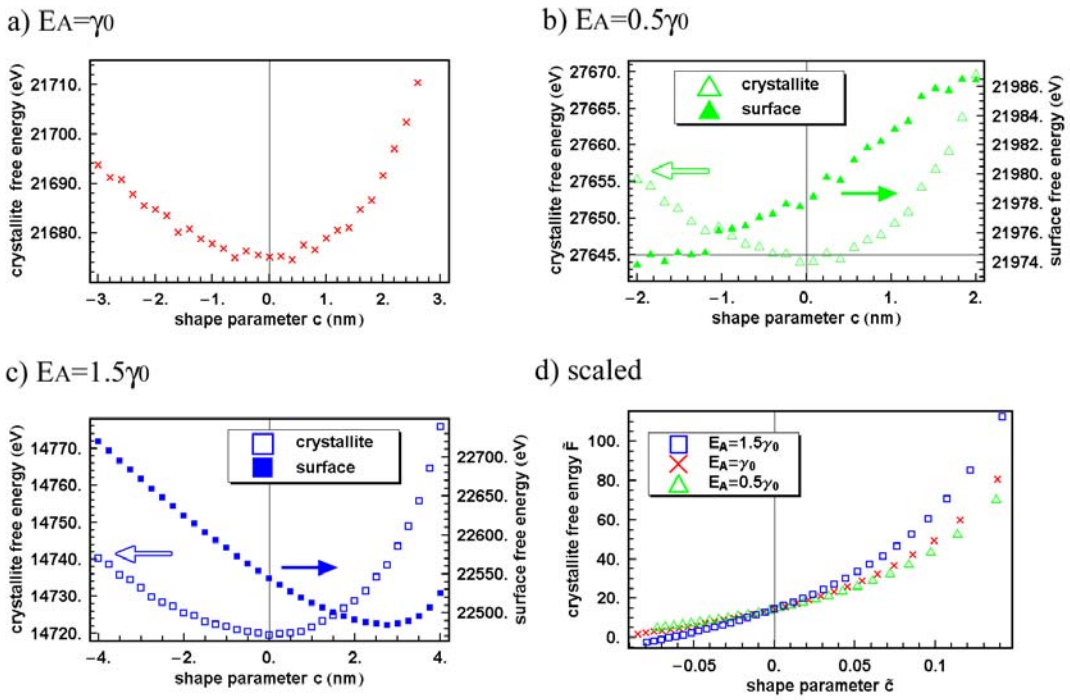

Figure 2-5 gives the crystallite free energy as a function of c up to c_{max} with same volume for a) the "free standing boundary" condition ($E_A=\gamma_0$) Thermodynamic parameters γ_0=1.7 eV/nm[272], β=0.34 eV/nm and g=0.65 eV/nm^2 [57, 58] where used for Pb at 27 ˚C. b) with adhesion energy $E_A=0.5\gamma_0$ (open) and c) with $E_A=1.5\gamma_0$ (open), respectively. The surface free energy alone (filled) is also given as closed symbols in b) and c). d) gives the scaled total surface free energy $\tilde{F}$ as a function of $\tilde{c}$ up to 1/6. Size and adhesion energy scaling is given as eq. (A-6)

$$\frac{\mu_S(c,E_A,V)}{2v}=\frac{\beta\rho_c\Omega-3cgv}{v\rho_c^2}=\frac{2\gamma_0-E_A}{z_h} \tag{2-19}$$

As a result, the excess chemical potential is now a function of the shape parameter, the adhesion energy and volume. In this case the surface and total free energies do not have the same c dependence. Here we consider first the surface free energy then the total crystallite free energy (e.g. including the interface terms). Filled triangles and squares in Figure 2-5 b) and c) give the surface free energy as a function of the shape parameter for the same volume crystallites but for different adhesion energies E_A=0.5γ_0 and E_A=1.5γ_0, respectively. Clearly, the minimum of the surface free energy shifts from zero with different shape parameters. For stronger adhesion, E_A=1.5γ_0, the minimum occurs at larger c, e.g. closer to the critical state, and for weaker adhesion, E_A=0.5γ_0, the shift is in the c<0 direction. The larger the adhesion energy, the greater the tendency toward a larger interface area, resulting in a flatter crystallite when the volume is fixed. This flattening gives smaller contact slopes at the interface (see eq.(14) for c=0), which results in a shift of the minimum of the surface free energy in the $c_{\max}$ direction. Similarly, when the adhesion energy is small, the interface area is small and the contact slope is large, which then shifts the minimum of the surface free energy in the c<0 direction. However, when adding on the interface energy to obtain the total crystallite free energy the minimum of the crystallite free energy is shifted back to c=0 independent of the adhesion energy. This is shown in Figure 2-5 b) and c) as open triangles and squares. Thus, when the total crystallite excess free energy is considered, the PT-ECS always stands independent of the adhesion energy. Notice that the crystallite free energy is the

smallest when the adhesion energy is largest, as expected, however this is not the case when considering only the surface free energy. This indicates that for calculating the properties of nano-size crystallites you must minimize the total crystallite excess free energy including the interface and not only the surface free energy. The specific free energy curves of Figure 2-5 b) and c) can be generalized by using the scaled (eqs. (A-3) and (A-6)) parameters as shown in Figure 2-5 d). All the curves collapse to one point at c=0. This result shows that we can relatively calculate the ECS using eqs. (A-1) and (A-2). Thus predicting variations in shape, due to e.g. changes in adhesion energy, can be done simply and relatively.

If we are interested in the possible metastable state represented by $c \neq 0$, then the use of the scaling forms of eqs. (A-3) is necessary, along with the function relationships of eqs. (A-4) and (A-5), which are represented in Figure 2-3, Figure 2-4 and Figure 2-5. Given, for instance experimental information as crystal height and facet radius, graphical prediction of Figure 2-4, (or the values in Table 2-1) all the other scaled parameters can be determined. Analytical solutions (eqs. (A-5)) yield excellent scaling results for crystal height, contact slope and excess chemical potential (Figure 2-4 a), c) and e)). The interface radius, the volume and total free energy have not yielded robust scaling relationships (Figure 2-4 b), d) and Figure 2-5 d)) and thus must be calculated individually if quantitative values are desired.

2.3.4 Application to Experiment

The consequence of the potential meta-stable states can be evaluated by comparison of the predicted crystal shape profiles with experimentally measured

Table 2-1 Table of values calculated from the analytical solutions (eqs. (A-5)) for different $\tilde{c}$, also given graphically in Fig. 4 and 7.

$\tilde{c}$	$\tilde{z}_h$	$\tan \tilde{\varphi}_b$	$\tilde{\mu}_S$	$\Delta\tilde{E}$
-0.08	0.806	0.08	2.48	2.77
-0.04	0.893	0.04	2.24	2.16
0	1	0	2	1.57
0.04	1.14	-0.04	1.76	1.03
0.08	1.32	-0.08	1.52	0.559
0.12	1.56	-0.12	1.28	0.192
0.16	1.92	-0.16	1.04	0.00483

results. Figure 2-6 shows a log-log plot of a 3 parameter fit (z_h, ρ, β/g) of eq. (2-10) (the ECS) and eq.(2-17) (the metastable state at c_{max}) to a cross section of a defect-free Pb crystallite measured with an STM at ~ 27 ˚C [14]. The solid line is the fit to a PT-shape and the dashed line to the shape where $c=c_{max}$. Both shapes visually fit the crystal shape well. However, the ratios of the interaction coefficient to the step free energy g/β obtained from the fits are very different, g/β=17.2 nm^{-1} for the PT-ECS and g/β=3.6 nm^{-1} for the critical state fit. This presents an interesting comparison with experiments by Nowicki et al. [58], where they have used fits to a PT-ECS and obtained the ratio of g/β=4.96 nm^{-1} for an equilibrated crystallite and g/β=13.11 nm^{-1}for a non-equilibrated crystallite at similar temperatures. (In their experiment they characterize crystallites that have screw dislocations on the facet as equilibrated as these structures can rearrange without the need to overcome a nucleation barrier [14, 64, 65].) Since the crystallite fit in Figure 2-6 did not have such a dislocation, we can speculate that the PT-ECS fit in this case and in Nowicki's non-equilibrated case both yield a spuriously high value of g, as previously predicted by Thürmer [14], because the crystallites are trapped in meta-stable ($c \neq 0$) states. The fit to the parabolic state seems to correct properly for the possible meta-stable structure as it yields a value of g/β consistent with these measured for crystallites that have relaxed via motion of screw dislocation.

2.4 Discussion

The use of the physically-based functional form of eq. (2-3) for the orientation dependence of the surface free energy yields a ready formalism for evaluating the

behavior of nanoscale crystallites supported on substrates of varying interaction strength. The use of the scaling formulas developed in the Appendix makes the results easy to extend to variable material systems. As already noted by Muller and Kern [41], increasing binding energy yields more severely truncated crystal shapes. Here we explicitly show also how the shape at the facet edge will respond to such substrate interactions: specifically the shift in the surface free energy minimum (shown in Figure 2-5 b) and c)) due to the presence of the interface. This would seem to indicate the break down of the Wulff theorem, however, when the interface energy is added to obtain the total crystallite free energy, the minimum of the total free energy is shifted back to c=0, the PT-ECS. This is physically reasonable, for large adhesion energy a large interface area is desired leading to a shift in the negative direction and for small vice versa. Thus we obtain an interesting result that the Wulff theorem gives the minimum of the total free energy even for finite crystallites and also with interfaces. The interesting effect of substrate interactions on the edge shapes are a direct consequence of the finite size effect, e.g. the new behavior that results from explicitly considering the shape of the crystallite that becomes important at small volumes.

Explicitly considering the effects of the curvature yields a family of crystal shapes that all have constant surface chemical potentials, only one of which represents an absolute minimum in the total surface free energy. The others, because they will have no strong driving force for rearrangement by mass transport, are likely to represent meta-stable states. This conclusion gives interesting results, such as on

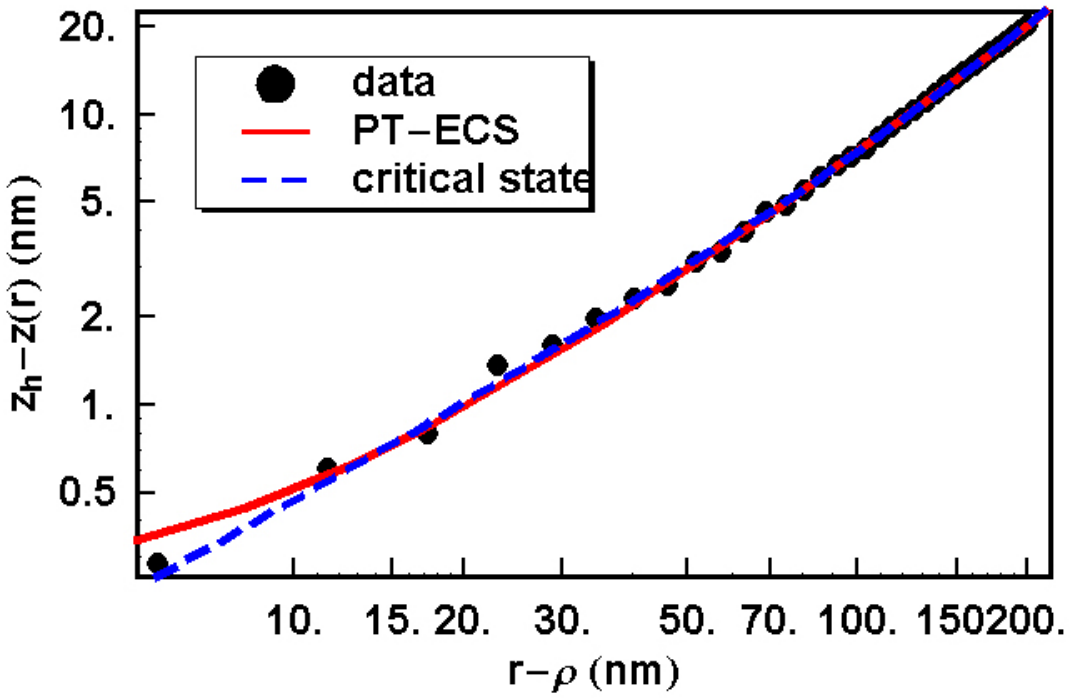

Figure 2-6 A log-log plot of a 3 parameter fits to the PT-shape eq. (2-10) and the critical state shape eq. (2-16) to the measured cross section of the defect-free Pb crystallite, taken with an STM at ~ 300K. The fits yield ratios of g/β=17.2 nm^{-1} and g/β=3.6 nm^{-1}, respectively.

the vapor-solid coexistence curve: though the vapor (and bulk) chemical potentials may be fixed, stable crystallites with different numbers of atoms (volume) will still be possible due to the difference in shape parameter, although only one of the shapes (volume) is the ECS.

The possibility of meta-stable crystal shapes, trapped by barriers to rearrangement has been proposed by Rohrer and Mullins [64, 65]. The barriers to shape evolution ΔE can be estimated by the method they proposed [9, 64, 65] considering only formation of steps

$$\Delta E(r) = 2\pi\beta(r - \rho_c) + \frac{\pi\mu_S(V)(\rho_c^2 - r^2)}{\Omega} \tag{2-20}$$

The critical radius is $r^*=\beta\Omega/\mu_b$ and with eq.(8) the barrier height is

$$\Delta E(r_C) = \frac{\pi(\beta\rho_c\Omega - 6cgv)^2}{2\Omega(\beta\rho_c\Omega - 3cgv)} \tag{2-21}$$

Figure 2-7 shows the scaled barrier height $\Delta\tilde{E}$ as a function of $\tilde{c}$ (eq. (A-3) and (A-5)) for different adhesion energies. It can be seen that the barrier disappears at $\tilde{c}_{\max}$ =1/6, in agreement with Uwaha's identification of this point as a "critical state"[16]. The barrier can be understood in more detail by working in the continuum step model where the concept of steps is included. This will be presented elsewhere [71].

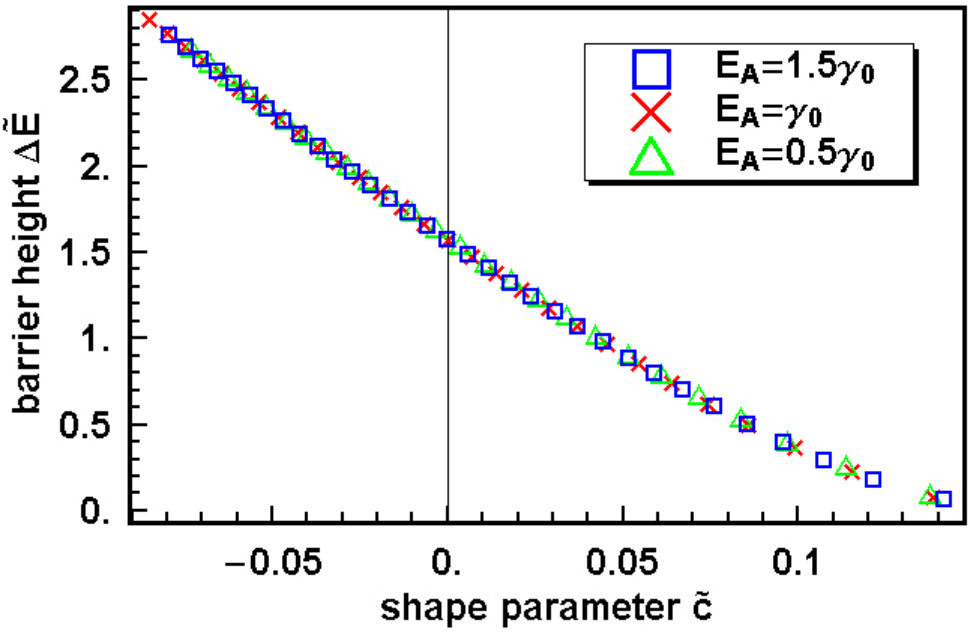

Figure 2-7 Scaled barrier height $\Delta\tilde{E}$ as a function of $\tilde{c}$ with constant volume and different adhesion energies (E_A=0.5γ_0, γ_0, 1.5γ_0) using the method by Rohrer and Mullins [64, 65]. Size scaling is given by eq. (A-3) and results in eq. (A-5)

Chapter 3: Barriers to shape evolution of supported nano-crystallites

Continuum solutions for supported crystallite shapes are combined with the continuum step model to yield a quantitative description of the physically-allowed metastable states, including the dependence on interfacial adhesion energy. Using a model of layer-by-layer shape evolution, the activation barriers for transitions between metastable states are calculated. The results collapse to a universal scaled form and for which the barrier height decreases (increases) for metastable states taller (shorter) than the equilibrium structure. Following Rohrer and Mullins [64, 65], we evaluate the smallest crystal volume where the energy barrier is less than $10k_BT$ as a function of the metastable state and interfacial energy. The results yield a family of curves showing the lowest energy accessible structure as a function of the dimensionless volume for different adhesions energies. Increasing adhesion energy correlates with increasing activation barriers at the same volume. Using realistic parameters for Pb, the equilibrium structure can only be reached by peeling for volumes $\leq$ 50 nm^3, and crystals of volume $\geq 10^6$ nm^3 will be trapped in the least favorable metastable state.

3.1 Introduction

Supported crystallites have been of great importance from the classical problems of catalysis [73, 74] to the recent studies of quantum dots [6, 37, 75, 76]. In both cases the properties, catalytic, electronic or luminescent, depend strongly on the crystallite size. As the size shrinks to the order of nanometers, the shape becomes an important factor as well [2, 5]. Shapes of supported crystallites are strongly affected by external perturbations such as adhesion energy and stress caused by the substrate interface [43, 77] and shapes can include unstable and metastable states of the crystallite. Crystallites trapped in metastable states and their shape evolution are observed experimentally [78, 79].

Where the desired properties of nanocrystals are closely tied to their shapes, shape evolution following fabrication or in response to environmental factors will be of concern (or possibly of interest). At size scales of 10^3 nm^3 or below, both the effects of curvature and the discrete nature of crystalline layers will play an important role in shape evolution [40, 64, 65, 68]. These factors can be addressed quantitatively by combining the continuum step model with thermodynamic predictions for the crystal shape [10, 11, 18].

A question of particular focus will be the possibility of activation barriers that may trap a structure in a non-equilibrium state [9, 64-66]. Such barriers cannot of course be predicted thermodynamically, but must be based on models for the transition states. For a small crystallite (see Figure 3-1) undergoing transformation toward a form with larger facets, a common mechanism is layer peeling [67, 68]. Rohrer and Mullins [64, 65]

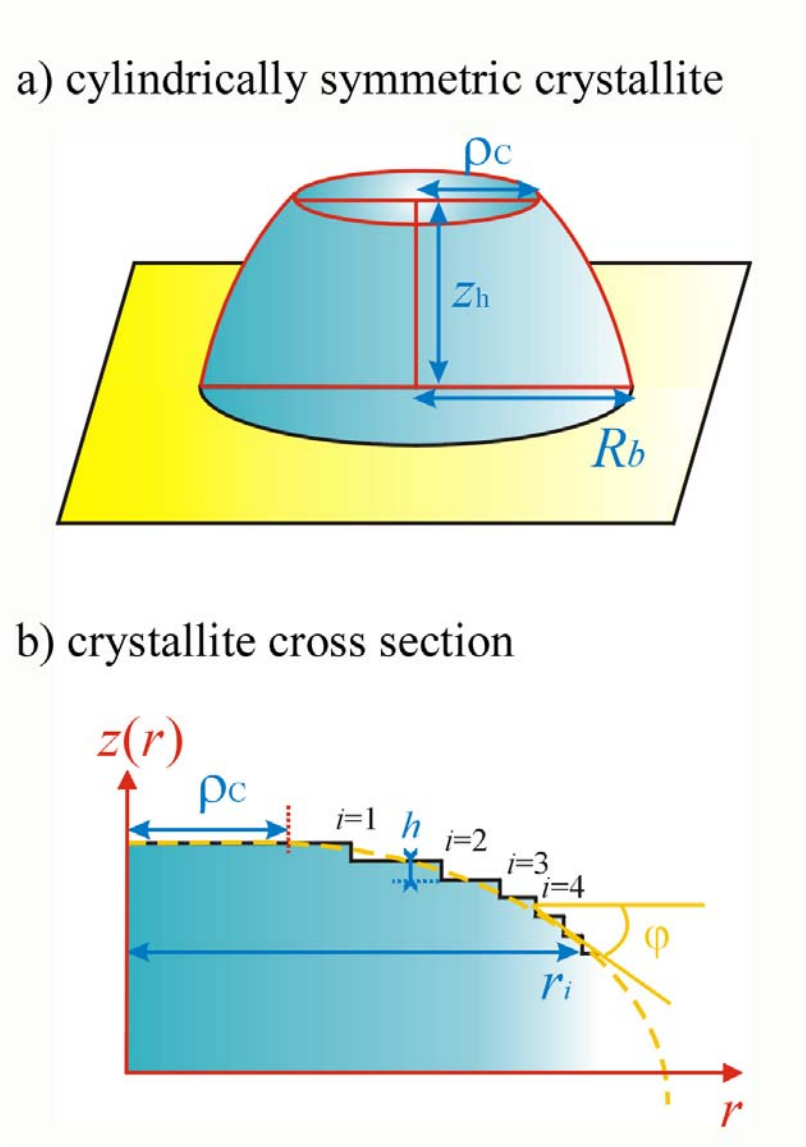

Figure 3-1 a) Schematic drawing of a cylindrically symmetric finite volume crystallite in the continuum model. A single flat facet is bounded by rounded regions that terminate at the substrate. Here the crystal height obeys the Wulff-Kaishew theorem [41]. b) Schematic drawing of a cross section of a crystallite in both the continuum model (dashed line) and continuum step model. i denotes the layer number and r_i is the radius of that layer. Notice that the radius of the top layer ρ_c in the continuum step model is not identical to the facet radius in the continuum model.

have shown that near equilibrium, removal of a layer involves a substantial activation barrier as the increasing Gibbs-Thompson free energy of the shrinking top layer competes with the decrease in free energy for material transferred to the more stable crystal configuration. They estimate that only for crystals with a radius smaller than ~100nm will the activation barrier be small enough (< $40k_BT$) to be overcome thermally. Here we will show how these results can be quantified in terms of measurable continuum step parameters and the nature of the interfacial adhesion energy between the crystallite and supporting substrate. The size dependence will be illustrated for the specific case of Pb crystals.

3.2 Background

In a previous paper [80] we defined the shapes of constant surface chemical potential for cylindrically symmetric crystallites, specifically including the finite size (curvature) effects of the crystallites and the effects of interfacial energy for supported crystallites. For these calculations we used the Pokrovsky-Talapov surface free energy density [15] in the radial direction of the cylindrically symmetric crystallite as in Figure 3-1 b).

$$f(\varphi) = \gamma_0 + \frac{\beta}{h}\tan\varphi + g\tan^3\varphi\,, \qquad (3\text{-}1)$$

where φ is the angle of the surface relative to the low-index terrace, h is the step height, β and g are the thermodynamic step free energy and step-step interaction coefficient, respectivel; γ_0 is the surface tension of the low-index terrace. The results gave a family of shapes (height vs. radius as in Figure 3-1 a)):

$$\frac{dz(r)}{dr} = \sqrt{\frac{\mu_s(V)r - 2\beta\Omega}{6g\nu} + \frac{c}{r}} \qquad (3\text{-}2a)$$

of constant chemical potential

$$\mu_S(V) = \frac{2(\beta\rho_c\Omega - 3cg\nu)}{\rho_c^2} = \frac{2(2\gamma_0 - E_A)\nu}{z_h}, \qquad (3\text{-}2b)$$

where ρ_c is the facet radius, z_h is the crystallite height, E_A is the adhesion energy and Ω and ν are the atomic area and volume, respectively. Specific forms for $\mu_S(V)$ in terms of the material parameters (β etc.) are given in eqs. (2-12) to (2-15) of the previous chapter, with the results needed to determine the values of the facet radius and crystal height summarized in Appendix C. The key result is that the family of crystal shapes is governed by a shape parameter *c,* of which only one value (c=0) gives the equilibrium crystal shape (ECS). The $c\neq0$ shapes all correspond to metastable states, which are local minima of the total crystallite free energy. There also exists a maximum value of the shape parameter *c* for a stable facet to exist, the c_{max} state as previously described by Uwaha [16].

Experimental observations [40, 68] show that a common mechanism of transformation is layer peeling, so it is appropriate to consider a model with the steps (layers) as fundamental building blocks, which naturally leads us to the continuum step model. The continuum step model, illustrated in Figure 3-1 b) allows a physical description of layer peeling that is consistent with the envelope of solutions predicted by the continuum model illustrated in Figure 3-1 a). The step chemical potential is obtained as

$$\mu_i(r_{i-1}, r_i, r_{i+1}) = \frac{\Omega}{r_i}\left(\frac{\partial\left[\left(r_i^2 - r_{i-1}^2\right)f(l_i)\right]}{\partial r_i} + \frac{\partial\left[\left(r_{i+1}^2 - r_i^2\right)f(l_{i+1})\right]}{\partial r_i}\right). \qquad (3\text{-}3)$$

With the Pokrovsky-Talapov surface free energy density, eq. (3-1), rewritten in terms of the terrace width

$$f(l_i) = \gamma_0 + \frac{\beta}{l_i} + g\frac{h^3}{l_i^3}, \tag{3-4}$$

where r_i is the radius of the ith step as shown in Figure 3-1 b) and $l_i = r_i - r_{i-1}$ is the spacing between the ith and (i+1)th steps. Eqs. (3-3) and (3-4) yield

$$\mu_i(r_{i-1}, r_i, r_{i+1}) = \Omega\left(\frac{\beta}{r_i} + \frac{gh^3}{2r_i}\left(\frac{1}{l_i^2} + \frac{1}{l_{i+1}^2}\right) - \frac{gh^3}{r_i}\left(\frac{r_{i-1}+r_i}{l_i^3} - \frac{r_i + r_{i+1}}{l_{i+1}^3}\right)\right) \tag{3-5a}$$

$$= \Omega\left(\frac{\beta}{r_i} - \frac{gh^3}{2r_i}\left(\frac{3r_{i-1}+r_i}{l_i^3} - \frac{r_i + 3r_{i+1}}{l_{i+1}^3}\right)\right). \tag{3-5b}$$

The first term in eq. (3-5a) is the 2D Gibbs-Thomson term, the second is the step-step interaction term due to the difference in circumference length of the layers and the last term is the step-step interaction term also obtained in the thermodynamic limit. This expression is quantitatively consistent with the results of the continuum model [80].

3.3 Results

In the following sections we will review the description of the crystal shape in the context of discrete steps, then present a simple model for predicting the energy barrier for peeling. We will then show how the barrier can be derived for supported crystallites of arbitrary interface energy. Finally, we will follow the approach of Rohrer and Mullins [64, 65] in evaluating the crystal-size dependence of the activation barrier for layer peeling in crystallite reshaping.

3.3.1 Crystallites with discrete step heights

Here we construct a crystallite starting from the solutions obtained in the continuum model using the shape parameter c. Combining the discrete height of the step with the continuum model shape parameter limits the metastable states to ones that are only physical structures. The radius of the layers can be written down by taking discrete points along the crystallite shape (See Figure 3-1), chosen at equal intervals of the step height h in the z direction, e.g. for the PT-ECS (c=0) and $c_{\max}$ states this yields

$$c\text{=}0\text{:}\quad r_i = \rho_0 + \left(\frac{27gh^3\rho_0(i-1/2)^2}{4\beta}\right)^{1/3} \qquad : i\text{=}1,2,\cdots, n_0 = \frac{(2\gamma_0 - E_A)\rho_0}{\beta}$$

$$c_{\max}\text{:}\quad r_i \cong \rho_{c\max} + \left(\frac{24gh^3\rho_{c\max}^2(i-1/2)^2}{\beta}\right)^{1/4}$$

$$: i\text{=}1,2,\cdots, n_{c\max} = \frac{2(2\gamma_0 - E_A)\rho_{c\max}}{\beta}. \qquad (3\text{-}6)$$

The equations given for the number of layers n_c (crystallite height) are defined by the Wulff-Kaishew theorem [41, 81]. (see Figure 3-1 a)) Note that the position of the first step is not identical to the facet radius in the continuum model (see Figure 3-1 b)). Figure 3-2 a) shows the scaled cross section (details of the scaling given in Appendix B) of the PT-ECS and the $c_{\max}$ state with the discrete positions of the steps. The difference between the quadratic and $\sim x^{3/2}$ shape profiles of the $c_{\max}$ state and PT-ECS is clearly evident. The cross sectional shape of the crystallite is independent of volume because of the scaling, however, the number of points along the cross section does depend on size, in that it is defined by the numbers of layers.

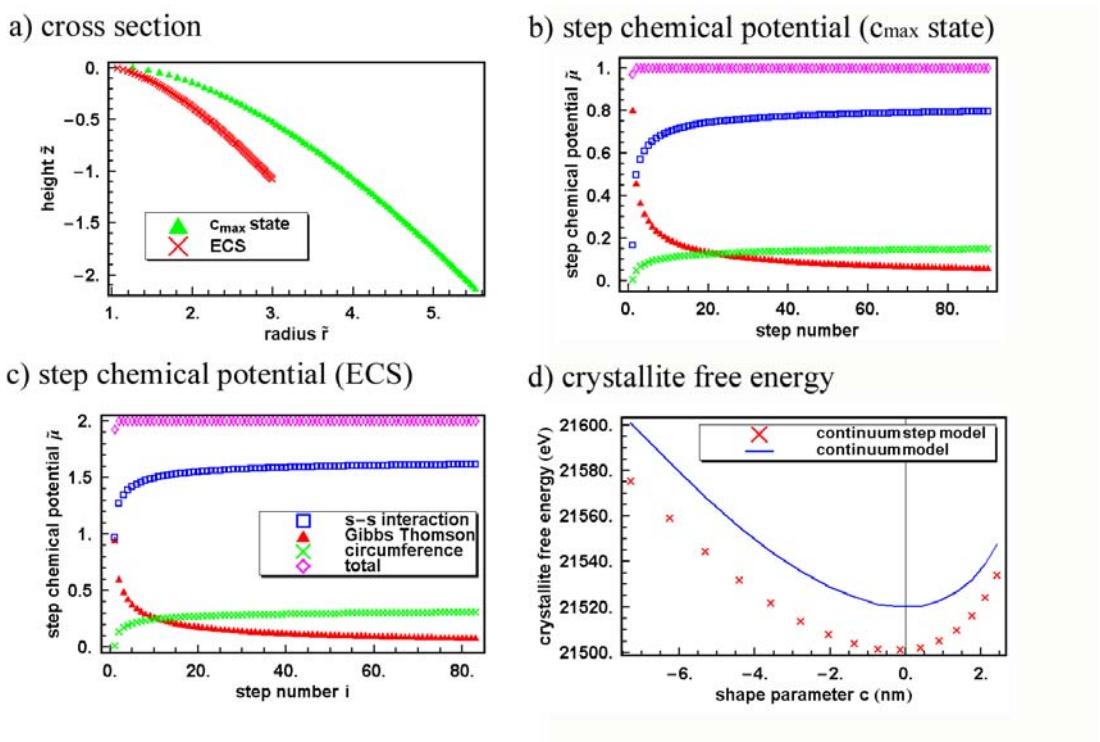

Figure 3-2 a) shows the scaled cross section of the ECS and the c_{max} state calculated for a crystal with same volume. b), c) are the scaled step chemical potentials for the c_{max} state and the ECS, respectively, as a function of step number. Triangles show the 2D Gibbs-Thomson term, crosses show the circumference interaction term, squares show the thermodynamic step interaction term and the diamonds show the total step chemical potential, respectively. The size scaling is done as in eq. (B-1) and (B-2). d) gives the total crystallite free energy of a Pb crystallite of volume 10^5 nm^3 calculated in the continuum and continuum step model [80]. The minimum of the total crystallite free energy is close to c=0 although this state does not exist for shapes consisting of layers of discrete separation. The shape parameter that gives the minimum shifts depending on where the position of the top layer is chosen along the continuous shape profile.

Inserting eqs. (3-6) into eq. (3-5) yields the contribution of each term to the total step chemical potential for each layer. Scaled results for the PT-ECS and the c_{max} state for which $\tilde{\mu}$=1 and $\tilde{\mu}$=2, respectively, are given in Figure 3-2 b), c) as a function of layer number. Closer to the facet edge or equivalently for smaller crystallites (fewer layers), the contribution from the Gibbs-Thomson term becomes stronger and the step-step interactions become weaker. However, the total step chemical potential stays a constant for all layers. The deviation of the total step chemical potential seen at the facet edge, results from breakdown of the continuum model when the step density varies rapidly, and becomes important when the crystallite size becomes smaller. However, the shape parameter does give a very good approximated solution of the stable crystallite shape, though not exact. Thus eq. (3-2b) can be used as the "reservoir" chemical potential to solve eq. (3-6) for the individual layers.

Finally, by numerically solving eq. (3-2a) to obtain the equivalent of eqs. (3-6) for all metastable ($c\neq0$) shapes, the surface crystallite free energy as a function of the shape parameter c can be obtained, as shown in Figure 3-2 d). The parameters used in the calculations are for Pb at 27˚C, $\gamma_0=E_A$=1.7 eV/nm[272], β=0.34 eV/nm and g=0.65 eV/nm^2 [57, 58] with volume $V=10^5$ nm^3. The discrete points of the shape parameter are a real effect due to the discrete height of the steps. For comparison the total crystallite free energy calculated in the continuum model eq. (3-3) in ref. [80] is also given in Figure 3-2 d). Qualitatively, they have similar behavior, however,

quantitatively they differ by about 20 eV (0.1%). This again is due to the fact that the continuum model solutions are an approximation to the continuum step model.

3.3.2 Metastable states and barriers

The discrete shape parameter values of Figure 3-2 d) represent local minima in the total free energy. We will use these states as starting and ending points for the "layer peeling" model of evolution of the crystallites. A full calculation of the barrier would require relaxation of the whole crystallite, e.g. all the layers. However, qualitative understanding can be obtained by fixing most layers.

As a first approximation, one can fix all layers but the top one, ignoring completely mass conservation. We also assume that the layer undergoes a uniform circular fluctuation, the so-called "breathing mode" [82] although it is well possible that other modes have a lower energy path. Under these conditions, the relative energy required to shrink the top layer from its stable facet radius ρ_c to an arbitrary radius r can be calculated by

$$\mu_1(r_1) = \Omega\left(\frac{\beta}{r_1} + \frac{gh^3(r_1 + 3r_{20})}{2r_1(r_{20} - r_1)^3}\right) \tag{3-7a}$$

$$\Delta E(r) = \frac{2\pi}{\Omega}\int_{\rho_c}^{r}\{\mu_1(r_1) - \mu_S(V)\}r_1 dr_1 . \tag{3-7b}$$

The step chemical potential of the top layer is obtained from eq. (3-5) with the fixed radius of the second layer r_{20}. Fixing the positions of all layers is equivalent to setting the second layer step chemical potential equal to the chemical potential of the metastable state, which defines a "reservoir" as mentioned in Sec. 3.1. The scaled

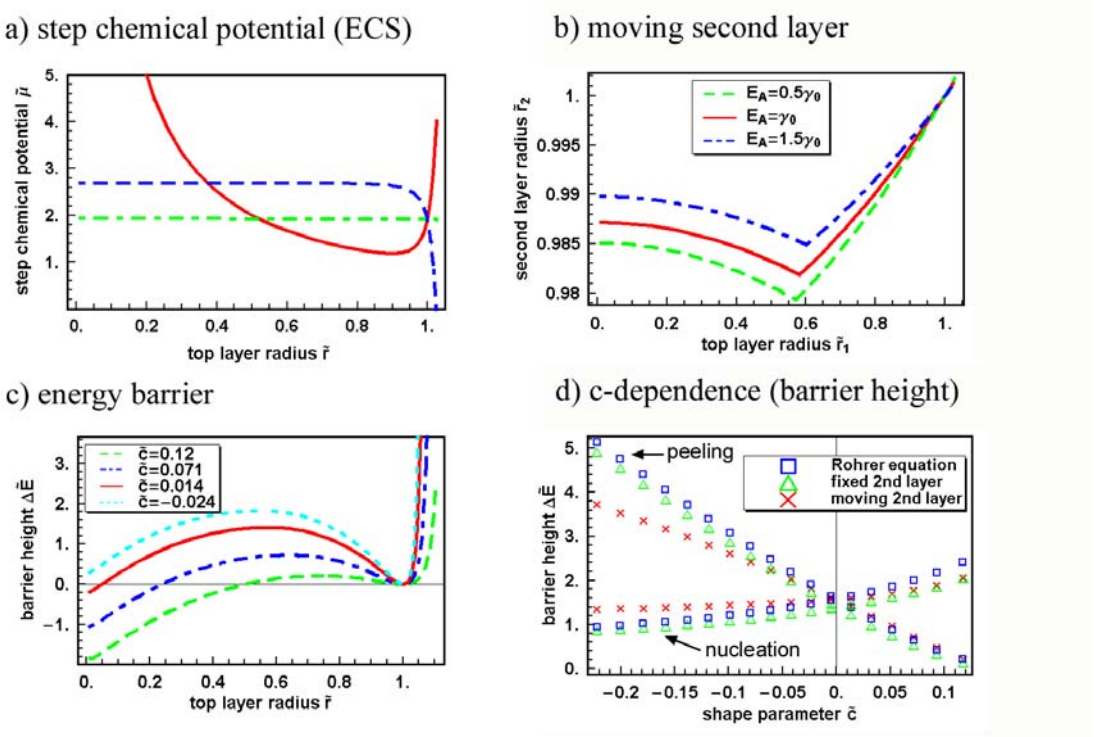

Figure 3-3 a) shows the scaled step chemical potential of the top (solid) and second layer (dashed) and the reservoir (dot-dashed) chemical potential as the function of the radius of the top layer r_1 for the ECS (c=0), assuming that the second layer radius is fixed. b) shows the motion of the variable second layer relative to the top layer as it shrinks, each radius scaled by its initial value. Solid line corresponding to $E_A = \gamma_0$, dash-dot line to $E_A = 1.5\gamma_0$ and dashed line to $E_A = 0.5\gamma_0$. c) shows the scaled barriers as a function of $\tilde{r}$ for various $\tilde{c}$ calculated by eq. (9) for $E_A = \gamma_0$. d) shows the scaled barrier height as a function of the shape parameter for both peeling and nucleation. Triangles calculated by eq. (7b), crosses calculated by eq. (9), which collapse for all the interfacial energies and squares obtained by Rohrer's equation [64, 65], respectively. Size scaling is given as eq. (A-1) and (A-2).

step chemical potential, eq. (3-7a), of the top layer and the reservoir chemical potential are shown in Figure 3-3 a) as a function of the top layer radius r_1 for the closest state to the $\tilde{c}$=0. (Scaling given in Appendix B.) The change in the reservoir chemical potential from the initial to the final metastable state is approximated as a linear function in r_1. As the top layer shrinks, its step chemical potential initially becomes smaller than the reservoir surface chemical potential and as a result there is a net tendency for it to gather mass and grow back to its stable facet radius. This is the origin of the "transition" energy barrier to structural reorganization.

The approximation above misses some significant physical aspects of the layer peeling, specifically mass conservation, which communicates the influence of the substrate interaction. When the first layer begins shrinking, the chemical potential of the second layer increases (also shown in Figure 3-3 a)) and so (if allowed to move) the second layer will shrink, transferring mass to both the first and lower layers. As the radius of the first layer deceases, its chemical potential increases and eventually surpasses that of the second layer. We will label the radius at which this occurs $\rho_{crossover}$. At this point mass transfer to the second layer is favorable and the second layer radius will increase. This crossover from shrinking and increasing of the second layer is confirmed in numerical simulations and experimental observations [68, 83]. The magnitude of the variations in the radius of the second layer r_2 is small, and we define an empirical form to describe this behavior:

$$r_2(r_1) = \sqrt{r_{20}^2 - A(\rho_c - r_1)^2} \qquad \rho_c > r_1 > \rho_{crossover}$$

$$r_2(r_1) = \sqrt{r_{2crossover}^2 + A(\rho_{crossover} - r_1)^2} \qquad \rho_{crossover} > r_1 > 0. \qquad (3\text{-}8)$$

The parameter A is the ratio between the net rate of attachment (or detachment) at the second layer, and the rate at the first layer. We determined the values of A and $\rho_{crossover}$ for different adhesion energies self consistently by calculating the energy barrier using eqs. (3-5) and (3-8) in the more complete form of eq. (3-7b):

$$\Delta E(r) = \frac{2\pi}{\Omega}\left(\int_{\rho c}^{r} \{\mu_1(r_1, r_2) - \mu_2(r_1, r_2)\} r_1 dr_1 + \int_{r20}^{r_2(r)} \{\mu_2(r_1, r_2) - \mu_S(V)\} r_2 dr_2 \right), \quad (3\text{-}9)$$

where the position of the third layer r_{30} is assumed fixed. The requirement that the energy barriers for peeling and nucleation are identical at $\tilde{c}$=0 (the ECS) yields A=7.1% $\tilde{\rho}_{crossover}$=0.57 , A=6.25% $\tilde{\rho}_{crossover}$=0.58, A=5.3% $\tilde{\rho}_{crossover}$=0.6 for E_A=0.5γ_0, E_A=γ_0 and E_A=1.5γ_0, respectively. The resulting variations of r_2 with r_1 is shown in Figure 3-3 b) and the energy barrier, eq. (3-9), with r in c). The energy difference between the facet radius and peak position gives the peeling barrier and the difference from the origin (r≈0) gives the nucleation barrier. The decrease of the peeling barrier as $\tilde{c}$ approaches $\tilde{c}_{\max}$=1/6 is evident. Close to $\tilde{c}$=0, the barriers to peel and to nucleate are close to identical. The peeling barrier and nucleation barrier, indicated by arrows, are shown in Figure 3-3 d) as a function of the shape parameter. Scaling described in Appendix B causes the curves for all the interfacial energies to collapse, providing a universal set of values for estimating the energy barriers. For instance at equilibrium, from the values of $\Delta\tilde{E}$≈1.5, it is possible to evaluate the energy barrier for a given volume and adhesion energy using scaling relationships of eqs. (B-1) and the relationship between chemical potential and materials parameters given in eq. (3-2) along with the results for $\mu_S(V,E_{A,}\, c)$ from our previous report [80] which is summarized in Appendix C.

The results for the fixed 2nd layer radius and from Rohrer's equation [64, 65] are also included in Figure 3-3 d) for comparison with the variable layer approach. It is interesting to see that the results from Rohrer's equation are a better approximation than the fixed 2nd layer results. This is because the effects of including step-step interactions and adding more layers seems to cancel out.

3.3.3 Structure evolution

If a crystallite is fabricated in an initial non-equilibrium state, or if it undergoes a change in temperature or chemical environment, it will relax towards its equilibrium structure. For most starting structures that are taller than the equilibrium state, [83] the evolving structure will encounter the metastable structures beginning with $c=c_{\max}$. Evolution after that point requires surmounting energy barriers between each pair of metastable states. Here we evaluate quantitatively the size dependence of evolution through the metastable states.

To evaluate the final state we must estimate the size of the largest fluctuation compatible with a measurable rate of transition. Following Rohrer and Mullins [64, 65] we use a fixed multiple of the thermal energy, here of $10k_BT$, as the maximum barrier height that can be traversed at a reasonable rate due to thermal fluctuations. Given ΔE the barrier height, the corresponding shape parameter c of the final state can be determined by the universal curve of Figure 3-3 d). Then we can calculate the crystallite height (z_h or the number of layers n_c) using eq. (3-2b) and thus the volume as

$$V = \pi h \sum_{i=1}^{nc} r_c^2\left((i-1/2)h\right), \qquad : i=1,2,3,\cdots,n_c \qquad (3\text{-}11)$$

where $r_c(z)$ is the cross section of the crystallite in state c, obtained by numerical integration of eq. (3-2a). Scaled results of the final state shape parameter $\tilde{c}$ as a function of volume $\tilde{V}$ are given in Figure 3-4 for different adhesion energies. The dashed line is $\tilde{c}_{max}$=1/6, for which the activation energy for peeling is zero for all volumes. With decreasing crystallite volume the thermal energy is enough to surmount the activation barrier between c states, yielding values closer and closer to equilibrium. At larger crystallite volumes, the structure is trapped in a metastable state. Structures for which the final state is below $\tilde{c}$=0 also have the possibility to nucleate layers. Notice also that crystallites evolve more easily with smaller adhesion energy.

The number of layers that will be removed between the first metastable state (c=$c_{\max}$) and the final state depends on the crystal volume. Here we give an example for a Pb crystallite with step height 0.286 nm and theoretically and experimentally observed thermodynamic parameters at 300K of $\gamma_0(\approx E_A)$=1.7 eV/nm^2 [72], β=0.34 eV/nm [84] and g/β=3.6 nm^{-1} (g=1.224 eV/nm^2) [80]. We compare the initial ($c_{\max}$) state shape parameters with the ECS(c=0) and the thermally accessible final state structure in Table 3-1. The maximum number of layers that would peel absent an activation barrier can be determined from the difference in height of the $c_{\max}$ state and the ECS. Obviously, the absolute difference in height is strongly dependent on crystal volume, as shown in column 6 of Table 3-1. The crystal height of the actual final state accessible via thermal activation is close to the crystal height of the $c_{\max}$ state in all cases, as shown in the last column of Table 3-1. Only the smallest crystal sizes,

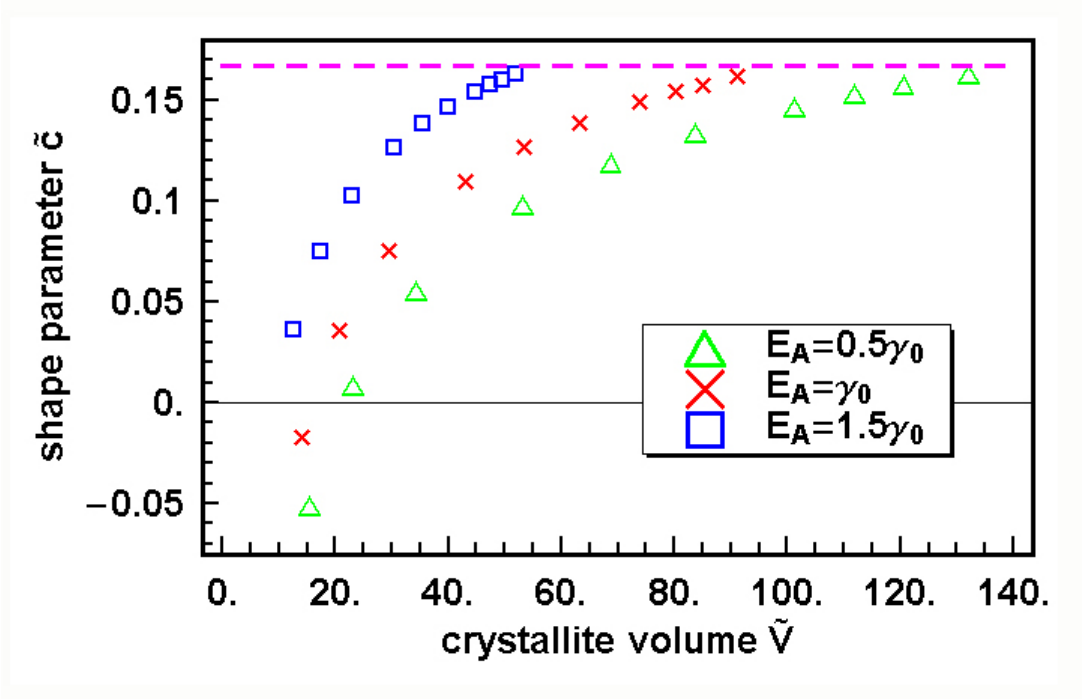

Figure 3-4 The scaled shape parameter $\tilde{c}$ corresponding to the metastable state accessible via peeling with an activation barrier no greater than 10 k_BT is shown as a function of scaled volume $\tilde{V}$ for different adhesion energies. Triangles, crosses and squares correspond to E_A=0.5γ_0, γ_0, 1.5 γ_0, respectively. The dashed line is $\tilde{c}_{max}$=1/6, the critical state where the activation barrier for peeling is zero. As a function of adhesion energy the equilibrium shape can only be attained for $\tilde{V}$ < 15 (E_A = 1.5 γ_0), $\tilde{V}$ < 20 (E_A = γ_0) and $\tilde{V}$ < 25 (E_A = 1.5 γ_0).

Table 3-1 Calculated crystallite height and facet radius for the initial state structure (c_{max} state), the equilibrium structure and the thermally accessible final state.

Volume	ρ_0	z_{h0}	ρ_{cmax}	z_{hcmax}	Δz_h (c_{max}-0)	ρ_f	z_{hf}	$\tilde{c}_f$	Δz_h (c_{max}-f)
30 nm^3	1.02 nm	1.46 nm	0.55 nm	1.58 nm	1	1.07 nm	1.43 nm	-.0254	1
220 nm^3	1.97 nm	2.83 nm	1.05 nm	3.01 nm	1	1.83 nm	2.86 nm	0.0275	1
1650 nm^3	5.52 nm	3.85 nm	2.06 nm	5.91 nm	2	3.17 nm	5.72 nm	0.0686	1
1.53×10^6 nm^3	37.5 nm	53.8 nm	20.0 nm	57.5	13	23.5 nm	57.2 nm	0.1367	1
189 μm^3	1.87 μm	2.68 μm	1.00 μm	2860.6 nm	667	1.03 μm	2860.0 nm	0.162	2

where the equilibrium state is within a layer spacing of the c_{max} state, achieve thermal equilibration.

3.4 Discussion

The evolution of an isolated crystallite due to surface diffusion can be separated into two regimes, one is deterministic evolution driven by gradients in the surface chemical potential, the other is a stochastic process where the crystallite is trapped in a metastable state and needs fluctuations to evolve to a lower energy state. The later evolution is the result of the built in *discreteness* of steps in the continuum step model as introduced here for the first time. Notice when the step height goes to $h \rightarrow 0$ (thermodynamic limit), there are no metastable states, $\tilde{\mu}=2$ (PT-ECS) and $\Delta\tilde{E}=\tilde{r}-\tilde{r}^2$ reducing to a well known nucleation theory of 2D islands [9], which however does not include a confining boundary and thus cannot address peeling. (Notice, however, that this formulism is still symmetric between $\tilde{r}=0$ and $\tilde{r}=1$ as pointed out in ref. [9]).

Another important fact is that, though the system is finite, the calculation of the barrier height is still done by using *thermodynamic* parameters and *thermodynamic* results. With increasing advances in computer speed, calculation of shape changing barriers of nano-crystallites from *ab initio* calculations and kinetic Mote Carlo are now possible [66]. It will be a great challenge to relate the two calculations and be able to extract thermodynamic parameters from microscopic properties, specially for the step-step interactions.

To obtain barriers from experiment, Figure 3-3 d) shows that the observation of the facet radius and cross section of the crystallite is sufficient to obtain the state. This is because the facet radius defines the amount of material that must be moved by

the fluctuations and the state defines the reservoir. Details of the crystallite volume or the interface boundary are not required, although partial information can be obtained from the motion of the second layer, as mentioned in Sec. 3.2. Similar results are obtained during the kinetic evolution presented elsewhere [83].

The crossover in size of the dominant evolution process from deterministic to stochastic is one of the main results in this work. However, there are some issues that must be addressed as the crystallite size gets smaller where the discreteness of the steps becomes more important. As the size decreases, the solution of the continuum model and continuum step model deviates and the shape parameter solution cannot be used to approximate the "reservoir" chemical potential. Even more critical, the concept of a "reservoir" itself breaks down as the crystallite gets smaller and motions of all layers up to the interface and interface boundary condition must be known to calculate the barrier. However, for such small enough system, more realistic models can be used and mass conserved Monte Carlo simulations can be performed to simulate the motion of all layers [70].

Chapter 4: Kinetic Parameters of Pb Obtained from Crystallite Evolution

Issues in modeling the evolution of supported crystallites are addressed by fitting scanning tunneling microscopy (STM) measurements of the evolution of Pb crystallites using the formalism of the continuum step model. Initial and final states used in the calculations are the least-stable metastable states for a cylindrically symmetrical crystallite with step-step repulsions varying as the inverse separation squared. The step-step interaction strength is determined from fits to the final shape. The kinetic parameters (terrace diffusion and step detachment rate) are determined by fits to the rate of evolution of individual layers of the crystallite. Using the obtained experimental values, a numerical simulation with a fixed step chemical potential for the boundary condition is performed. The results greatly overestimate the critical slowing down as the crystallite approaches the final state.

4.1 Introduction

With the rapid advances of nano-technology, nano-size crystallites are of interest as ideal models of quantum dot systems [6, 37, 75, 76]. The electronic or luminescent properties of quantum dots are well known to depend on their size, but as the size approaches the nano-scale, they also depend on crystallite shape [2, 5]. In addition, with shrinking structure size, shapes of a nano-crystallite become more vulnerable to external perturbations such as the substrate stress or adhesion energy [43, 77-79]. The influence can be so strong that a stable crystallite cannot exist on the surface and the structure simply decays [40, 68]. Such issues are important in gaining control over constructing and manipulating stable nano-structures and quantum dots.

Finite size of a crystallite is an important issue theoretically, which requires addressing the extensive variables explicitly [80]. Also the discrete nature of steps becomes more evident as the system size shrinks, which is also an interesting theoretical problem [85]. One approach to both problems is to use the continuum step model in cylindrical coordinates. With this approach, it is possible to demonstrate that finite size results in metastable states and the discrete steps define transitions between the metastable states [64, 65, 85]. Dynamical modeling of shape evolution can also be done within the same framework by modeling microscopic mass transport mechanisms, which introduces kinetic parameters that govern the rate of mass transport for each mechanism [38, 39].

Kinetic parameters are of importance, along with the substrate boundary condition, to determine the total time of the crystallite reshaping process when there is a change in external environment such as temperature or chemical environment.

Independent measurement of kinetic parameters is needed to distinguish the kinetics-limited and the boundary condition-limited parts of the deterministic evolution. Kinetic parameters obtained from island or mound decay experiments are derived under the approximation that there is one rate-limiting mass transport mechanism for the kinetics [22, 40, 68, 86]. This approximation is good for a decaying structure where the boundary condition does not constrain mass flow. However, describing the kinetics of the structure evolution becomes subtle when considering a volume-conserving reshaping process, because in this case the substrate boundary condition is crucial. Here we present results obtained by fitting decay curves of a reshaping crystallite, which is already under the influence of the boundary condition imposed through the step-step interactions. The ratio between two kinetic process, adatom diffusion and attachment-detachment at the step edges is determined.

4.2 Experiment and results

Pb crystals 200-300 nm in radius were formed in ultra high vacuum (UHV) by depositing a 20-30 nm Pb film on a clean Ru(0001) substrate at room temperature and subsequent dewetting of the film at a high temperature, a few degrees below the melting point. More details of sample preparation are given in refs. [14, 68]. The crystals were then cooled rapidly to the desired temperatures of experiment and observed using a variable-temperature scanning tunneling microscope (VT-STM). After the evolution, the crystallite reaches a stable shape defined by the temperature and crystal volume [80]. Figure 1 of ref. [14] gives a good example of an image of such a stable crystallite. It has a flat, circular facet with an (111) orientation, which

smoothly connects to the vicinal part of the crystallite as schematically shown in Figure 4-1 a).

Time evolution of the crystallite is observed with STM after the rapid cooling. The evolution proceeds by a layer-by-layer peeling as demonstrated in refs. [14, 68]. Figure 4-1 b) shows the radius of the top and second layer as a function of time for a cooled crystallite at 95˚C close to the end of the evolution. The second layer does not start to shrink until the first layer disappears, indicating the conservation of mass. The transient increase in the radius of the second layer just as the top layer disappears shows that a fraction of the mass expelled from the top layer initially attaches to the second layer (see also Figure 4-1 c)). The facet size increases every time the top layer disappears, eventually reaching the steady state facet radius. The decay time of each layer becomes longer as the reshaping process gets closer to the final steady state, a critical slowing down. This increase is due to the first layer staying close to the second layer for a significant amount of time before it decays away rapidly. Arrows in Figure 4-1 b) indicate the inflection point in the decay curves, which approximately gives the temporal midpoint where the first layer stays close to the second.

The transient increase in the radius of other layers (conservation of mass) is more clearly seen by observing the step-step distances on the vicinal part of the crystallite close to the facet. Figure 4-1 c) shows the step-step distances (between the second and third, third and fourth, and so on) during three subsequent peeling events for a crystallite at 80˚C. All step-step distances become smallest when the top layer disappears. They then increase, reach a maximum, indicated by arrows, and

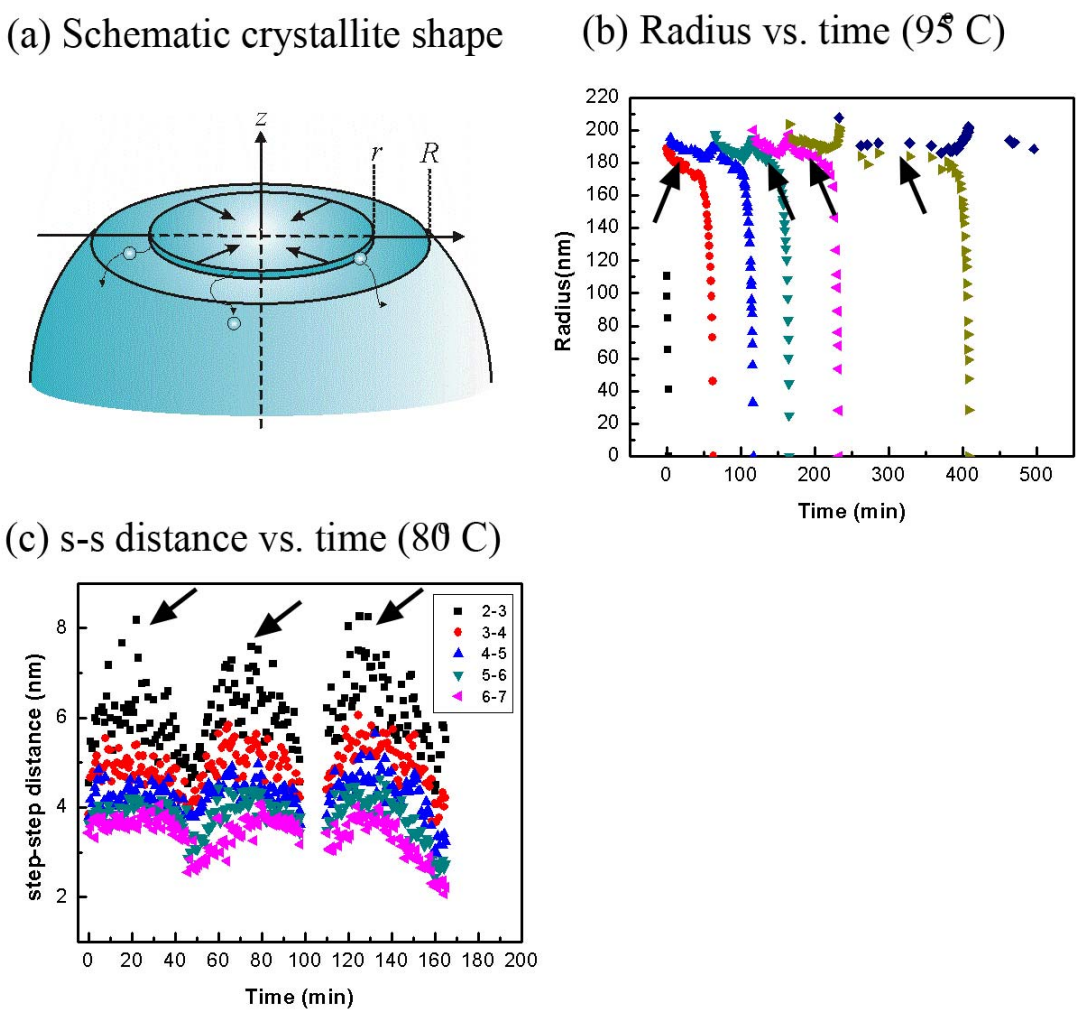

Figure 4-1 a) Schematic drawing of the top part of the crystallite. *r* is the top layer radius and *R* is the second layer radius (fixed) b) The radius of the two top layers as a function of time for a crystallite rapidly cooled to 95˚C. Inflection points of the top layer decay curves are indicated by arrows. c) The step-step distance between the 2nd and 3rd, 3rd and 4th , 4th and 5th, 5th and 6th, 6th and 7th layers during three subsequent peelings for a crystallite rapidly cooled to 80˚C. The maximum distances, indicated by arrows, are at the same times as the inflection points in b).

decrease again until the top layer disappears. The process is repeated until the crystallite reaches a steady state and the step-step distances become stationary. The arrows in c) corresponds to the same point in time as the arrows in b), thus the inflection point in the decay curves give the maximum point in the step-step distances, another indication of the conservation of mass.

4.3 Analysis

The surface chemical potential of a crystallite, subsequent to rapid temperature change, is locally variable and as a result there is a deterministic mass transfer process for the evolution of the crystallite to a more stable shape. With the use of the continuum step model, such evolution can be modeled by deriving kinetic equations of motions of the steps (layers) [13, 38, 39]. Considering only surface diffusion, the kinetic equation of motion of the top layer can be written down by the use of the kinetic parameters, the surface diffusion constant D_S, the linear kinetic coefficient κ and the equilibrium adatom concentration of a straight step c^0_{eq} as

$$J = 2\pi D_S c^0_{eq} \frac{\exp(\frac{\mu_{top}}{k_B T}) - \exp(\frac{\mu_{2nd}}{k_B T})}{\ln\frac{r}{R} + \frac{D_S}{\kappa}\left(\frac{1}{r} + \frac{1}{R}\right)} \tag{4-1a}$$

$$\frac{dr}{dt} = \Omega\frac{J}{2\pi r}, \tag{4-1b}$$

where t is time, Ω the adatom area, r and R are the top and second layer radius, respectively, as shown in Figure 4-1 a). μ is the step chemical potential, which is introduced below. Eq. (4-1a) gives the adatom flux detaching from the top layer to the lower terrace and eq. (4-1b) gives the velocity of the top layer as it shrinks. Note

that we assume there is no incoming flux to the top layer from the upper facet. The kinetics are governed by a dimensionless ratio between the surface diffusion constant and the linear kinetic coefficient $\tilde{d}=k_BTD_S/\Omega\tilde{\beta}\kappa$ [13, 39], where $\tilde{\beta}$ is the step stiffness, here assumed to be isotropic thus equal to the step free energy β. When $\tilde{d} \cong 0$ the evolution is diffusion limited and when $\tilde{d} \cong \infty$ it is attachment-detachment limited.

The step chemical potential is calculated from the total surface free energy, which is itself obtained by the surface free energy density and the shape of the crystallite. Using the Pokrovsky-Talapov surface free energy density in cylindrical coordinates the step chemical potentials for the top two layers are given as [85]

$$\mu_{top} = \Omega\left(\frac{\beta(T)}{r} + \frac{g(T)h^3(r+3R)}{2r(R-r)^3}\right) \tag{4-2a}$$

$$\mu_{2nd} = \Omega\left(\frac{\beta(T)}{R} - \frac{g(T)h^3}{2R}\left(\frac{3r+R}{(R-r)^3} - \frac{4R+3d}{d^3}\right)\right). \tag{4-2b}$$

where d is the step-step distance between the second and third layer, g is the interaction coefficient.

The step free energy for Pb is obtained by using the exact solution for a hexagonal lattice Ising model [87] with an experimentally obtained kink energy of 42 meV [88, 89]. For the interaction coefficient we use the ratio of g/β=3.6 nm^{-1}, experimentally obtained at temperature close to ≈300 K, from a fit to a steady state crystallite shape, in most cases chosen as the least stable metastable shape [80]. Combining eqs. (4-1) and (4-2) gives the kinetic equation of motion of the top layer. The unknowns are the radii of the 2nd and 3rd layer ($R + d$) as the first layer shrinks. From the experimental results in Sec. 2, since the motion of the 2nd and 3rd layer are

small compared to that of the top layer, we begin with the assumption that R and d can be held fixed during each peeling event. The fit is done as follows.

Starting where the decay has reached half the initial radius, the rapid decay at the end of each peeling is fitted in the same way as the island decay experiments in ref. [22], with the interaction term assumed irrelevant, $g/\beta=0$. The fitting parameters are the product $D_S c^0_{eq}$ and ratio D_S/κ. Table 4-1 gives D_S/κ for different $D_S c^0_{eq}$ values for experiments at a) 80ºC (β=0.33eV/nm) and b) 95ºC (β=0.32eV/nm). Figure 4-2 a) is an example (Layer 20 in Table 4-1 and Table 4-2) with fitting parameters $D_S c^0_{eq}$=14000 s^{-1} and D_S/κ=8 nm. It is clear that the results are consistent with a broad range of relative values of the terrace diffusion and detachment rate.

To refine the determination of the kinetic parameters, the entire peeling curve is fitted, including step interactions with the ratio g/β=3.6 nm^{-1} layer (see also Figure 4-1 c)). The facet size increases every time the top layer disappears, and using the obtained pairs of $D_S c^0_{eq}$ and D_S/κ from Table 4-1. Figure 4-2 b) is an example of the fit to the entire peeling curve, the same curve in a), also shown with the position of the second layer. The best value of the step-step distance fitting parameter found to be d=7.6 nm. Table 4-2 gives d with different values of $D_S c^0_{eq}$, using the corresponding value of D_S/κ in Table 4-1, for experiments at a) 80ºC (g=1.19eV/nm^2) and b) 95ºC (g=1.15eV/nm^2).

From the ratio of the standard deviation over the average for d in Table 2, we achieve the most consistent fitting over the entire data set with parameters of $D_S c^0_{eq}$=14000 s^{-1} and D_S/κ =11.1 nm for 80ºC, and $D_S c^0_{eq}$= 40000 s^{-1} and D_S/κ =14.5 nm for 95ºC. This gives d=9.8nm at 80ºC and d=7.2 nm at 95ºC, which is in fairly

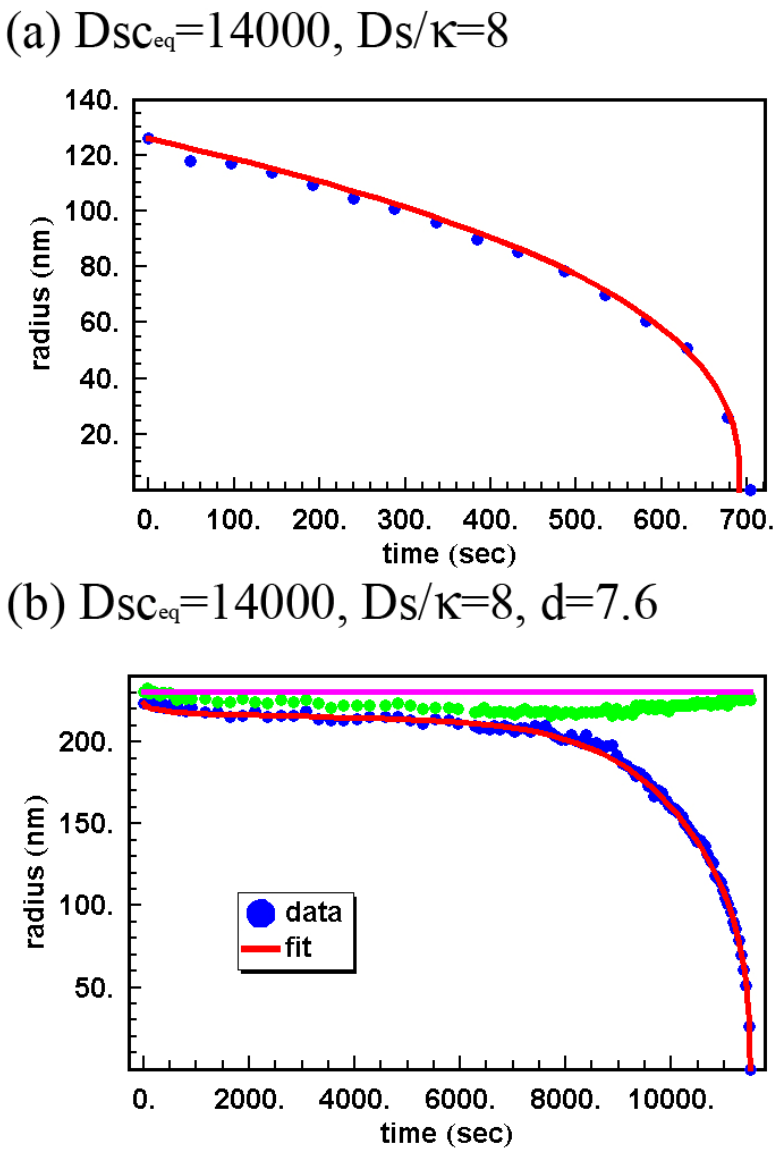

Figure 4-2 Fitting curves to a peeling layer (Layer 20 in Tables 1 and 2) or a crystal at 80˚C. a) Fit to the rapid decay with parameters $D_S c^0_{eq}$=14000 s^{-1} and D_S/κ=8 nm. b) Fit to the whole peeling curve using the ratio g/β=3.6 nm^{-1} for the interaction term. The position of the second layer is also shown for the experiment and fit. $D_S c^0_{eq}$=14000 s^{-1} and D_S/κ=8 nm for the kinetic parameters results in the fitting parameter d=7.6 nm.

Table 4-1 Table of ratio D_S/κ (nm) for all peeling events observed at a) 80ºC and b) 95 ºC. In a), boldface letters (Layers 21 and 22) are not included in the averaging and standard deviation.

a)

Layer / $D_S c^0_{eq}$ (s^{-1})	2	3	4	5	6	7	8	9	10	11	12	20	**21**	**22**	Ave	StDev
15000	12	10	12	13	16	12	21	18	15	14	25	13	**42**	**41**	15.1	4.34
14000	8	7	8	10	12	9	17	14	10	10	20	8	**37**	**34**	11.1	4.01
13000	5	3	5	6	8	5	12	10	6	6	15	4	**30**	**28**	7.08	3.55
12000	2	0.5	2	2	4	2	8	5	2	2	10	0	**23**	**21**	3.29	3.0
11000				0	1	0	4	1	0	0	5		**13**	**14**	1.38	2.0
10000							0				0		**7**	**8**		

b)

Layer / $D_S c^0_{eq}$	1	2	3	4	5	Ave	StDev
80000	74	76	59	42	86	67.4	17.17
70000	60	62	46	31	69	53.6	15.14
60000	45	46	33	20	52	39.2	12.76
50000	31	31	20	8	35	25	11.0
40000	17	16	7		18	14.5	5.067
30000	3	1			1	1.67	1.155

Table 4-2 Table of the (assumed fixed) spacing between the 2d and 3d layers, *d* (nm), obtained as a fitting parameter for all data in Table 4-1, observed at a) 80ºC and b) 95 ºC

a)

Layer	2	3	4	5	6	7	8	9	10	11	12	20	21	22	Ave	StDev
$D_S c^0_{eq}$																
15000 s^{-1}	11.6	10.1	50	14.5	15.5	9.5		13.1	9	9		7.68	8.6	7.83	13.9	11.7
14000 s^{-1}	9.6	9.3	13	12.5	11.8	9		11.3	8.4	8.6		7.635	8.54	7.79	9.79	1.87
13000 s^{-1}	8.8	8.2	10.9	9.9	10	8.3	19	10	8	8.15	25	7.605	8.37	7.76	10.7	5.02
12000 s^{-1}	8.15	7.85	9.4	8.6	8.8	7.9	12.5	8.6	7.65	7.75	13.5	7.575	8.2	7.72	8.87	1.83
11000 s^{-1}				8.3	8.2	7.75	10.1	7.95	7.54	7.66	9.9		7.91	7.68	8.3	0.928
10000 s^{-1}							8.7				8.3		7.79	7.65	8.11	0.482

b)

Layer	1	2	3	4	5	Ave	StDev
$D_S c^0_{eq}$ (s^{-1})							
80000	7.354	7.59	7.505	7.285	7.304	7.4076	0.1336
70000	7.321	7.545	7.451	7.263	7.297	7.3754	0.1186
60000	7.272	7.455	7.379	7.238	7.289	7.3266	0.0888
50000	7.221	7.362	7.294	7.207	7.279	7.2726	0.0622
40000	7.156	7.245	7.195		7.267	7.2158	0.0499
30000	7.076	7.112			7.255	7.1477	0.0946

good agreement with the experimentally observed step-step distance in Figure 4-2 c) (80ºC), considering that it being fixed during the fit. Also the ratio D_S/κ at both temperatures suggests that on Pb(111), the kinetics is closer to attachment-detachment limited.

4.4 Simulation

The Pb parameters used in the simulation are nearest-neighbor atomic spacing a=3.5 Å, atomic step height h=2.86 Å and atomic area Ω=10.6 Å^2. The thermodynamic and kinetic parameters used in the simulation are β=0.32 eV/nm, g=1.15 eV/nm^2, $D_S c^0_{eq}$= 40000s^{-1} and D_S/κ=14.5 nm, the results obtained above for 95ºC. The surface chemical potential is fixed at the boundary and is calculated for the least stable metastable state [80], $\mu=\beta\Omega/\rho_{cmax}$ with ρ_{cmax}=210 nm determined from the final state of the experiment (Figure 4-1 a)). The initial shape is the least stable metastable state calculated at a higher temperature and smaller facet radius (ρ_{cmax} = 120 nm). More details of the simulation setup, including careful discussion of the boundary condition, will be given elsewhere [71].

The results of the simulation are given in Figure 4-3. The final shape fits nicely to the *chosen final* state as shown in Figure 4-3 a), albeit with a larger ratio g/β=3.8nm^{-1}, than the simulation value. The evolution of the crystallite for the last several layers, radius (nm) as a function of time (min), is given in Figure 4-3 b). As in the experiments, the top layer stays close to the second layer, where the step-step interactions are important. Once the Gibbs-Thomson term of the first layer takes over, it starts to peel rapidly and the decay time from here is mainly kinetically limited.

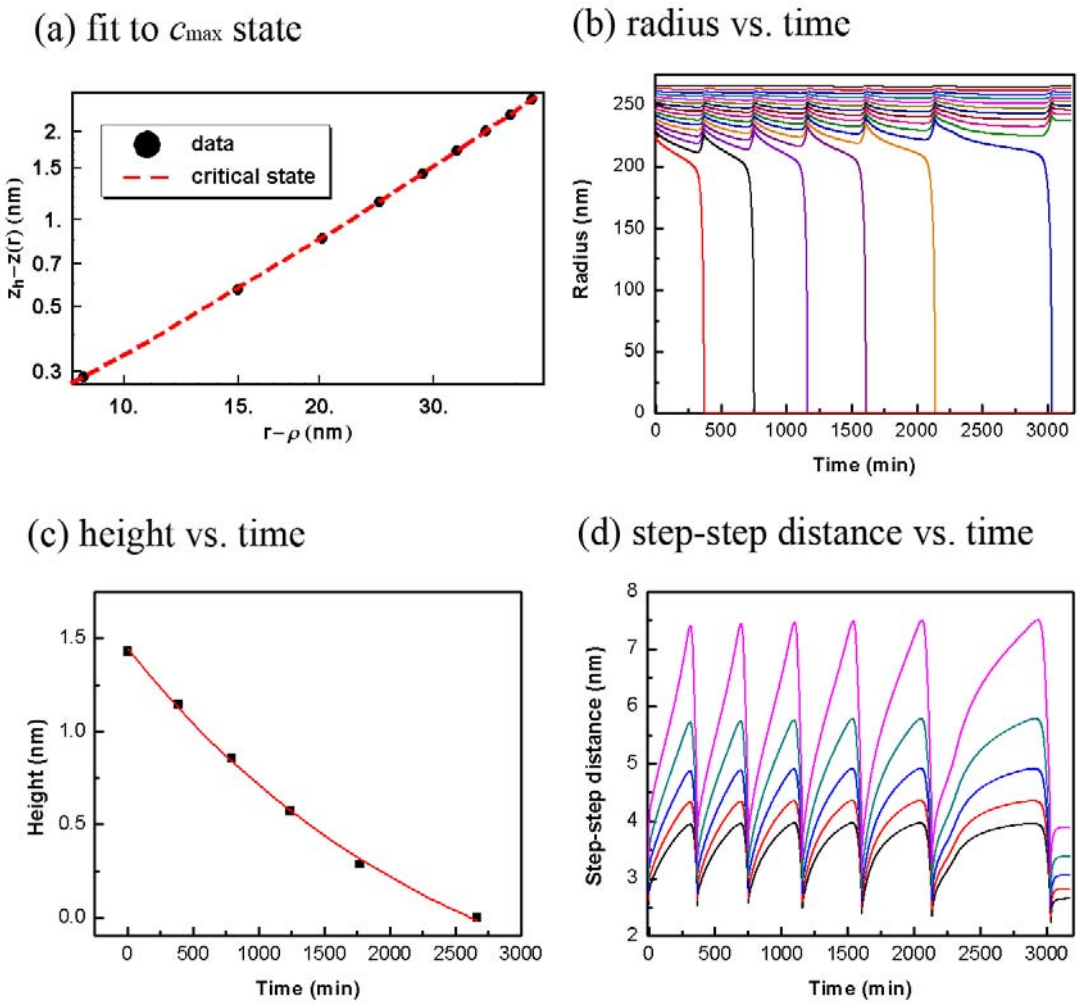

Figure 4-3 a) The final steady shape of the crystallite evolution simulation. Fit to the c_{max} state shape gives g/β=1.24nm^{-1}, close to the input of g/β=1.15nm^{-1}. b) Radius (nm) as a function of time (min) for the last six peeling events. c) Height (nm) as a function of time (min) to show clearly the critical slowing down. d) Step-step distances as a function of time. The maximum distance between the second and third layer is in good agreement with experiment and also results obtained form the fit in Table 2 b).

The critical slowing down of the peeling as it gets close to the end is also evident, due to the interface boundary condition imposed through the step-step interactions. The slowing down is more clearly seen in the height vs. time in Figure 4-3 c). Figure 4-3 d) gives the step-step distances as a function of time. As in the experiments, they are smallest at the time of peeling and have a maximum in between, although from the shapes of the curves are much less symmetrical than in the experiment. The maximum step-step distance between the second and third layer, which is about 7.5 nm is in fairly good agreement with the experiment in Figure 4-1 c) (though the temperature is different) and also to the results from the fit to the peeling curves in Table 4-2 b). The overall time scale for the evolution, however, is much longer than observed for experiment. For instance the first full peeling occurs in 60 min experimentally, whereas in the simulation it takes 385 min. This indicates that improvement in modeling the boundary conditions is needed.

4.5 Discussion

The simulation results give very good qualitative agreement, reproducing the region where the top layer stays close to the second layer in the individual peeling curves and also the critical slowing down as it reaches the final steady state. However, quantitatively the decay time for each layer is much longer than the ones experimentally observed, even though we are using the kinetic parameters obtained from the experimental data. One possible reason for this is that we are simply not using the correct pair for D_S/κ and $D_S c^0_{eq}$ in Table 4-1. Although the standard deviation may not be the smallest, it is very likely that the true value is given by other

pairs. This will be tested in future work [71]. However, although this may change the time scale of an individual peeling of the top layer, it does not help in simulating the critical slowing down seen at the end of the evolution. This is the difficulty in setting the interface boundary condition and modeling the approach to the final state. More detailed discussions will be given elsewhere [71]. Furthermore in these experiments, not only is there the interface between the substrate but side facets also on the crystallites themselves, which may play a key role in defining the effect boundary conditions. Such physical conditions make it more difficult to make a model concerning the critical slowing down at the end of the evolution, and from it obtain information about the boundary condition that defines the crystallite shape. Further work will focus on determining whether the constant step chemical potential assumption for the boundary condition is responsible for the discrepancy.

Chapter 5: Constrained evolution of Nano-Crystallites

Deviations from the universal predictions of shape-preserving structure evolution have been investigated in the context of realistic physical boundary conditions for supported nano-scale crystallites. Structural evolution was simulated using the continuum step model with volume conservation, variable interface free energy and incorporating analytical solutions for equilibrium and metastable crystallite shapes. Early stages of evolution following a simulated temperature drop are consistent with the kinetics of shape-preserving evolution. Later stages of decay show a distinct slow down, with an empirically-determined exponential form. The time constant of the slow final evolution increase linearly with the length scale of the crystallite, and also increases monotonically with interface adhesion strength. Under normal evolution, where the interface area is constant or increasing, the evolution progresses through the metastable states accessible to the volume. If a decreasing interface area can be induced, an alternative progression ending much closer to equilibrium is possible. The late-stage slow-down provides additional kinetic information that allows the non-uniqueness of early-stage modeling to be resolved. The slow down observed in the late stages of relaxation of Pb crystallites has been fit, with a unique determination of the relative values of the terrace diffusion constant and step attachment constant.

5.1 Introduction

Nano-size crystallites have become of great interest with the rapid developments of nano-technology e.g. quantum dot systems [6, 37, 75, 76]. Electronic or luminescent properties of such quantum dots depend on their size and recent studies show that they also depend on the shape [2, 5] as the dot size approaches the nano-scale. In addition they become more vulnerable to external perturbations such as the surrounding vapor or the substrate adhesion energy [43, 77-79] with shrinking size. The influence can be so strong that a stable nano-crystallite may not exist and the structure simply decays away [40, 68]. Alternatively, environmental effects on the free energies and boundary conditions for mass transport can constrain both the final structure and the kinetics by which it is formed. Such issues become important the demand grows for control over constructing and manipulating stable nano-structures on surfaces.

The work presented here demonstrates the issues of crystallite evolution, using supported Pb crystallites as a specific example. Pb crystallites have been used for ECS experiments since the early 80s [52, 90] since they are ideal model systems with clean observable facets at moderate temperatures. Early studies were done using scanning electron microscopy (SEM), and confirmed the $\sim x^{3/2}$ shape of the PTECS [52, 53, 90]. More recently, scanning tunneling microscope (STM) experiments allowed more detailed observation of the facet-to-vicinal transition and gave qualitative results of the prefacter, which yields the thermodynamic parameter, the step-step interaction coefficient [58, 91, 92]. However, results showed a strong difference of the obtained values for defective (screw dislocation) and defect-free, equilibrated crystallites. The reason for the difference was proposed originally by Mullins et al. [14, 64, 65, 93], and

involves barriers for evolution of the crystallite when the volume is conserved. For a volume-conserved crystallite, the evolution from a non-equilibrium to an equilibrated steady shape proceeds by a layer-by-layer peeling mechanism of the top "facet" [68]. From individual peeling events it is possible to obtain some of the kinetic parameters, given information about the key free energies [68, 71]. However, the resulting values are effective parameters, that are primarily useful for describing the initial stages of the evolution where mass transport is not constrained by boundary conditions [38, 69]. Here we specifically address the influence of the boundary conditions as the crystallite approaches the final state.

When a crystallite is in a non-equilibrium shape, the surface chemical potential is local and the kinetically driven, deterministic evolution of crystallites can be simulated. In this paper, with use of the continuum step model, we simulate a rapid cooling of a finite volume crystallite supported on a substrate surface. We use experimentally observed and theoretically proven temperature dependence of the thermodynamic parameters, specifically for Pb, to model the rapid cooling. Most importantly the Wulff-Kaishew theorem is used for the interface boundary condition. The variety and complexity of the evolution with volume, substrates and initial shapes are presented with comparisons with experiment.

5.2 Background

We follow previous workers [38, 39] to construct kinetic equations for steps of a cylindrically symmetric crystallite. A cross section of such a crystallite in the continuum step model is shown schematically in Figure 5-1 a). Mass transport is

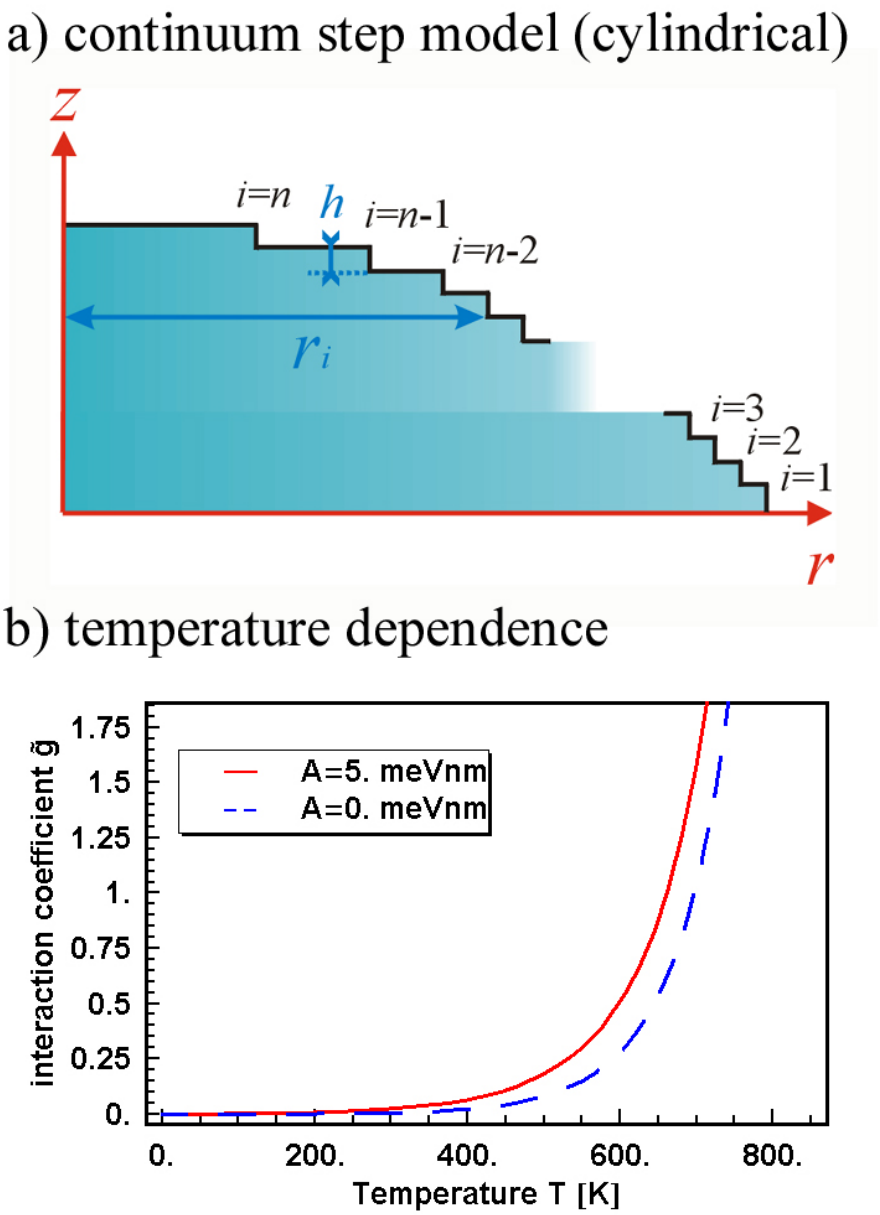

Figure 5-1 a) Schematic drawing of the continuum step model in cylindrical coordinates. Step height is denoted as h and layers are numbered from the bottom. b) Temperature dependence of the dimensionless step-step interaction coefficient, eq. (D-1) for Pb. The step free energy is calculated with eq. (5-5) with kink energy 42 meV [72, 84]. Dashed line gives entropic step-step interaction and solid line gives interaction with A=5 meV×nm [94].

restricted to surface diffusion with no evaporation or condensation or flow onto the surrounding substrate, so the crystallite volume is conserved. Taking the static approximation, the concentration of adatoms $c(r)$ on a terrace obeys a Laplace equation. For the ith terrace bounded by the ith and (i+1)th layer (layers numbered from the bottom, Figure 5-1 a)), this is

$$D_S\left(\frac{\partial^2}{\partial r^2}+\frac{1}{r}\frac{\partial}{\partial r}\right)c_i(r)=0\,, \tag{5-1}$$

where D_S is the diffusion constant of adatoms on the surface. The boundary conditions for this equation at the ith layer edge is

$$-D_S\left.\frac{\partial c_i}{\partial r}\right|_{ri}=\kappa\left(c_i(r_i)-c_{eq}^{i}\right), \tag{5-2}$$

where r_i is the radius of the ith layer, κ the linear kinetic coefficient and c^i_{eq} the equilibrium adatom concentration at the ith layer edge. Similar boundary conditions for the (i+1)th layer lead to two equations of motion for the layers,

$$J_i=2\pi D_S\frac{c_{eq}^{i+1}-c_{eq}^{i}}{\ln\dfrac{r_i}{r_{i+1}}+\dfrac{D_S}{\kappa}\left(\dfrac{1}{r_i}+\dfrac{1}{r_{i+1}}\right)} \tag{5-3a}$$

$$\frac{dr_i}{dt}=\Omega\frac{J_i-J_{i-1}}{2\pi r_i}\,, \tag{5-3b}$$

where t is time and Ω the adatom area. Eq. (5-3a) gives the adatom flux J_i attaching to (detaching from) the ith layer from (to) the ith terrace and eq. (5-3b) gives the velocity of the boundary of the ith layer. The kinetics is governed by the dimensionless ratio, $\tilde{d}$, between D_s, the surface diffusion constant, and κ, the linear kinetic coefficient, $\tilde{d}=k_BTD_S/\Omega\beta\kappa$ (eq. (D-1)). Frequently discussed limiting physical

cases occur when $\tilde{d} \cong 0$ so the evolution is diffusion limited, and when $\tilde{d} \cong \infty$ so the evolution is attachment-detachment limited.

The equilibrium adatom concentration at the *i*th layer edge is obtained from the step chemical potential μ_i, which is calculated from the step dependence of the surface free energy. We use results from the previous paper [93] based on the Pokrovsky-Talapov surface free energy density

$$f(l_i) = \gamma_0 + \frac{\beta(T)}{l_i} + g(T)\frac{h^3}{l_i^3} \tag{5-4a}$$

$$\mu_i = \Omega\left(\frac{\beta(T)}{r_i} - \frac{g(T)h^3}{2r_i}\left(\frac{3r_{i+1}+r_i}{l_i^3} - \frac{r_i+3r_{i-1}}{l_{i-1}^3}\right)\right) \tag{5-4b}$$

$$c_{eq}^{i} = c_{eq}^{0}\exp\left(\frac{\mu_i}{k_B T}\right), \tag{5-4c}$$

where $l_i=r_i-r_{i+1}$ is the *i*th terrace width, β, g are the step free energy and step-step interaction coefficient, respectively, and c^0_{eq} is the equilibrium adatom concentration of a straight step.

To summarize the properties of the crystal shape based on eq. (5-4b): there is a family of stable states, which are characterized by a shape parameter c obtained in the continuum model [80]. Every value of c corresponds to a unique shape, which is a stable state with transition states corresponding to layer peelings in between [93]. There is a maximum value of c that yields a limiting metastable state, called the $c_{\max}$ state, which has a $z\sim r^2$ shape, to leading order, and the highest crystal height of all states for the same volume. As the shape parameter decreases from $c_{\max}$, at c=0, it corresponds to the Pokrovsky-Talapov shape (PT shape) with $z\sim r^{3/2}$, the equilibrium crystal shape

(ECS). The value of c also can be negative corresponding to a shape closer to a cone with $z \sim r$.

The initial stage of crystallite evolution after a rapid cool has been studied by Uwaha et al. [38] using similar formulae as above. Assuming that the dominant driving force is the 2D Gibbs-Thomson effect of the top layer, and also assuming a shape preserving evolution, the height of the crystallite as a function of time was found to obey a power law depending on the preserving shape. For the $c_{\max}$ shape ($z \sim r^2$) this is $z \sim t^{1/3}$ and $z \sim t^{2/5}$ for attachment-detachment and diffusion limited kinetics, respectively, and for a PT shape ($z \sim r^{3/2}$) this is $z \sim t^{3/10}$ and $z \sim t^{1/3}$. This power law behavior has also been observed experimentally, [38, 69], and is called "fast relaxation" since all layers are free to transfer mass without any limiting boundaries. Such behavior occurs physically in decay, where there is no equilibrium crystalline final state, as opposed to the case of relaxation to a stable final state discussed here.

5.3 Methods

5.3.1 Numerical Simulation

The initial crystallite shape is a $c_{\max}$ state shape with thermodynamic parameters calculated at 700K specifically for Pb, which is described in detail later. The simulation runs with thermodynamic parameters calculated at 300K, thus modeling a rapid cooling of ΔT=400K. Table 5-1 gives the values of the thermodynamic parameters at the initial temperature of 700K and the final temperature of 300K. Initial shapes of spheres and cones are also considered and are specified when used.

Table 5-1 Table of thermodynamic parameters, step free energy and step-step interaction coefficient for Pb. Temperature dependence is calculated by eq. (5-5) and (5-6) with kink energy of 42 meV [84] and step interaction energy of A=5 meV×nm [94]. See also Figure 5-1 b).

temperature	step free energy β	step-step interaction coefficient g
700K	0.208 eV/nm	1.87 eV/nm^2
353K	0.326 eV/nm	1.174 eV/nm^2 (g/β=3.6)
300K	0.339 eV/nm	0.652 eV/nm^2

Volumes of the crystallites evaluated in the simulations vary from 500nm^3 to 2.0×10^4 nm^3.

The boundary condition of the finite crystallite is the most important part of setting up the simulation. The interface boundary condition of the bottom layer defines the final constant step chemical potential and is most crucial. Here the Wulff-Kaishew theorem [95], the equilibrium boundary condition for a finite volume crystallite, is satisfied at the interface at all times giving the bottom layer step chemical potential as $\mu/2\nu=(2\gamma_0-E_A)/z(t)$, where E_A is the adhesion energy. Fixed volume is obtained by setting $J_0=0$ (Eq. 3a)) at the bottom layer boundary. The top layer radius is set to 0 whenever it becomes smaller than one lattice spacing.

Modeling the kinetics requires values for the structural properties of Pb, which are the nearest-neighbor atomic spacing a=3.5 Å, atomic step height h=2.86 Å and atomic area Ω=10.6 Å^2. A reasonable value of 1.7 eV/nm^2 is used for the surface tension of a Pb(111) surface [72]. The temperature dependence of thermodynamic parameters is obtained from microscopic models. The step free energy is quantified by using an hexagonal lattice Ising model [87] with an effective kink energy ε_k,

$$\beta(T)\big|_{[110]} = \frac{2k_BT}{a}\cosh^{-1}\left(-\frac{1}{2}+\frac{1}{2}\sqrt{3+\frac{1+3W^4(T)}{W^2(T)(1-W(T))(1+W(T))}}\right)$$

$$:W(T)=\exp\left(\frac{-\varepsilon_k}{k_BT}\right), \qquad (5\text{-}5)$$

where a is the nearest-neighbor atomic spacing. For the kink energy we use 42 meV for A-type steps obtained experimentally [84] and confirmed theoretically [72]. The step-step interaction coefficient is obtained from the interacting step model [10, 33]

$$g(T) = \frac{(\pi k_B T)^2}{24 h^3 \beta(T)} \left(1 + \sqrt{1 + \frac{4A\beta(T)}{(k_B T)^2}} \right)^2 , \qquad (5\text{-}6)$$

where A is a step interaction energy. Note that the step free energy is assumed isotropic ($\beta=\tilde{\beta}$) with circular layers. A=5 meV×nm is used for the step interaction energy [94]. Figure 5-1 b) gives an example of the temperature dependence of the scaled step-step interaction coefficient $\tilde{g}=g\Omega(hk_BT/\Omega\beta)^3/k_BT$ as in eq. (D-1) for Pb. The specific values used for different temperatures are listed in Table 5-1. The kinetic parameters (D_S, κ and c^0_{eq}) are scaled into a dimensionless time as in Appendix A that has no influence on the thermodynamic properties of the crystallite.

The results for the kinetic evolution are obtained by numerical integrations of eq. (5-3) using a first order Runge-Kutta method (Euler's method). The value of the time increment is $\Delta\tilde{t} = 1.0\times10^{-3}$ when scaled as in eq. (D-1). Sequential cycles of step motion were performed from the bottom layer (i=1) to the top (i=N). For a concrete demonstration, we use a value of D_S/κ =16 nm, in the regime of attachment-detachment kinetics, as was estimated in previous work [71]. At 300K, the dimensionless parameters are $\tilde{\gamma}_0$=7.0, $\tilde{g}=2.3\times10^{-2}$ and $\tilde{d}$=11.5 (The relationship of the scaled to the physical values is shown in Table 5-2 for for Pb at 300K).

When a crystallite is rapidly cooled, the step chemical potentials become local and there is a self-driven mass transfer process from high to low step chemical potential, resulting in a reshaping of the crystallite. An example of the reshaping of a $V=2.0\times10^4$ nm^3 crystallite evolution with an adhesion energy of $E_A=\gamma_0$, is shown in Figure 5-2. The initial shape is a $c_{\max}$ shape with thermodynamic parameters calculated at 700K. Simulations were run with thermodynamic parameters at 300K,

Table 5-2 Table of proportionality factors, eq. (D-1) and (D-2), relating the scaled to real Pb parameters at 300K calculated by eq. (5-5), (5-6). $E_A=\gamma_0$ is used for the adhesion energy and $D_S c^0_{eq}=20000\ s^{-1}$ experimentally obtained in section 5.3.2.

$\tilde{r}/r$	$\tilde{z}_h/z_h$	$\tilde{t}/t$	$\tilde{E}_A/E_A$	$\tilde{V}/V$	$\tilde{c}\,\rho/c$
0.720	3.50	1098.5	6.97	1.81	0.551

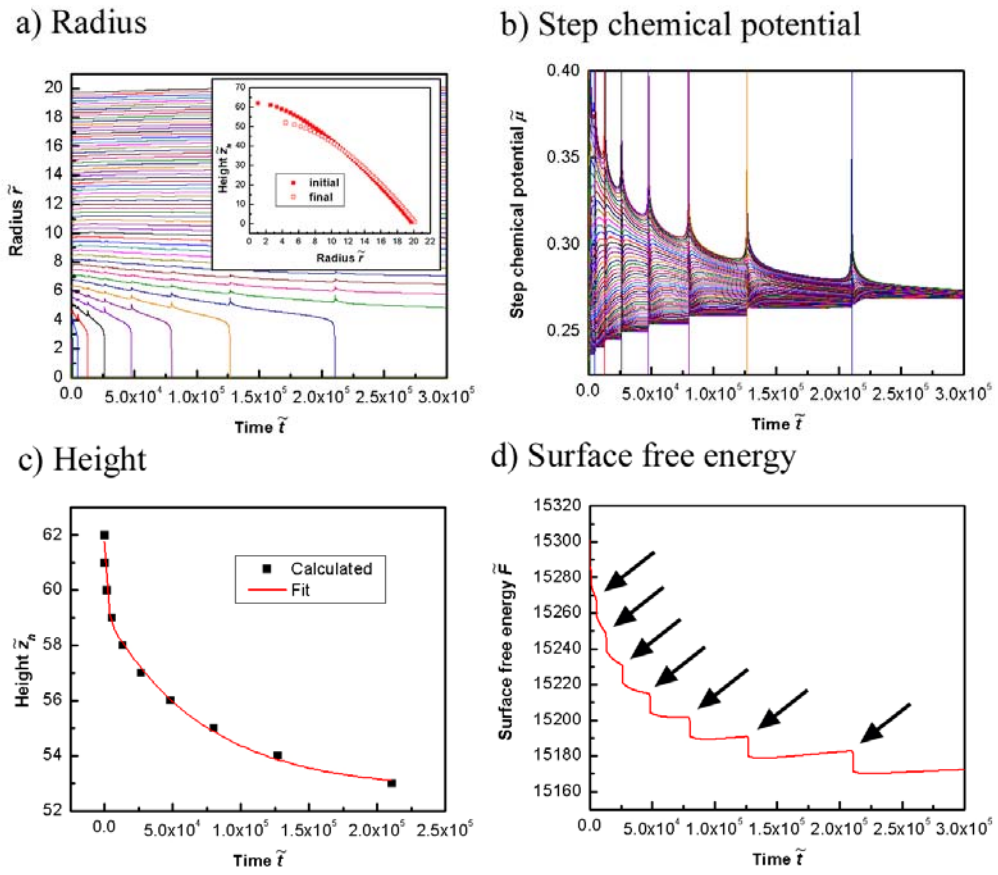

Figure 5-2 Evolution of shape following a temperature drop of 400K. a) Layer radius, b) step chemical potential, c) crystallite height and d) surface free energy (including interface free energy) as a function of time. Inset in a) is the initial and final crystallite shape. 2nd order exponential fit to the data with two time constants is also given in c). Arrows in d) indicate the discrete jumps in the surface free energy when the layers peel. Crystallite volume V=2.0×10^4 nm^3, adhesion energy $E_A=\gamma_0$, step-step interaction g=0.652 eV/nm^2 and D_S/κ=16 nm, gives dimensionless parameters of $\tilde{V}$=3.48×10^4, $\tilde{\gamma}_0$=7.0, $\tilde{g}$=2.3×10^{-2} and $\tilde{d}$=11.5

a temperature drop of 400K. Figure 5-2a) shows the time dependence of the radii of all the layers of the crystallite. As also observed in experiment, the top layer undergoes a rapid decay ("peeling") coupled to slow evolution of the other layer radii. Only after the top layer disappears does the next layer decay and disappear. Eleven such peeling events occur during this simulation and the crystallite reaches the final shape shown in the inset of a) along with the initial shape ($c_{\max}$ shape). The corresponding evolution of the step chemical potentials is shown in Figure 5-2b). Initially, there are strong gradients from the top to the bottom of the crystallite, with increasing time, the differences become smaller and thus the driving force for mass transport also becomes smaller.

Also evident in Figure 5-2a) is that the time interval between top layer peeling events increases with time (and with the decreasing chemical potential gradients shown in Figure 5-2b). The height vs. time in Figure 5-2c) fits very well to a 2nd order exponential with a fast τ_f and slow τ_s time constant.

$$z = z_0 + A_f \exp(\frac{-t}{\tau_f}) + A_s \exp(\frac{-t}{\tau_s}) \qquad (5\text{-}7)$$

As mentioned in section 2, the initial fast relaxation is more physically fit to a power law, however the fast τ_f time constant is parametrically useful in separating the initial behavior from the final slowing down. The specific values of the time constants for this case are $\tau_f=(1.61\pm0.539)\times10^3$ and $\tau_s=(7.27\pm1.22)\times10^4$. The value of the time constant τ_s was also determined for $\tilde{d}<1$ (diffusion limited kinetics) yielding a smaller value. The as the crystallite relaxes, the surface free energy decreases as shown in Figure 5-2d), indicating the deterministic nature of the evolution. The discrete jumps

in the free energy, indicated by arrows, are due to the sequential peeling events of the layers, a unique result of the built-in steps of the continuum step model.

The boundary conditions governing the late stages of evolution are physically determined by the initial shape and volume, and by the interfacial free energy. The volume dependence of crystallite evolution is shown in Figure 5-3 for a specific interfacial energy condition, $E_A=\gamma_0$, and the same value of D_s/κ as in Figure 5-2. The initial shapes used are similar $c_{\max}$ shapes with the same facet radius to height ratio. As a result they have a decreasing interface area to volume ratio as the volume increases as shown in Figure 5-3c). The two characteristic time constants τ_f and τ_s as a function of volume are given in Figure 5-3a) and b), respectively. They both increase approximately linearly with volume, however, the rate of increase is much larger for τ_s indicating that the final slowing down is more sensitive to the interface/volume ratio than the initial fast relaxation. The total number of peeling layers and the ratio of the interface area to volume are shown in Figure 5-3c). The number of layer peelings increases as a 1/3 power law with volume (linear in length). The final /initial interface area ratio is independent of volume. To quantify the nature of the final shape, the final value of the shape parameter c is calculated approximately from the final height z_h and top layer radius r_f

$$c_f \cong \frac{r_f}{3g}\left(\frac{\beta}{h}-\frac{(2\gamma_0 - E_A)r_f}{z_h}\right), \qquad (5\text{-}8)$$

The volume dependence of the shape parameter is shown in d) (scaling in eq. (D-3)). All c values are positive and close to $c_{\max}$. The small increase the value of c with volume is due to the fact that smaller crystallites have fewer states available due to the discreteness of the step [93]. This is not an effect of the interface/volume ratio. The

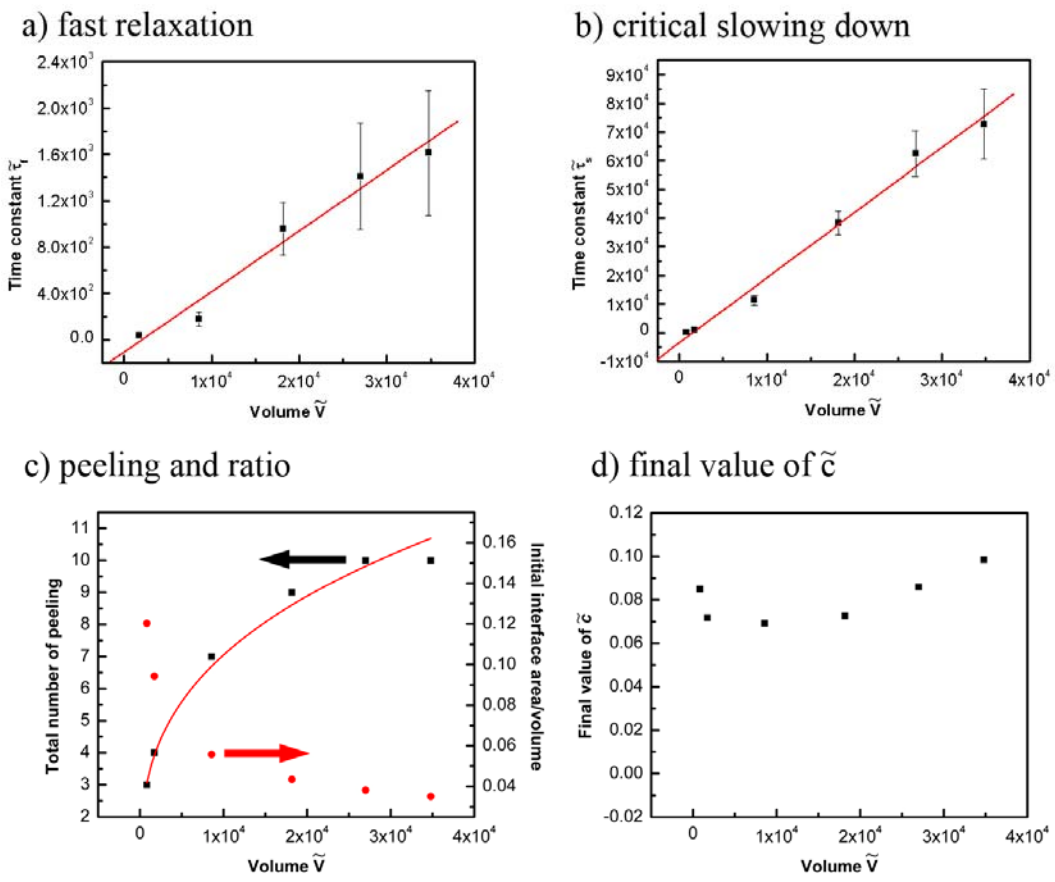

Figure 5-3 Dependence of structural relaxation as a function of volume. Initial shape c_{max} shape, temperature drop of 400K from 700K, D_S/κ =16nm. a) Fast relaxation time constant τ_f and b) critical slowing down time constant τ_s as a function of volume. Solid line is a linear fit. c) Total number of layer peelings and initial interface area to volume ratio. The solid line is a fit of the number of layer peelings to the 1/3 power of the volume. d) Final values of the shape parameter c calculated from the final shape using eq. (5-8).

results of c) and d) indicate that the influence of the interface/volume ratio is fairly weak and most crystallites end close to the $c_{\max}$ state for $E_A=\gamma_0$.

The adhesion energy dependence of crystallite evolution is shown in Figure 5-4 for the same initial shape as the crystallite in Figure 5-2. The two characteristic time constants as a function of dimensionless adhesion energy (eq. (D-1)) are shown in a) and b), respectively. The fast time constant τ_f has a very weak adhesion energy dependence. However, the slow time constant τ_s increases dramatically with adhesion strength (Note: smaller $\tilde{E}_A$ is larger adhesion). The total number of layer peeling events and the final/initial interface area ratio is shown in Figure 5-4c). Both increase approximately linearly with adhesion strength. For weak adhesion the interface area shrinks, and the interface area expands for strong adhesion. The shape parameter of the final state, calculated using eq. (5-8), is shown in Figure 5-4d). For most adhesion energies the crystallite ends in a state near c_{max}. However, when the adhesion energy is weak, the crystallite ends up in a state much closer to equilibrium (c=0). These results show a strong dependence on the adhesion energy. Specifically for weak adhesion, since the interface area prefers to shrink, an uphill mass flux is generated causing more layers to peel due to mass conservation, thus enabling the crystallite to reach other states. Notice in c) that the total number of peeling layers deviates from its linear behavior and is larger for weak adhesion.

Finally, the evolution of structures with different initial shapes, but with the same volume and adhesion energy ($E_A=\gamma_0$) are compared. The initial shapes are a $c_{\max}$ shape (700 K), a truncated sphere and two cones with different interface area as shown in Figure 5-5 a), the final shapes in b). The characteristic time constants, total

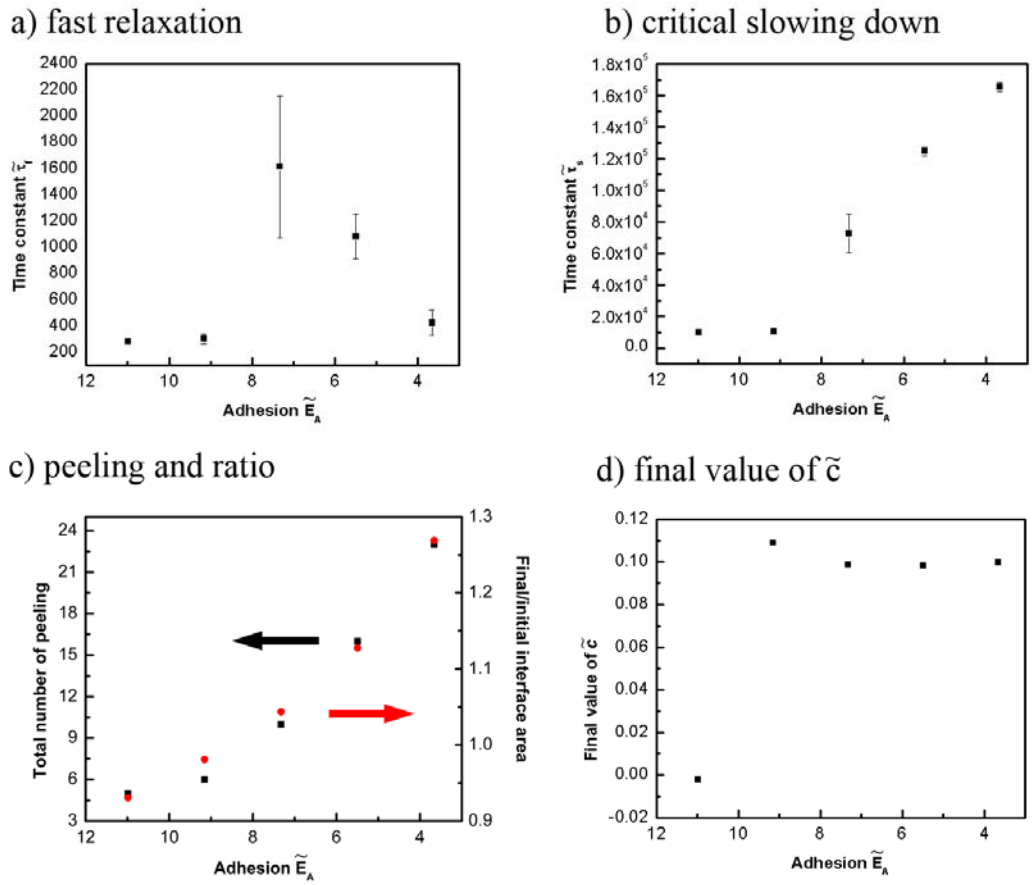

Figure 5-4 a) Fast relaxation time constant τ_f and b) critical slowing down time constant τ_s as a function of adhesion energy. Initial shapes are the same c_{max} shape. c) Total number of peeling and final/initial interface area ratio. d) Final value of c calculated from the final shape using eq. (5-8).

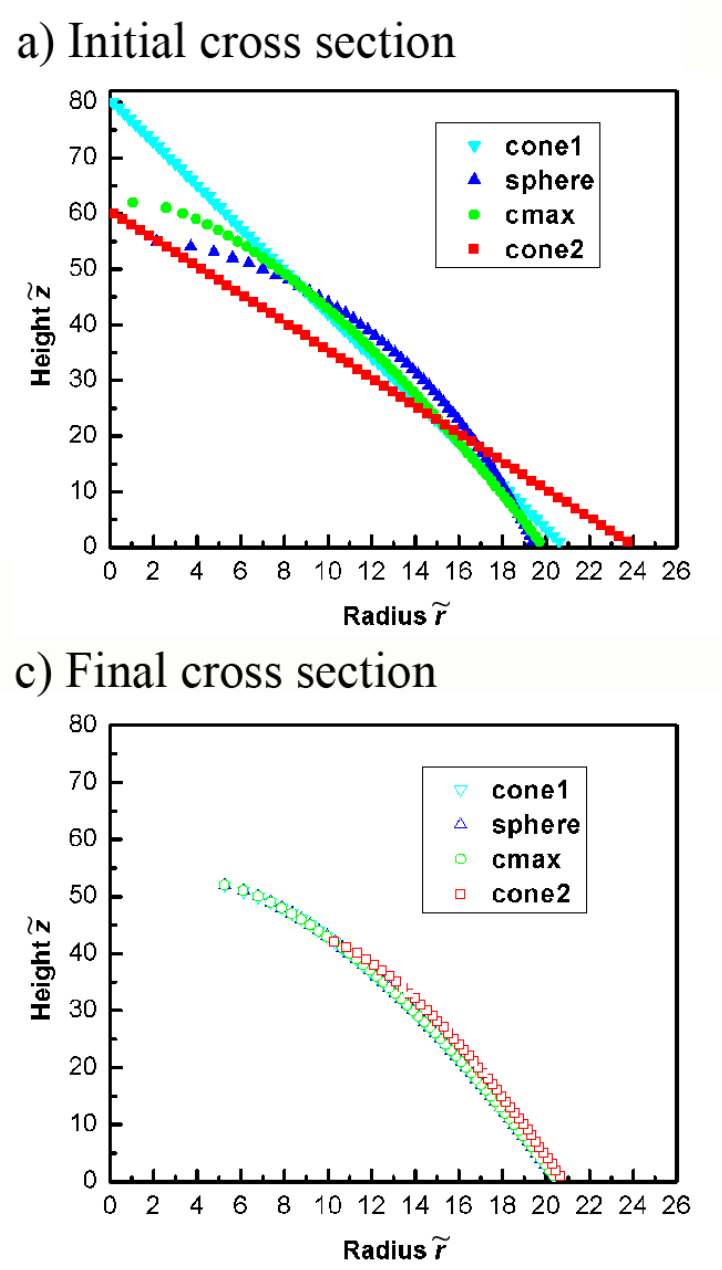

Figure 5-5 a) Different initial shapes for same volume and adhesion energy (E_A=γ_0) crystallite. b) Final shape after the evolution for different initial shapes in a).

number of peeling event, final/initial interface area ratio and the final value of c with eq. (5-7) are summarized in Table 5-3. For any initial shape if the initial and final interface areas are approximately the same, the relaxation ends in the same state close to c_{max}. However, for different initial interface area such as cone2, than the final state is different. From the final/initial interface area ratio, it is clear in the latter case that there is an uphill mass flux similar to the effect of having weak adhesion. However, even when the final state is identical the time constant for both fast and slow differ with different initial shapes.

The Wulff-Kaishew theorem is physically intuitive and useful in defining the boundary condition. However, the approximation of a fixed boundary chemical potential used in modeling the large crystallite is questionable. The true time dependence of the boundary condition should be more gradual compared to the sharp one in the simulation. There is also the fundamental question of whether Wulff-Kaishew theorem is truly satisfied during the evolution, since it is a boundary condition only satisfied at equilibrium. Obviously this is an approximation, however, it should be quite valid since the crystallite volume is conserved at all time and the change in the height of the crystallite is still very small. For very small crystallites this becomes more questionable, however, in such case a thermodynamic approach itself is questionable with appearance of the discrete nature of the atoms.

From the results it can be concluded that when the interface area is expanding during relaxation the crystallite always settles in the c_{max} state whatever the volume or adhesion energy. Thus the adhesion energy can be obtained from eq. (8) with c_f equal to 1/6 and the known thermodynamic parameters. With known adhesion energy, the

Table 5-3 Table of the two characteristic time constants (τ_f and τ_s) and the final c state calculated by eq. (5-7) from the shapes in Figure 5-5 b) for crystallites with different initial shapes but with same volume and adhesion energy ($E_A=\gamma_0$).

	c_{max} state	sphere	cone1	cone2
time constant $\tilde{\tau}_f$	1613. ±539.9	-	346.3 ±85.00	152.0 ±42.68
time constant $\tilde{\tau}_s$	72680. ±12210.	894.47	21460. ±2092.	13490. ±2830.
number of peeling	10	3	28	18
final/initial area	1.044	1.109	1.003	0.7456
final value of $\tilde{c}$	0.09856	0.09856	0.09856	-0.235

slow time constant τ_s as a function of volume has a universal slope for a given D_S/κ ratio, which can determine the product of $D_S c^0_{eq}$. However, difficulty still remains in obtaining τ_s experimentally, due to the need to separate the power law regime of the initial fast relaxation and the final slowing down. As noted above, the former depends strongly on the initial shape of the crystallite while the later depends on the interface boundary condition. The two regimes become more and more difficult to separate as the crystallite size approaches the nano-scale.

5.3.2 Experiment

The computational results presented above serve as the basis for evaluating experimental results on the evolution of Pb crystallites. Pb crystals with radius of 200~300nm were formed in UHV by depositing a 20~30 nm thick Pb film at room temperature on a Ru(0001) substrate. The film dewets when the sample is heated, and then it is left to equilibrate a few degrees below the melting temperature. Details of sample preparation are given in refs. [14, 57, 68, 88, 96]. The crystals were then rapidly cooled and observed by a variable-temperature scanning tunneling microscope (VT-STM). Figure 1 of ref. [14] gives an good example of a stable crystallite with a flat, circular (111) facet, which smoothly connects to the vicinal of the crystallite. The height of the crystallite as a function of time (open circles) during the evolution is given in Figure 5-6 a), identical to Figure 2 d) in ref. [14]. The data fits very well to an exponential (dashed line) giving a time constant of 798±26 min. Since it is difficult experimentally to capture the initial fast relaxation, this is considered to give τ_s of the

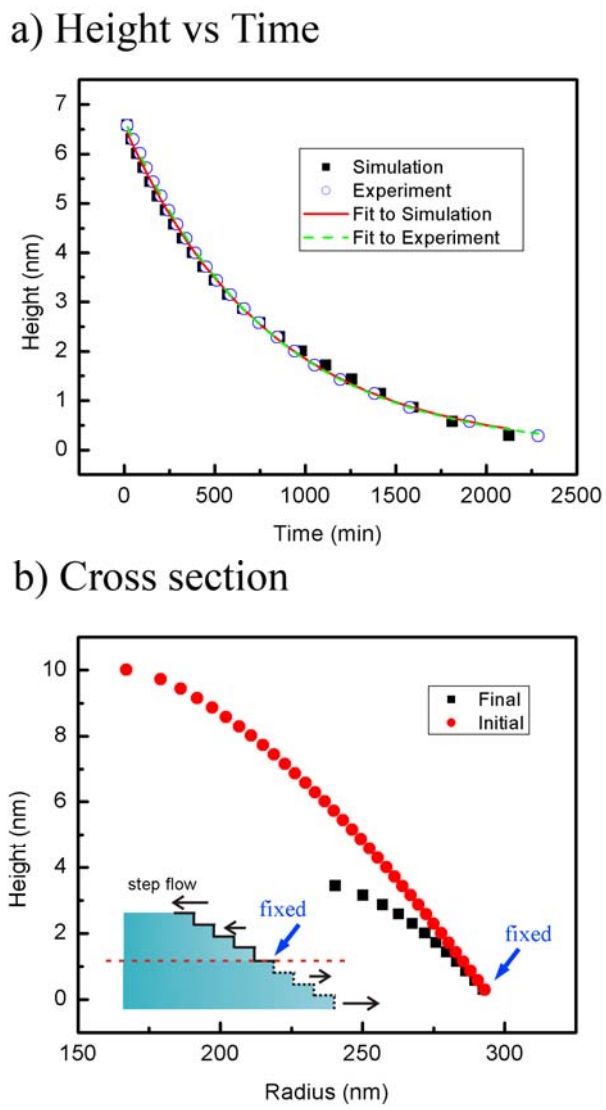

Figure 5-6 a) Height as a function of time for both experiment (open circles) and simulation (squares) at 80ºC (experimental data from ref. [14]). τ_s for experiment and simulation is 798 and 777 min, respectively. Values for $D_S c^0_{eq}$ and D_S/κ in the simulation are 20000 s^{-1} and 0.1 nm. b) Initial (circles) and final (squares) shape of the simulation. Fit to a c_{max} shape of the final shape gives ρ_{cmax}=227.7 and g/β=3.88. Boundary condition of the simulation is schematically shown in the inset in b).

critical slowing down. The final facet radius was 230 nm, large enough that the final state can be approximated to be in a c_{max} state [93].

Simulations were performed to reproduce the above experiment. The value of the step free energy is calculated with eq. (5-5) for 80ºC giving β=0.326 eV/nm and the value of the step interaction parameter was set to g=1.174 eV/nm^2 based on the experimentally obtained ratio of g/β=3.6 [80] (see Table 5-1). For the physical crystallite under consideration, there are facets on the sides of the crystallite that are equivalent in symmetry to the top facet [14, 53]. Because of this symmetry, the structural evolution can be modeled by considering a subset of all the layers with an appropriately chosen boundary condition, schematically shown in the inset of Figure 5-6b). For volume-conserving shape evolution there is a layer midway between the symmetry-equivalent facets that does not move. As suggested in the inset of Figure 5-6b), the growth of the two adjacent facets requires equivalent mass flow toward this layer from the two adjacent facets. Therefore, the boundary condition for simulating the experiment is to cut the crystallite at this layer and use it as a bottom layer with fixed radius. This fixed layer is obtained from the point of intersection of initial and final shapes of the crystallite (here assumed PT shape for initial and c_{max} shape for final), calculated using the observed value of the initial and final facet radius during the experiment. Then, instead of conserving the volume (J_0=0) for the resulting subset of the entire crystallite, the step chemical potential at this layer is fixed to the final surface chemical potential $\mu=\beta\Omega/\rho_{final}$. This is not an exact description since the chemical potential at this point must evolve with time (see Figure 5-3b)). However this condition reproduces the experimentally observed final shape. This boundary

condition was compared to the Wulff-Kaishew boundary condition with volume conservation for a small crystallite and the results show a slightly shorter slow time constant τ_s. The values of $D_S c^0_{eq}$ and D_S/κ estimated in ref. [71] were used as initial estimate for the values of $D_S c^0_{eq}$ and D_S/κ used as fitting parameters to match simulation and experiment. The initial and final shapes of the simulated crystal shape are given in Figure 5-6 b). The final shape fits well to a c_{max} shape giving values of ρ_{cmax}=227.7 and g/β=3.88, consistent with experiment. The height as a function of time (squares) is given in Figure 5-6 a). The fit (solid line) gives the time constant τ_s=777±6.9 min, in very good agreement with experiment. The used values for $D_S c^0_{eq}$ and D_S/κ are 20000 s^{-1} and 0.1 nm, respectively.

The agreement in experiment and simulation is very good, however, the fitting parameters of $D_S c^0_{eq}$ and D_S/κ are different compared to results from ref. [71], especially for D_S/κ, which now suggests diffusion limited kinetics. Apart from considering a larger number of layers than in ref. [71], there are two main causes for this. The first is the precise specification of the initial and final shape of the crystallite, since this does have an affect on the observed τ_s as shown in the previous section. The second is again the boundary condition where ref. [71] used a fixed step-step distance between the second and third layer (fixed slope), while here the step chemical potential is kept fixed. However, if the physical situation of the boundary condition is accurately known, in principal it is possible to determine a unique pair of $D_S c^0_{eq}$ and D_S/κ (Table 1 of ref. [71]) from the fitted value of τ_s due to the extra constraint of the late stage slow-down.

5.4 Discussion

Previous studies of the global evolution of nanostructures within the continuum step model have focused on the case of shape-preserving solutions. This approximation is useful for systems undergoing complete decay, where mass is being transferred to a "reservoir" of constant chemical potential independent of the changes of the decaying structure. However, in the case of structural evolution, mass is being redistributed within the structure with concomitant changes in the chemical potential of the areas to which mass is being transferred. This correlated evolution of the chemical potential is clearly illustrated in Figure 5-3b). Therefore in the case of relaxation, the boundary conditions that limit the final state structure play an important role in defining the late-stage kinetics, and deviations from the universal behaviors of shape-preserving processes will be observed. Here we have simulated the late-stage behavior that arises from some physically reasonable scenarios for the boundary conditions.

The calculations quantify the expectation that as the evolution of a supported crystallite comes to an end, close to a stable state, the driving force for mass transport becomes small, and the time intervals between the sequential peeling events, which govern the reshaping, become very long. This slowing down is exponential with a time constant that scales linearly with the linear dimension of the crystallite. At this late stage of evolution the dominant driving force is no longer the 2D Gibbs-Thomson effect as it was in the initial stages of evolution. Instead, the kinetic process is dominated by cooperative mass transport between layers, ultimately mediated by the interface boundary condition. Thus the adhesion energy (within the formalism of the

Wulff-Kaishew theorem) and interface area define the approach to the final state. If the total interface energy is low the bottom layer expands during the evolution and the crystallite becomes trapped in the least stable of the metastable states, the c_{max} state, which is the first state to be reached by peeling. On the other hand if the interface energy is higher in the final state, the bottom layer shrinks and since the volume is conserved the crystallite bypasses the c_{max} state and stops at the first metastable state that matches the interface boundary condition.

As the size of nanostructures shrink, metastable states can not be avoided completely and must be considered for fabrication. With an ideal selection of the crystallite and substrate it is possible to control morphological changes and drive an evolving structure to the target state, even the ECS. Another control would be to have the boundary condition mediated by a vapor pressure surrounding the crystallite, in this way controlling the chemical potential of the interface and/or the steps on the surface, although controlling the volume would be difficult in this case.

Chapter 6: Distinctive Fluctuations in a Confined Geometry

Spurred by recent theoretical predictions [70, 97], we find experimentally using STM line scans that the fluctuations of the step bounding a facet edge exhibits scaling properties distinct from those of steps on vicinal surfaces. The correlation functions go as $t^{(0.14\pm0.03)}$ decidedly different from the $t^{(0.27\pm0.04)}$ behavior for fluctuations of isolated steps. From the exponents, we categorize the universality, confirming the prediction that the non-linear term of the KPZ equation, long known to play a central role in non-equilibrium phenomena, can also arise from the curvature contribution to the step free energy.

6.1 *Introduction*

Technological demands on the fabrication and properties of nano-structures [6, 37, 75, 76] provide renewed motivation for understanding the atomistic properties that control morphology changes on the nanoscales. In the past decade, the continuum step model has led to many quantitative successes in correlating direct observations of step fluctuations to kinetic and thermodynamic descriptions of nanoscale structural evolution [10, 22, 27, 98-100]. For complex structures where mass transport is constrained by geometry, the fundamental question of how fluctuations behave in a constrained environment becomes experimentally accessible. For an isolated step on a flat fcc(111) metal surface, experimental results often show that the principal mass transport mechanism is periphery diffusion (PD), with time correlations $\sim t^{1/4}$ [22, 27, 99, 100]. However, for smaller structures, issues of finite volume (shape effects and volume conservation) become non-negligible [80, 101]. Although the step can still be viewed as a 1D interface obeying a Langevin-type equation of motion, not only local deformation but global effects must be considered when calculating the step chemical potential. These considerations alter the equation of motion, including the noise term, resulting in different university classes of dynamic scaling [102].

6.2 *Background*

Finite-volume effects on nano-crystallites with a Gruber-Mullins-Pokrovsky-Talapov surface free energy density [15] have been found to produce metastable states with different crystal shapes [16] for a given crystal-substrate interface boundary

condition [41, 80, 81]. All shapes have a facet smoothly connected to a vicinal region, which obeys an $x^{3/2}$ shape-power law in equilibrium [8, 9, 52, 53, 59] and different power laws otherwise. Once a crystallite attains a stable state, the step that serves as the interface between the facet and the vicinal region (see Figure 6-1 b)) fluctuates around its stable position, which is defined by step-step interactions and the "reservoir" chemical potential of the crystallite. The shape effect (global curvature of the facet) can be directly evaluated for step chemical potential [103], and then enters the equation of motion as a non-linear term of the form $(\nabla x)^2$, characteristic of the Kardar-Parisi-Zhang equation (KPZ term). If the fluctuations are small compared to the inter-step spacing, the reservoir chemical potential and step-step interactions enter the step chemical potential as additional polynomial terms. Such terms also contribute to the KPZ term depending on the kinetics of the step. Furthermore, they affect the noise term and restrict the amplitude of fluctuation, which leads to different scaling properties of the noise. In recent theoretical work, such considerations were shown to give rise to the dynamic scaling of the facet-edge fluctuations, a roughness exponent of $\alpha=1/3$, different from that of a random walk, and a growth exponent $\beta=1/5$ or $\beta=1/11$, depending on the limiting kinetics, attachment-detachment or periphery diffusion, respectively [97]. General considerations of the different universality classes that can arise for different types of spatial confinement for the two cases of limiting kinetics are summarized in Table 6-1.

Here we report the first results of experimentally observed facet-edge fluctuations on stable Pb crystallites on a Ru substrate. The time correlation function $G(t)$ and saturated width w

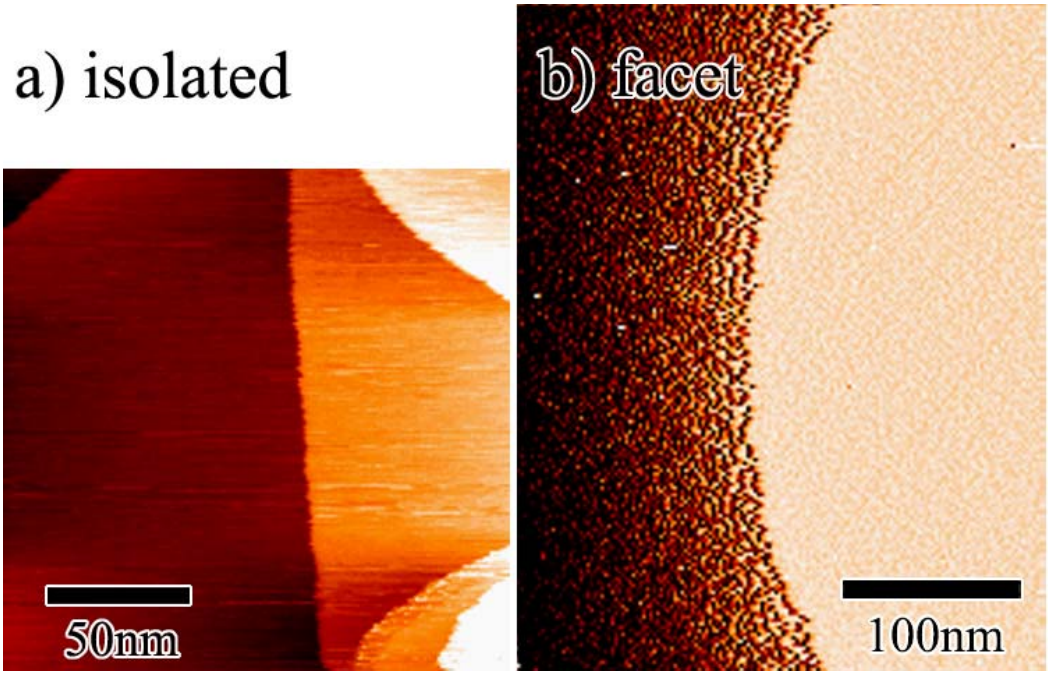

Figure 6-1 A STM image of a) an isolated step on a crystallite facet (room temperature) and b) a crystal facet edge or shoreline (80°C).

Table 6-1 Summary of the dynamical scaling universality classes for steps on solid surfaces. The geometries included are: Str-fr = an isolated step with no imposed curvature, Crv-fr = an isolated curved step such as boundary of an island, Str-cfn = straight steps confined by the presence of neighboring steps as in a step bunch, and Crv-cfn = curved steps confined by the presence of neighboring steps as at the edge of a finite-volume crystal. Following ref. [29], we characterize the relevant growth equations by 3 letters and a number. The first (L or N) indicates whether the equation is linear or non-linear (i.e. has a KPZ term). The second and the third (both C or N) indicate whether the deterministic part or the noise, respectively, is conservative or non-conservative. The number, 2 or 4, indicates the power of ∇ in the linear conservative term. We also indicate the dimensionality of the independent variable. Note that the universality classes associated with LCN2 and NNN2 are EW (Edwards-Wilkinson) and KPZ.

Geom.	A/D Class	α	β	z	PD Class	α	β	z
Str-fr	LCN2-1d	1/2	1/4	2	LCC4-1d	1/2	1/8	4
Crv-fr	NNN2-1d	1/2	1/3	3/2	NCN4-2d	2/3	1/5	10/3
St-fr	LCN2-2d	1/2 ($\rightarrow$0)	1/4 ($\rightarrow$0)	2	LCC4-2d	0	0	4
Crv-cfn	Cnstr-KPZ	1/3	1/5	5/3	NCC4-1d	1/3	1/11	11/3

$$G(t) = \left\langle \left[x(t - t_0) - x(t) \right]^2 \right\rangle_{t_0} \sim t^{2\beta} \tag{6-1}$$

$$w^2 = \left\langle \left[x(t) - \bar{x} \right]^2 \right\rangle_{t} \sim L^{2\alpha}, \tag{6-2}$$

are calculated from the temporal displacements $x(t)$ measured for the facet-edge fluctuations in a system of size L. At early times the time correlation function, eq.(6-1), has the indicated power-law increase, giving the growth exponent. For three different temperatures, results show that the exponents for facet-edge fluctuations are clearly different from isolated step-edge PD, and that they are close to the value of 2/11 predicted for facet-edge PD.

6.3 Experiment

Crystallites were formed by depositing a 20~30 nm thick Pb film at room temperature on a Ru(0001) substrate in UHV [58, 88, 104]. The film dewetted as it cooled and was left to equilibrate to a stable state at the temperature of experiment. Details of sample preparation are in refs. [14, 58, 68, 88, 104]. The crystallites are observed with a variable-temperature scanning tunneling microscope (VT-STM) after equilibration. Figure 6-1 depicts an STM image of a) an isolated step (room temperature) and b) facet-edge (80°C). A crystallite in a stable state as shown in b) has a flat, close to circular (111) facet and a smoothly connecting vicinal region. By repeatedly scanning over a single point on the facet-edge or step-edge, we obtain a line-scan STM image $x(t)$, as shown in Figure 6-2 for a) an isolated step (step from screw dislocation) and b) a facet-edge, both at 80°C. The time interval between measured time line scans is 0.02 s, and 2000 lines are measured per image. Digitized step positions $x(t)$

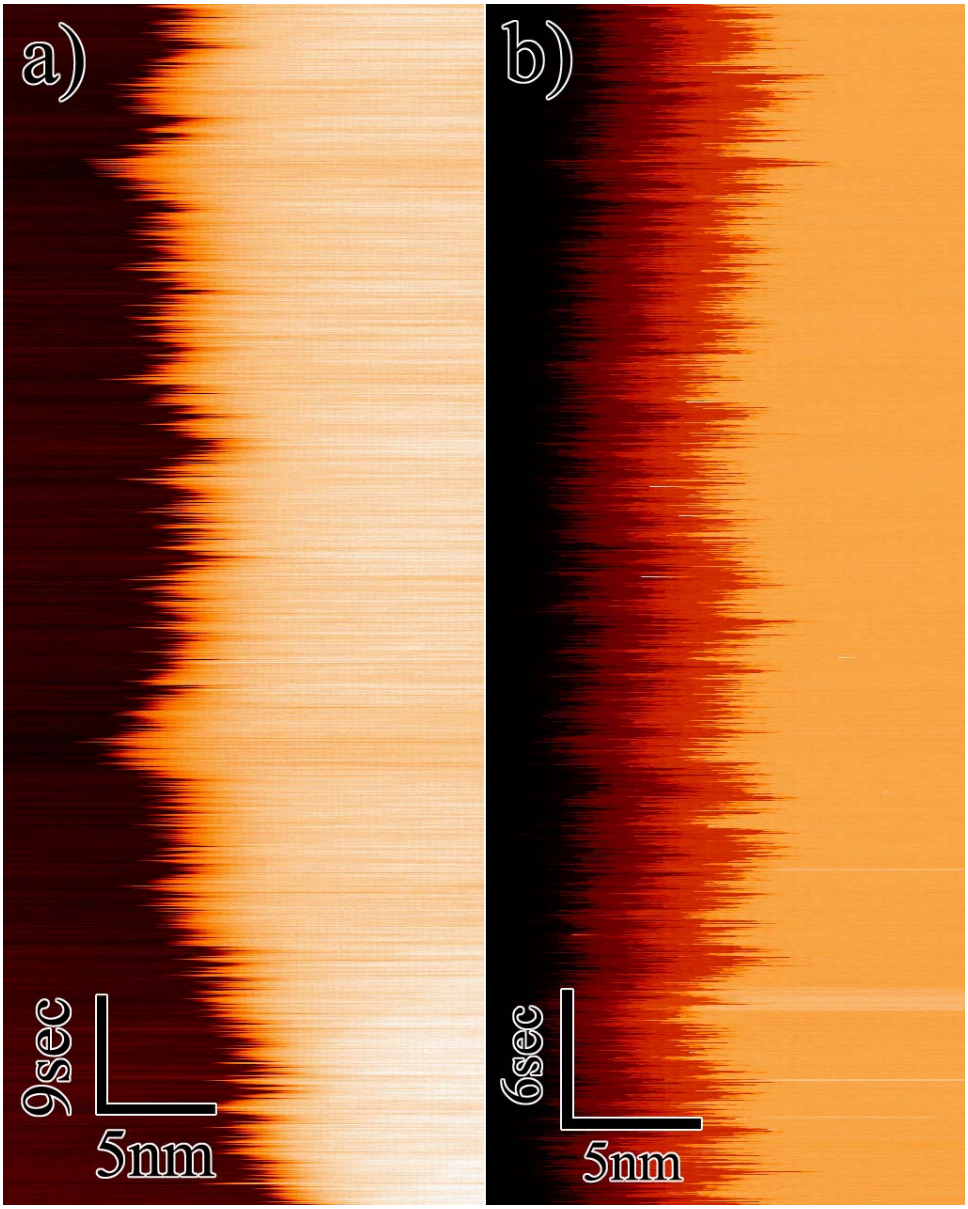

Figure 6-2 A line scan image of a) an isolated step (step from screw dislocation) and b) a facet-edge at 80°C, showing also the correlated fluctuations of the neighboring steps.

extracted from the line-scan images are used for statistical analysis. Correlation functions are calculated as an average over 10~30 individual measurements at one step position. For the confined steps, measurements were performed on facets of radii ranging from 60 to 190 nm.

6.4 Results

Time correlation functions, eq. (5-1), calculated from the data are shown in Figure 6-3 for a) facet-edges and b) isolated step-edges. Square, circle and triangle symbols correspond to room temperature, 80°C and 127°C, respectively. Different data sets for the same temperature are from different facets or steps. From all data sets, regardless of temperature, the average exponent is $2\beta = 0.14\pm0.03$ for facet-edge fluctuations, and $2\beta = 0.27\pm0.04$ for isolated step-edge fluctuations. These values are close to the predicted 2/11 and 1/4 for PD kinetics along a facet-edge and isolated step-edge.

For the isolated steps, the magnitude of the correlation function shown in Figure 6-3 increases monotonically with temperature, as expected [99]. For the confined steps (Figure 6-3 a)), the substantial variability in amplitude for different measurements at the same temperature is due to experiments performed on crystals of different facet radius. For instance, the three upper sets of data at 80°C, were taken on larger crystallites (radius > 100 nm). The size effect should yield a dependence of the mean squared width of the fluctuations that scales as $L^{2\alpha}$ (eq. (6-2)). This experimental dependence is shown in Figure 6-4, where the value of $L = w^2\tilde{\beta}/k_B T$ is plotted as a function of facet radius, where $\tilde{\beta}$ is the step stiffness (= 0.339 eV/nm at

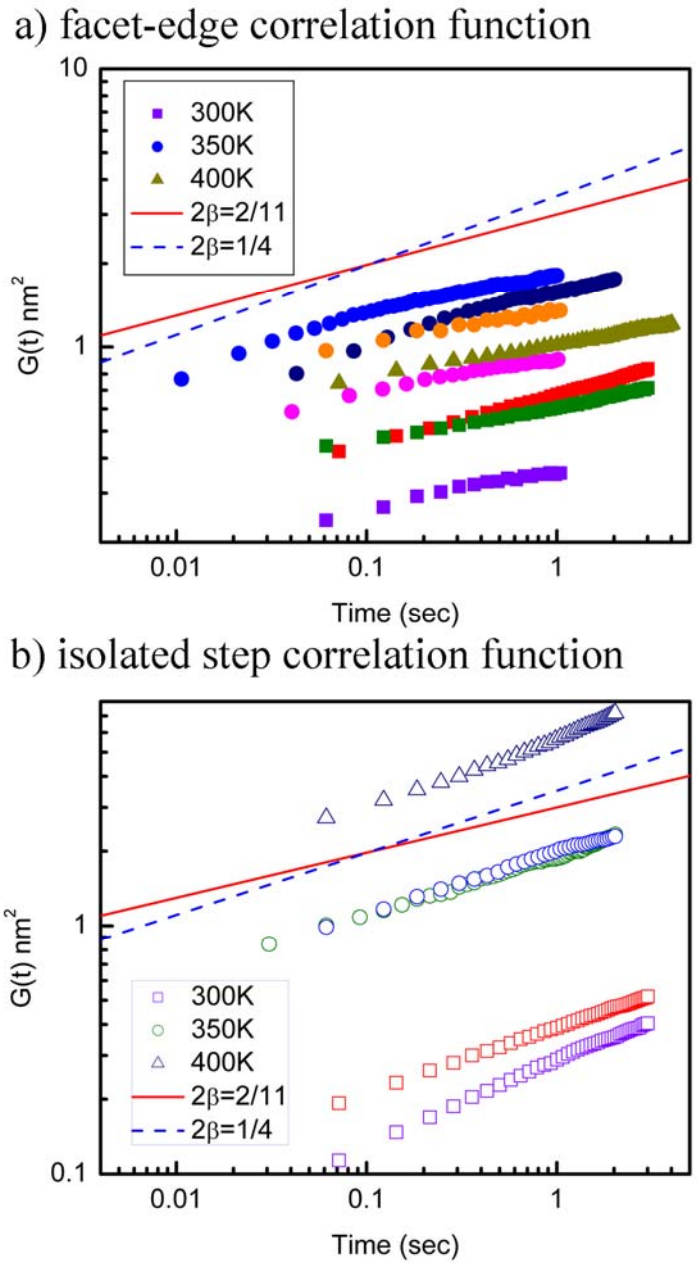

Figure 6-3 Log-log plot of time correlation functions, at different temperatures, of a) facet edges and b) isolated steps: room temperature (squares), 80°C (circles) and 127°C (triangles). Results from the fit give an average exponent β of 0.14±0.03 for shoreline fluctuations and 0.27±0.04 for isolated- step fluctuations. For guidance, solid and dashed lines show slopes 2/11 and 1/4, respectively.

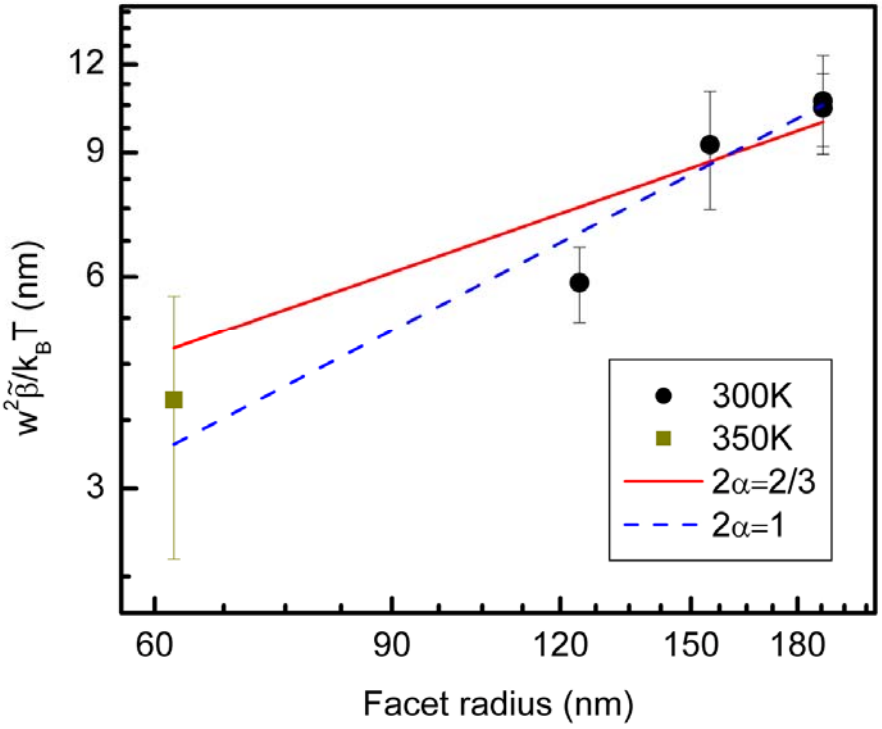

Figure 6-4 Saturation width as a function of facet radius (facet-edge only). Circles and squares are room temperature and 80°C, respectively. Solid and dashed lines are a fit to the 80°C data with $\alpha=1/3$ and $\alpha=1/2$, respectively.

room temperature and 0.327eV/nm at 80°C [87, 89]). The square and circles correspond to values at room temperature and 80°C, respectively. Based on the assumption that the system size is proportional to the facet radius, the data are fit by $\alpha=1/3$ (solid) and $\alpha=1/2$ (dash). Although $\alpha=1/2$ gives a better fit, there is not enough data to draw a definitive conclusion. Direct experimental observation, such as the spatial correlation function on a quenched crystallite, is needed to obtain α for facet-edge fluctuations.

6.5 Discussion

The facet-edge fluctuations clearly show a different universality class of dynamic scaling than that of an isolated step on a surface. Unlike previous experimental studies of the step exponents [10, 22, 105, 106] the origin of this difference is not in the underlying physical mechanism of the kinetics. Instead the effect results from the coupling of the step chemical potential, which is a thermodynamic quantity defined by the configuration and environment of the step, to the fluctuations. The "isolation" of any non-confined step can be easily perturbed by the environment, resulting in changes in the measured prefactor or even the exponent of the time correlation function. Changes in the prefactor are expected for instance due to the asymmetry in step stiffness[107]. Perturbation of an isolated step by an external electric field reportedly produces higher-order corrections-to-scaling to the leading $t^{1/4}$ term. Thus, it is extremely important to control the step environment (fields or densities) when performing quantitative analysis.

For facet-edge fluctuations the step confinement is due to an increase in local step chemical potential when the step is displaced from equilibrium. The functional behavior of $\mu(x)$ results from a competition between the step-repulsions from the vicinal region and the 2-d pressure of the adatom density on the facet, which in turn in defined by the constraints governing the crystallite shape[16, 80]. For a step symmetrically confined on a vicinal surface, the confinement corresponds to a force that is quadratic in displacement[108]. For the facet-edge step, the asymmetry in the $\mu(x)$ corresponds to an asymmetric confining force that includes a cubic term in displacement [109]. These thermodynamic conditions of the confined facet-edge step lead to the dynamic universality class explained above. The value $\alpha=1/3$ is obtained in a TSK model with entropic interactions between steps and volume conservation of the crystallite using statistical methods [70]. Although there are not yet any experimental results for a system with attachment/detachment kinetics, our theoretical prediction for that case (Table I) seems to correspond to MC results on a restricted solid-on-solid (RSOS) model, which additionally includes a somewhat artificial mechanism to limit the fluctuation width[110]. To investigate the issue further, we are carrying out MC simulations of a model in which step interactions and volume conservation should naturally limit the fluctuation width, and the kinetics is PD limited [111].

We have experimentally, for the first time, observed a growth exponent of $\beta\approx1/11$, for the case of geometrically confined fluctuations. The value $\beta=1/11$ belongs to a universality class of dynamical scaling with $\alpha=1/3$ and $z=11/3$, which can be obtained from the KPZ equation (without the linear term) for small-amplitude

fluctuations [29, 97, 112]. This is the first time that a KPZ type equation of motion, traditionally used to explain non-equilibrium properties, was observed in the context of equilibrium. Change in the fluctuations and equation of motion for steps in a perturbed environment, may introduce new opportunities in controlling the fabrication of nano-structures, or in new aspects of their dynamic properties. More detailed discussion of the evolution of nano-structures in which fluctuations are confined will be presented elsewhere [83].

Chapter 7: Facet-edge fluctuations with periphery-diffusion kinetics

7.1 Introduction

Due to the rapidly growing interest in quantum computing and the related demand for creating quantum dots, controlled fabrication of nano-structures becomes of importance [6, 37, 75, 76]. To accomplish this, the control of step dynamics is crucial, since the steps are the fundamental building blocks of crystalline structure, and thus understanding the step equations of motion is the key. For steps on flat surfaces this is well established with the use of the continuum step model, having success in the description of e.g. MBE growth or step bunching etc. The continuum step model is a powerful model applied to both analysis of experimentally observed motion of steps [10, 22, 98, 99] and comparsion to microscopic models, such as the terrace-step-kink (TSK) model, and for connecting atomistic energies to kinetic or thermodynamic parameters using statistical methods [22, 109]. Langevin-type analysis with the continuum step model has also had great success, revealing the equilibrium properties of isolated steps on surfaces. The experimentally accessible correlation function scale as $\sim x^{2\alpha} t^{2\beta}$, where α and β are the roughness and growth exponents, respectively. For isolated steps it is well known that $\alpha=1/2$, characteristic of a random walk and β depends on the principal mass transport mechanism, for attachment-detachment (A/D) $\beta=1/4$ and periphery diffusion (PD), $\beta=1/8$ [10, 22].

For nano-structures, the determination of the step equation of motion is non-trivial compared to steps on flat surfaces due to the issues of finite volume of the nano-structure [80, 101]. Although the steps can still be viewed as a 1D interface, not only local deformations but global effects such as shape and volume conservation must be considered in the determination of the equations. These considerations alter

the step chemical potential and even the noise term of the Langevin equation, resulting in different university classes of dynamic scaling [97, 110, 113]. In a previous paper, we have shown that a global curvature of a step (e.g. facet or island) results in a non-linear equation of the step equation of motion [97] illustrated in Figure 7-1. Furthermore for a facet the fluctuation amplitude is strongly suppressed by the existence of a neighboring step and volume conservation, and is not a "random walk" in contrast to an isolated step. Such suppression of the fluctuation results in a different scaling behavior of the fluctuation width [110], which gives $\alpha=1/3$ [70].

However, it was also concluded in this work that for the curvature effect to be strong, the facet must be small compared to the capillary length and this condition can be washed out by the 2D Gibbs-Thomson effect [12, 86]. In this paper, we show with the use of the continuum step model that even with no curvature (straight steps), interactions with the neighboring step and conserved dynamics can result in a nonlinear term, similar to the curvature effect, in the equation of motion of the facet. Monte Carlo simulations are performed to confirm the proposed model.

7.2 Background

The continuum step model is a discrete array of 1D continuous interfaces, which represent the steps on the surface. Here we consider a crystallite facet-edge with infinite volume thus straight steps on average with no global curvature, also illustrated in Figure 7-1. With appropriate approximations, the step equation of motion, can be written down as a Langevin equation

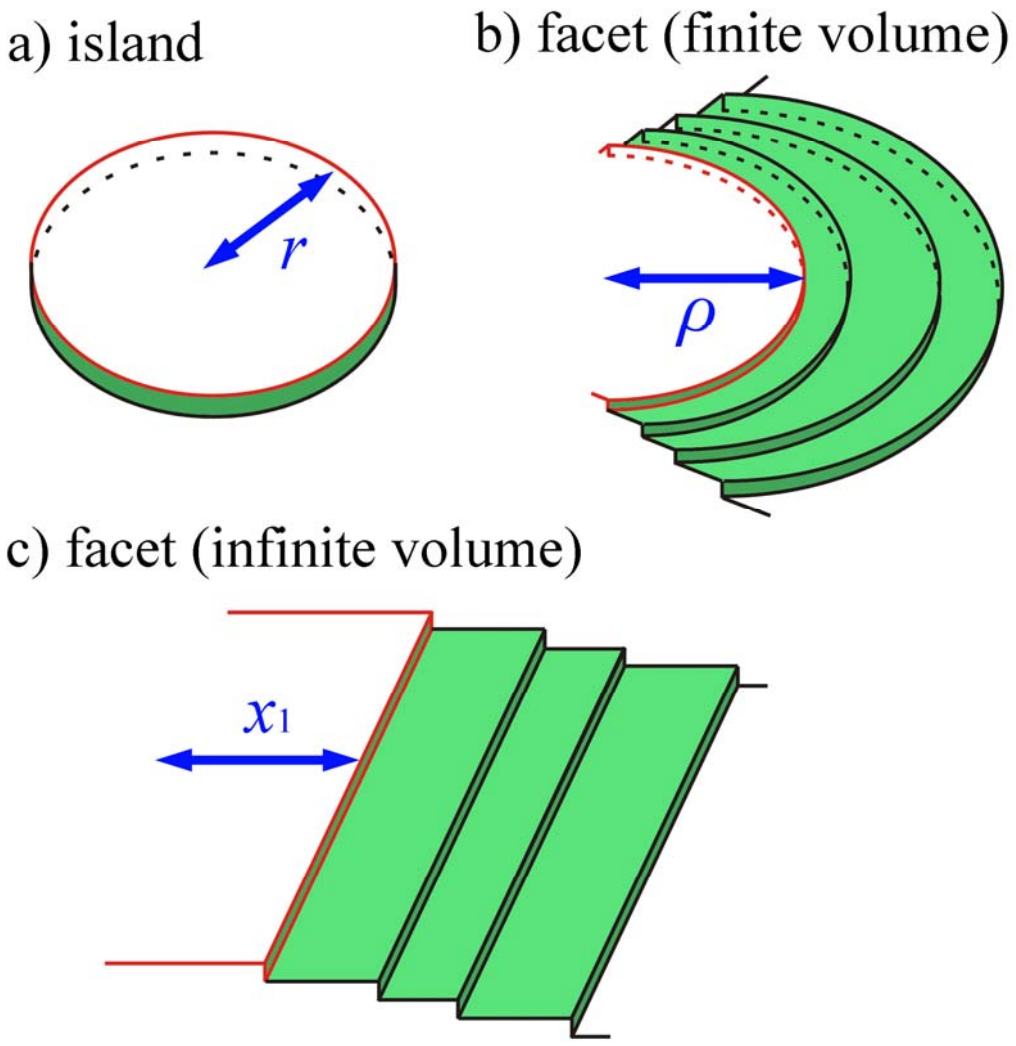

Figure 7-1 Schematic drawing of the continuum step model in the three cases of a) an island with radius r b) a facet of a finite volume crystallite (with curvature) with radius ρ and c) a facet of a infinite volume crystallite (straight steps) with radius x_1.

$$\frac{\partial x(y,t)}{\partial t} = f[x(y,t)] + \eta(y,t), \tag{7-1}$$

where $x(y,t)$ is the position the facet edge at time t, $f[\bullet]$ is a function of $x(y,t)$ describing the deterministic relaxation process, and $\eta(y,t)$ is a noise term, which can be conservative or non-conservative depending on the nature of $f[\bullet]$. The deterministic process $f[\bullet]$ is obtained by starting from the total free energy of the facet layer. The free energy of the step is the sum of the step creation energy and interaction from the neighboring step. For a straight step with arbitrary length L, this is

$$F = \int_0^L \left(\beta(\theta) \sqrt{1 + \left(\frac{\partial x}{\partial y} \right)^2} + \frac{g h^3}{(x_2 - x)^2} \right) dy, \tag{7-2}$$

where β is the step free energy per length, g the interaction coefficient and x_2 the (mean) position of the neighboring step, which is here fixed. Then the step chemical potential is derived as

$$\mu[x, \dot{x}, \ddot{x}] = \frac{\delta F}{\delta N} = \Omega \left(\frac{-\tilde{\beta} \ddot{x}}{\sqrt{(1 + \dot{x}^2)^3}} + \frac{2 g h^3}{(x_2 - x)^3} \right), \tag{7-3}$$

where Ω is the atomic area, $\tilde{\beta} = \beta + \partial^2 \beta / \partial \theta^2$ is the step stiffness and the superscript dot denotes differentiation with respect to y. Once the step chemical potential is derived, the deterministic part of the Langevin equation is determined by modeling the microscopic transfer processes at the step edge. For A/D, this is represented by non-conserved dynamics with adatoms attaching and detaching at random positions on the step edge from a thermodynamic reservoir

$$\frac{\partial x(y,t)}{\partial t} = \frac{-\Gamma_{AD}}{k_B T} \mu[x, \dot{x}, \ddot{x}] + \eta(y,t), \tag{7-4}$$

where Γ_{AD} is the attachment-detachment mobility and $\eta(y,t)$ is non-conserved white noise. Similarly for PD, we use conserved dynamics to represent atoms moving along the step edge as

$$\frac{\partial x(y,t)}{\partial t} = \frac{\Gamma_{PD}}{k_B T}\frac{\partial^2 \mu[x,\dot{x},\ddot{x}]}{\partial y^2} + \eta_C(y,t), \tag{7-5}$$

where Γ_{PD} is the step-hopping mobility and $\eta_C(y,t)$ is conserved white noise.

7.3 Results

To obtain the mean stable position x_1 of the facet edge, eq. (7-3) is set equal to a "reservoir" chemical potential μ_0 [80] neglecting the local curvature term, giving

$$x_1 = x_2 - h\left(\frac{2\Omega g}{\mu_0}\right)^{1/3} \qquad \text{or} \qquad d = h\left(\frac{2\Omega g}{\mu_0}\right)^{1/3} \tag{7-6}$$

where $d=x_2-x_1$ is the distance between the top two steps. Assuming that the fluctuations are small, eq.(7-3) is expanded about a x_1 ($\dot{x}=0$) as

$$\mu[x,\ddot{x}] = -\Omega\tilde{\beta}\ddot{x} + \mu_0 + \frac{3}{h}\left(\frac{\mu_0^4}{2\Omega g}\right)^{\frac{1}{3}}(x-x_1) + \frac{3}{h^2}\left(\frac{2\mu_0^5}{\Omega^2 g^2}\right)^{\frac{1}{3}}(x-x_1)^2 + \cdots. \tag{7-7}$$

Converting to dimensionless variables

$$\tilde{x} = \frac{x-x_1}{x_1}, \quad \tilde{y} = \frac{y}{x_1}, \quad \tilde{d} = \frac{d}{x_1}, \quad \tilde{\mu} = \frac{x_1\mu}{\Omega\tilde{\beta}}, \quad \tilde{g} = \frac{gh^3}{\tilde{\beta}x_1^2} \tag{7-8}$$

eq. (7-7) becomes

$$\tilde{\mu}[\tilde{x},\ddot{\tilde{x}}] = -\ddot{\tilde{x}} + \tilde{\mu}_0 + \frac{6\tilde{g}}{\tilde{d}^4}\tilde{x} + \frac{12\tilde{g}}{\tilde{d}^5}\tilde{x}^2 + \cdots. \tag{7-9}$$

In the PD case we obtain

$$x_1 \frac{\partial \tilde{x}(y,t)}{\partial t} = \frac{\Gamma_{PD}\Omega\tilde{\beta}}{k_B T x_1^3}\left(-\frac{\partial^4 \tilde{x}}{\partial \tilde{y}^4} + \tilde{\mu}_0 + \frac{6\tilde{g}}{\tilde{d}^4}\frac{\partial^2 \tilde{x}}{\partial \tilde{y}^2} + \frac{24\tilde{g}}{\tilde{d}^5}\left(\frac{\partial \tilde{x}}{\partial \tilde{y}}\right)^2 + \cdots \right) + \eta_C(y,t) \tag{7-10}$$

Notice the non-linear term in eq. (7-10), characteristic of the Kardar-Parisi-Zhang (KPZ) equation. This term arises only from the asymmetry of the effective potential that the facet feels due to the fact that it has a neighboring step only on one side. The scaling behavior at long time (still shorter than the crossover time) is determined by the relative magnitude of the terms, and the scaled distance between the top two steps must be at most $\tilde{d}$ = 4 for the KPZ term to dominate, otherwise the linear term dominates. When $\tilde{g}$=0, it is easy to see that eq. (7-10) reduces to the equation for an isolated step.

We turn to the effective thermodynamic potential that the facet edge feels during its fluctuation and understand its asymmetry. For a straight step, this potential is obtained by adding the "reservoir" term μ_0 to the free energy in eq. (7-2) giving

$$\tilde{\Omega}(\tilde{x}) = \frac{\beta}{\tilde{\beta}} + \frac{\tilde{g}}{(\tilde{d}-\tilde{x})^2} - \tilde{\mu}_0(\tilde{x}+1) \quad \text{where} \quad \tilde{\Omega}(\tilde{x}) = \frac{\Omega(x)}{\tilde{\beta}L}. \tag{7-11}$$

For small fluctuations this is expanded in $\tilde{x}$ giving

$$\tilde{\Omega}(\tilde{x}) \cong \left(\frac{\beta}{\tilde{\beta}} + \frac{\tilde{g}}{\tilde{d}^2}\right) + \frac{3\tilde{g}}{\tilde{d}^4}\tilde{x}^2 + \frac{4\tilde{g}}{\tilde{d}^5}\tilde{x}^3 + \cdots. \tag{7-12}$$

Comparing with eq. (7-9) the asymmetric $\tilde{x}^3$ term in the effective potential eq. (7-12) is responsible for the non-linear term in eq. (7-10).

7.4 Simulation

Metropolis Monte Carlo simulations (MCS) are performed based on a standard TSK model (square lattice closed-packed) with PD kinetics. In the TSK model the only excitations are thermally excited kinks with energy ε along a step denoted by a single-valued function $x_n(y)$. The Hamiltonian of the step includes a term $\varepsilon|x_n(y+1)-x_n(y)|$, which results in a high symmetry step free energy per length of $\beta = \varepsilon/a+k_BT\log(\tanh(\varepsilon/2k_BT))/a$ [30] (a is the atomic length) and step stiffness of $\tilde{\beta}=(2k_BT/a)\sinh^2(\varepsilon/2k_BT)$ [23]. There is also a non-touching constraint that requires $x_{n+1}(y)>x_n(y)$, which results in a entropic repulsion of $g=(\pi k_BT)^2/6h^3\tilde{\beta}$ [33]. Using these results of the TSK model, some of the thermodynamic parameters introduced above can be calculated. Assuming a Pokrovsky-Talapov equilibrium crystal shape (PTECS) yields $\mu_0=\beta\Omega/x_1$ [8], Figure 7-2 a) shows the product $\tilde{d}\times(x_1/a)^{2/3}$ as a function of temperature T [ε/k_B] (solid line) within the TSK model. This shows that, if the facet radius x_1 (crystallite volume) is not significantly small, the required condition $\tilde{d}\leq 4$ for the KPZ term to dominate the scaling behavior is satisfied for most temperatures. Also plotted in Figure 7-2 a) is the dimensionless capillary length $k_BT/\tilde{\beta}a$ (dashed line), which indicates that x_1 must be pretty small for the non-linear term due to curvature [97] to be effective. PD kinetics is obtained by moving atoms to their neighboring sites from randomly chosen step positions. When an atom moves to a neighboring position on the step it necessarily breaks and reforms bonds. With just nearest neighbor bonds, the net change in energy has only 3 possibilities, corresponding to the net gain/loss of 2 (±4ε), 1 (±2ε), 0 bonds.

For facet-edge fluctuation analysis, the spatial and time correlation functions, $G(y,t_0)$ and $G(y_0,t)$, respectively,

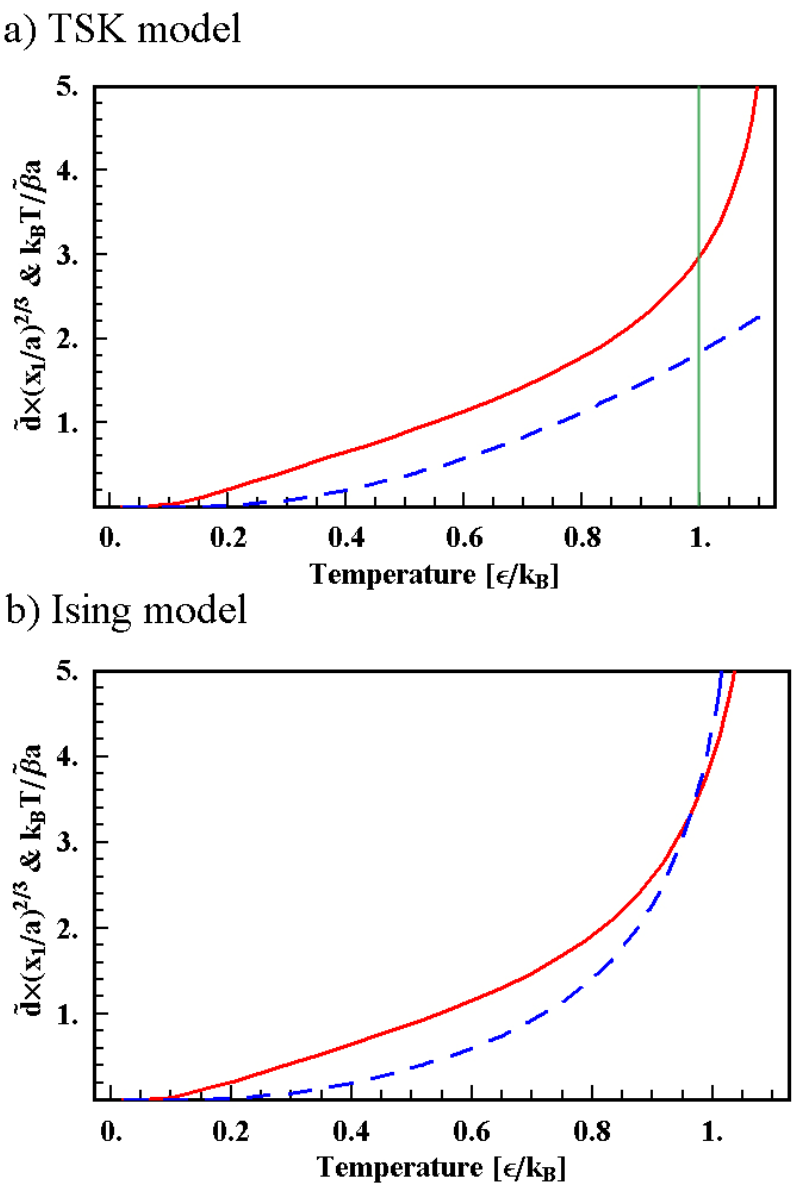

Figure 7-2 Product of the step-step distance and facet radius $\tilde{d}\times(x_1/a)^{2/3}$ (solid line) and capillary length $k_BT/\tilde{\beta}a$ (dashed line) as a function of temperature T [ε/k_B]. Thermodynamic parameters, step free energy β, step stiffness $\tilde{\beta}$ and step-step interaction coefficient g calculated within the a) TSK model and b) Ising model. Temperature of the simulation is given in a) as a thin vertical line.

$$G(y,t_0) = \left\langle \left[x(y+y_0,t_0) - x(y_0,t_0) \right]^2 \right\rangle_{y_0}, \tag{7-14a}$$

$$G(y_0,t) = \left\langle \left[x(y_0,t+t_0) - x(y_0,t_0) \right]^2 \right\rangle_{t_0}, \tag{7-14b}$$

are calculated for a fully equilibrated step (checked from the width). For lengths and time shorter than the correlation length and crossover time, respectively, the correlation functions scales as $G(y,t_0) \sim y^{2\alpha}$ and $G(y_0,t) \sim t^{2\beta}$, providing the roughness exponent α and growth exponent β. Figure 7-3 shows a snap shot of a MCS of an isolated step (d=500) for $T = \varepsilon/k_B$ (vertical line in Figure 7-2 a)) and L=100, initial (orange) and after equilibration (green). Here, the maximum amplitude of the fluctuation of an isolated step is approximately 8 lattice spacings. To simulate confinement, the neighboring step is placed a distance d=2,3,4,5,6, illustrated in Figure 7-3 for d=4 (solid red line). Figure 7-4 shows results of $G(y_0,t)$ obtained after equilibration for 10^5 MC steps and averaged over 10 realizations. Temperature and step length are the same as Figure 7-3. Figure 7-4 a) shows results for d=4 with a definite crossover. A fit to the data is also shown, first a slope with m~0.25 and later with m~0.18, very close to the predicted values of 2β=1/4 for an isolated step-edge, and 2β=2/11 for facet-edge fluctuations, with PD kinetics. Figure 7-4 b) shows results for d=2,3,4,5,6 and 500. For d=2 the neighboring step is so close that the 2β=2/11 regime cannot be identified, it shows a more logarithmic behavior β=0, characteristic of an isolated 2D system (also notice the quick saturation time). As the step-step distance increases the crossover point from 2β=1/4 to 2β=2/11 behavior also increases. Finally, when d>6 it is nearly equivalent to an isolated step with 2β=1/4 within the range of 10^5 MC steps. Figure 7-5 shows results of $G(y,t_0)$ obtained after equilibration as in Figure 7-4, for d=4 and d=500. Since the length of the step is too

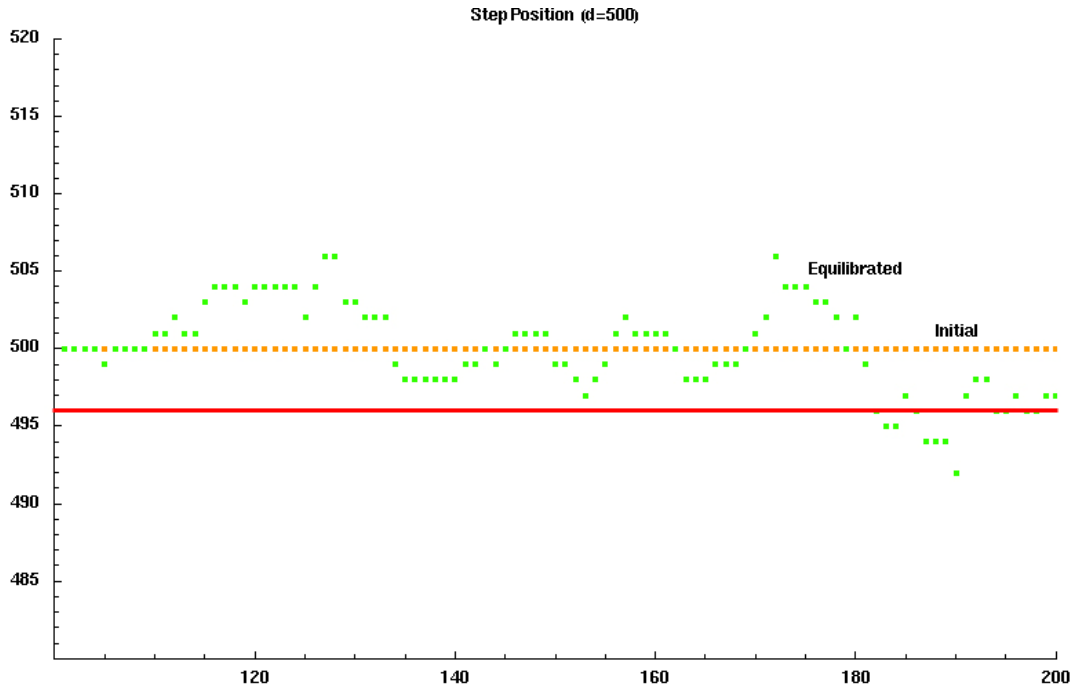

Figure 7-3 A snap shot of the MC salutation of an isolated step (d=500) for T= ε/k_B and L=100. Initial step (orange) and equilibrated step (green). The red line is an illustration of position of the neighboring step for d=4.

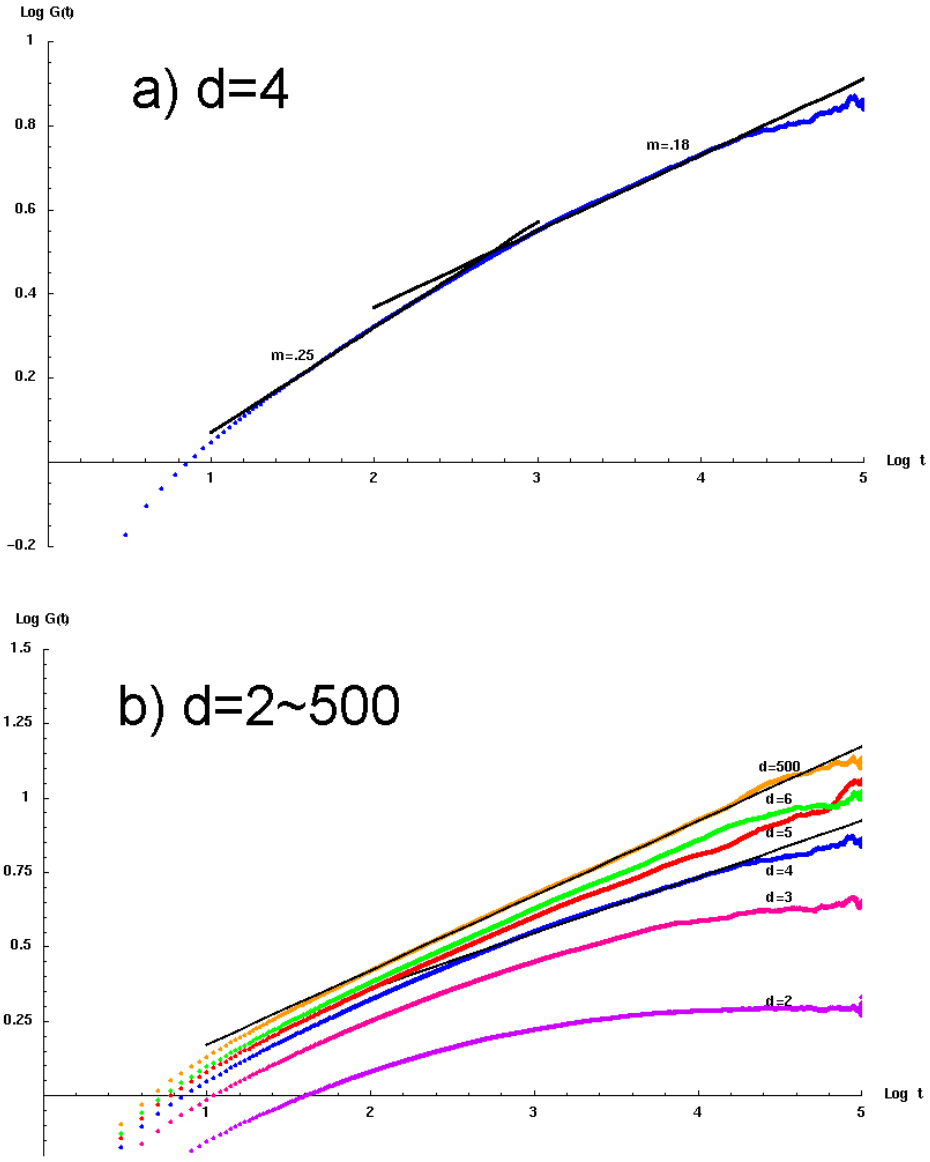

Figure 7-4 $G(y_0,t)$ obtained after equilibration. 10^5 MC steps and averaged over 10 realizations. a) shows results for d=4 with a fit to the slope of ~0.25 and ~0.18, close to the predicted values of $2\beta=1/4$ and $2\beta=2/11$. b) shows results for d=2~500. For d=2 the logarithmic behavior of $\beta=0$ is observed and for d=500 it is exactly $2\beta=1/4$.

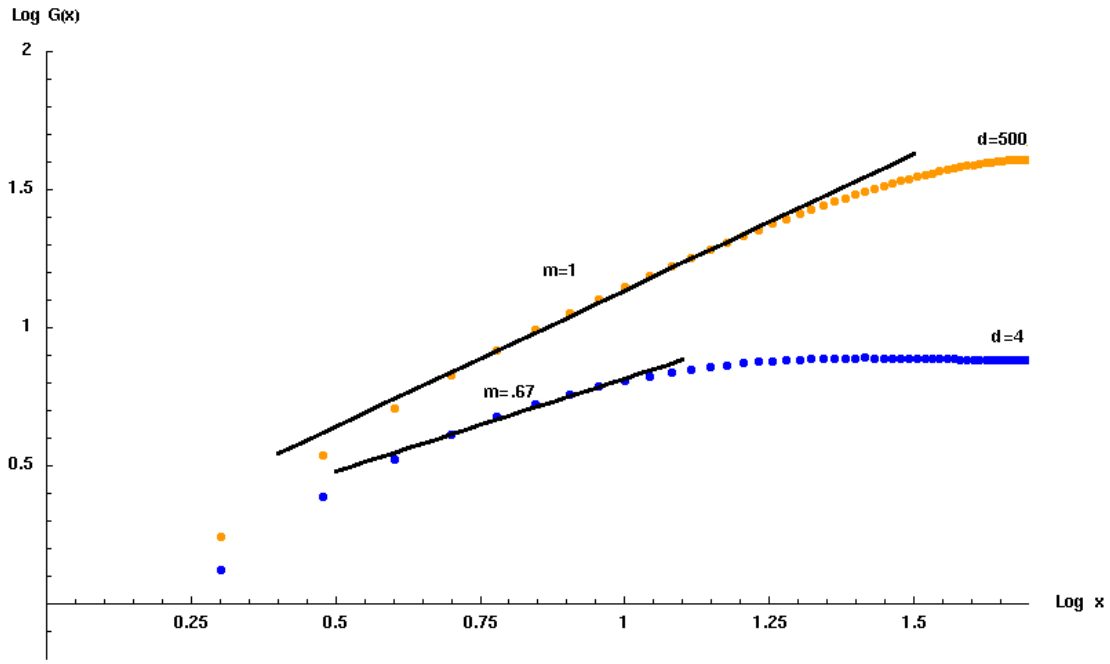

Figure 7-5 Results of $G(y,t_0)$ obtained after equilibration for d=4 (blue) and d=500 (orange). The fit is ~1 and ~0.67 for d=4 and d=500, respectively. Saturation values are 0.85 and 1.6 for d=4 and d=500, respectively.

short it is difficult to say anything conclusive, however, the initial portion of the data is fit to a slope of m~0.67 and m~1.0 for d=4 and d=500, consistent to the prediction for restricted and non-restricted steps, $2\alpha=2/3$ and $2\alpha=1$, respectively. From the saturation value of $G(y,t_0)$, 0.85 for d=4 and 1.6 for d=500, the interface width can be calculated as w=3.5 and w=20, respectively, consistent with the amplitude restrictions (see also Figure 7-3).

Although the TSK model is a good model to describe steps at low temperature it is not applicable for high temperatures since overhangs are prohibited. To include such behavior the Ising model must be considered. Figure 7-2 b) shows the product of the step-step distance and facet radius $\tilde{d}\times(x_1/a)^{2/3}$ and capillary length $k_BT/\tilde{\beta}a$ calculated within the Ising model. Although the Ising model gives larger values for both $\tilde{d}\times(x_1/a)^{2/3}$ and $k_BT/\tilde{\beta}a$ then the TSK model, the qualitative arguments are still valid that the facet radius must be significantly small for any of the conditions not to be satisfied.

7.5 Discussion

In the preceding sections we only discussed PD, and neglected A/D, which is certainly an important equilibration mechanism in many systems [10, 22]. It should be clear from eq. (7-4) and eq. (7-8) that A/D will not generate a KPZ term, so that the experimental relevance of our results may appear rather limited. In fact, that is not the case, and the reason is rather subtle. It has to do with conservation of mass. At equilibrium, since the volume of the crystallite is fixed, there is no size fluctuation from atoms coming on and off the crystallite itself. However, the individual layers

composing the crystallite may be seen as non-volume conserving systems that fluctuate around their stable shape and position, exchanging matter with an effective adjacent "reservoir", whose chemical potential is determined by the conservation of the crystallite volume. The key point here is that, strictly speaking, this is not a thermodynamic reservoir [93] and although the mass may not be conserved within one layer it must be overall. Now, for steps that obey the Gruber-Mullins-Pokrovsky-Talapov surface free energy density, the celebrated Wulff construction yields the stable positions that results in the Pokrovsky-Talapov equilibrium crystal shape (PT-ECS), which has a $z \sim x^{3/2}$ dependence near the facet edge with the step density increasing with x. As mentioned above, at equilibrium the layers fluctuate around their stable position, exchanging mass among the layers. However, far from the facet the fluctuations are strongly suppressed due to the high step density. Thus, it is energetically highly unfavorable for any mass to be transferred far away from the facet. As a result the facet is the layer that fluctuates the most. Since atoms cannot travel far away, the net result is that mass leaving the facet edge tends strongly to return to it, in a way reminiscent of step fluctuations in the presence of a strong Ehrlich-Schwoebel barrier [24].

Chapter 8: Open questions and Future work

In this final chapter I present some of the open questions in the theory and also some of the experimental work, which can be performed in the future. Such work will give more insight to how we can control and manipulate finite-volume nano-size systems and make use of them in the future of nano-technology.

8.1 Theory

Theoretical work on the Langevin theory of the facet with other mechanisms other than PD such as A/D should be considered. For the A/D case, when the curvature term is small, the KPZ term in the Langevin equation does not exist, however, the equation is still non-linear when including the asymmetric term in the expansion of the potential. It will be interesting to see their scaling behaviors.

Including more steps in the MCS will be interesting so that the neighboring step can also fluctuate. In such case an in phase fluctuation of the top layers may weaken the asymmetric effect of the top facet potential. Such effect should be different for different volume crystallites since even with more steps finally it will come down to the boundary condition again.

Boundary conditions for non-equilibrium systems must be further investigated to capture the late stages of the crystallite evolution. The expanding of the interface itself should be expressed in terms of its own thermodynamics and given as an input to the whole crystallite evolution. Not only adhesion energies but epitaxial stress [41, 95] should be considered in such thermodynamics.

The greatest challenge is the modeling of the projected surface free energy per area. Although the Gruber-Mullins-Pokrovsky-Talapov surface free energy density is a fairly good approximation, interaction between steps only depending on the distance in the radial direction is clearly wrong. Also asymmetry of the thermodynamic paramaters must be included to model low temperature properties, making the mathematical problem 2D raising more challenges.

8.2 Experiment

Despite the lack of statistics throughout the work, additional experiments should be done as follows.

The determination of the roughness exponent α of facet-edge fluctuations is challenging. A quench experiment from a fully equilibrated crystallite at high temperature to a temperature where the kinetics is practically frozen will enable direct observation of the spatial correlation function by STM giving the exponent α.

Fluctuation measurements of different orientation facets is also a challenge since different orientation give different mass transport mechanisms[22]. Such measurement can be done, although very difficult, on side facet, which have been observed[14, 92]. Or reports also show that changing the substrate or even just changing the crystallographic orientation of the substrate can lead to different orientation of the facet[78].

Changing the substrate or crystallographic orientation of the substrate is interesting for crystallite evolution experiments. For Pb, graphite is another candidate to create clean crystallites. To investigate if the physical interface really influences the later part of evolution or only symmetry arguments, side facets, is good enough to explain the evolution is interesting.

The metastable states should be investigated with other crystallites, Ag, He and others, which display facets with vicinal surfaces. Thermodynamic parameters obtained from such fact will play an important roll in shape and size control of these nano-size crystallites.

Appendices

Appendix A

For the PT-ECS (c=0) all calculations can be done analytically, and size scaling can be done using the volume of the crystallite. We define dimensionless quantities of the adhesion energy (temperature), volume, excess chemical potential, facet radius, crystallite height, interface radius and contact angle as follows

$$\widetilde{E}_A = \frac{(g(2\gamma_0 - E_A)^2)^{1/3}}{\beta / h}, \qquad \widetilde{V} = \frac{V}{h\Omega}, \qquad \widetilde{\mu}_S = \frac{\mu_S}{(\Omega^2(2\gamma_0 - E_A)\beta^2)^{1/3}},$$

$$\widetilde{\rho}_0 = \frac{\rho_0}{(\beta\Omega/(2\gamma_0 - E_A))^{1/3}}, \qquad \widetilde{z}_h = \frac{z_h}{h((2\gamma_0 - E_A)^2\Omega/\beta^2)^{1/3}},$$

$$\widetilde{R}_b = \frac{R_b}{(\beta\Omega/(2\gamma_0 - E_A))^{1/3}}, \qquad \tan\widetilde{\varphi}_b = \frac{\tan\varphi_b}{(\beta/gh)^{1/2}}. \tag{A-1}$$

This gives the following analytical relationships between dimensionless variables, which are shown in Figure 2-1

$$\widetilde{\mu}_S = \left(\frac{2\pi(140 + 252\sqrt[3]{2}\widetilde{E}_A + 135\sqrt[3]{2^2}\widetilde{E}_A^2)}{35\widetilde{V}}\right)^{1/3},$$

$$\widetilde{\rho}_0 = \widetilde{z}_h = \left(\frac{140\widetilde{V}}{\pi(140 + 252\sqrt[3]{2}\widetilde{E}_A + 135\sqrt[3]{2^2}\widetilde{E}_A^2)}\right)^{1/3},$$

$$\widetilde{R}_b = (2 + 3\sqrt[3]{2}\widetilde{E}_A)\left(\frac{35\widetilde{V}}{2\pi(140 + 252\sqrt[3]{2}\widetilde{E}_A + 135\sqrt[3]{2^2}\widetilde{E}_A^2)}\right)^{1/3},$$

$$\tan\widetilde{\varphi}_b = \frac{\sqrt{\widetilde{E}_A}}{\sqrt[3]{2}}. \tag{A-2}$$

For $c \neq 0$ states size scaling is not done in terms of the volume but in terms of the characteristic facet radius at each state numerically calculated for constant volume. Here we define dimensionless values of position, shape parameter, cross section, interface radius, crystal height, contact slope, excess chemical potential, crystallite volume, crystallite free energy and energy barrier ΔE as

$$\tilde{r} = \frac{r}{\rho_c}, \qquad \tilde{c} = \frac{cgh}{\rho_c \beta}, \qquad \tilde{z}(\tilde{r}) = \frac{z(r) - z_h}{\rho_c (\beta / gh)^{1/2}}, \; \tilde{R}_b = \frac{R_b}{\rho_c},$$

$$\tilde{z}_h = \frac{z_h \beta}{\rho_c h (2\gamma_0 - E_A)}, \;\; \tan\tilde{\varphi}_b = \frac{\rho_c R_b gh \tan^2 \varphi_b}{\beta (R_b^2 - \rho_c^2)} - \frac{R_b}{3(R_b + \rho_c)}, \tilde{\mu}_S = \frac{\rho_c \mu_S}{\beta \Omega},$$

$$\tilde{V} = \frac{V\beta}{\rho_c^3 h (2\gamma_0 - E_A)}, \;\; \tilde{F} = \frac{F}{\rho_c^2 (2\gamma_0 - E_A)}, \;\; \Delta\tilde{E} = \frac{\Delta E}{\rho_c \beta}. \qquad \text{(A-3)}$$

Notice the consistency with eq. (A-1) at $c=0$. Eqs. (A-3) yield specific expressions for the crystal shape for arbitrary values of c:

$$\tilde{z}(\tilde{r}) = -\int \sqrt{\frac{\tilde{r} - 1}{3} - \frac{\tilde{c}(\tilde{r}^2 - 1)}{\tilde{r}}} d\tilde{r}, \qquad \text{(A-4)}$$

$$\tilde{z}_h = \frac{1}{1 - 3\tilde{c}}, \quad \tilde{\mu}_S = 2(1 - 3\tilde{c}), \qquad \tan\tilde{\varphi}_b = -\tilde{c}, \quad \Delta\tilde{E} = \frac{\pi(1 - 6\tilde{c})^2}{2(1 - 3\tilde{c})}, \qquad \text{(A-5)}$$

$$\tilde{V} = \pi \left\{ \frac{\tilde{R}_b^2}{1 - 3\tilde{c}} - 2\tilde{E}_A^{-3/2} \int_1^{\tilde{R}b} \left(\int_1^{\tilde{r}} \sqrt{\frac{\tilde{r}' - 1}{3} - \frac{\tilde{c}(\tilde{r}'^2 - 1)}{\tilde{r}'}} d\tilde{r}' \right) \tilde{r} d\tilde{r} \right\},$$

$$\tilde{F} = \pi \left\{ \tilde{R}_b^2 + 2\tilde{E}_A^{-3/2} \int_1^{\tilde{R}b} \left[\sqrt{\frac{\tilde{r} - 1}{3} - \frac{\tilde{c}(\tilde{r}^2 - 1)}{\tilde{r}}} + \left(\frac{\tilde{r} - 1}{3} - \frac{\tilde{c}(\tilde{r}^2 - 1)}{\tilde{r}} \right)^{3/2} \right] \tilde{r} d\tilde{r} \right\}.$$

eq. (A-4) is shown in Figure 2-3 and eq. (A-5) are shown in Figure 2-4 and Figure 2-7. Notice that eq. (A-5) is already independent of adhesion energy (temperature), however, quantities such as the interface radius, crystallite volume and crystallite free

energy are not. Also because analytical results are not available here we have used the scaling results obtained for c=0 (eq. (A-2)) and applied them to other shape parameters.

$$\widetilde{R}_b = \frac{R_b - \rho_c}{\rho_c \widetilde{E}_A},$$

$$\widetilde{V} = \frac{V\beta}{\rho_c^3 h(2\gamma_0 - E_A)\widetilde{E}_A^2} - \frac{\pi(5 + 9\sqrt[3]{2}\widetilde{E}_A)}{5\widetilde{E}_A^2}$$

$$\widetilde{F} = \frac{F}{\rho_c^2 (2\gamma_0 - E_A)\widetilde{E}_A^2} - \frac{3\pi(5 + 9\sqrt[3]{2}\widetilde{E}_A)}{5\widetilde{E}_A^2}, \qquad \text{(A-6)}$$

eq. (A-5) are shown in Figure 2-4 and Figure 2-5. As is discussed in the manuscript, this is not a perfect scaling and some temperature dependence remains.

Appendix B

The scaling is performed in a same manner as it was in the continuum model in the previous paper [80]. We define dimensionless values of

$$\widetilde{r}_i = \frac{r_i}{\rho_c}, \qquad \widetilde{c} = \frac{cgh}{\beta\rho_c}, \qquad \widetilde{g} = \frac{gh^3}{\beta\rho_c^2}, \qquad \widetilde{\mu} = \frac{\rho_c \mu}{\beta\Omega},$$

$$\Delta\widetilde{E} = \frac{\Delta E}{\beta\rho_c}, \qquad \widetilde{z}(\widetilde{r}) = \frac{z(r) - hi}{\rho_c(\beta / gh)^{1/2}},$$

$$\widetilde{V} = \frac{V\beta}{\rho_c^3 h(2\gamma_0 - E_A)}, \quad \widetilde{F} = \frac{F}{\rho_c^2(2\gamma_0 - E_A)}. \qquad \text{(B-1)}$$

This gives the following analytical relationships between dimensionless variables, which are shown in Figure 3-3.

$$\widetilde{\mu}_S = 2(1 - 3\widetilde{c})$$

$$\tilde{\mu}_1(\tilde{r}_1,\tilde{r}_2)=\frac{1}{\tilde{r}_1}+\frac{\tilde{g}(\tilde{r}_1+3\tilde{r}_2)}{2\tilde{r}_1(\tilde{r}_2-\tilde{r}_1)^3}$$

$$\mu_1(\tilde{r}_1,\tilde{r}_2)=\frac{1}{\tilde{r}_2}-\frac{\tilde{g}}{2\tilde{r}_2}\left(\frac{3\tilde{r}_1+\tilde{r}_2}{(\tilde{r}_2-\tilde{r}_1)^3}-\frac{\tilde{r}_2+3\tilde{r}_{30}}{(\tilde{r}_{30}-\tilde{r}_2)^3}\right)$$

$$\Delta\tilde{E}=2\pi\left(\int_1^{\tilde{r}}\{\tilde{\mu}_1(\tilde{r}_1,\tilde{r}_2)-\tilde{\mu}_2(\tilde{r}_1,\tilde{r}_2)\}\tilde{r}_1 d\tilde{r}_1+\int_{\tilde{r}20}^{\tilde{r}_2(r)}\{\tilde{\mu}_2(\tilde{r}_1,\tilde{r}_2)-\tilde{\mu}_S\}\tilde{r}_2 d\tilde{r}_2\right) \quad \text{(B-2)}$$

Appendix C

The supported crystal shape can be determined completely given the material parameters (step stiffness, step interactions, surface free energy, interface free energy) and one physical constraint such as the volume of the crystallite. This can be done analytically for the ECS, and numerically for the metastable structures. For the ECS the surface chemical potential is:

$$\mu=\left(\frac{2\pi h\Omega^3\beta^2}{35V}\right)^{1/3}\left[140(2\gamma_o-E_a)+252\sqrt[3]{2}\,\frac{hg^{1/3}}{\beta}(2\gamma_o-E_a)^2+135\left(\frac{hg^{1/3}}{\beta}\right)^2(2\gamma_o-E_a)^3\right].$$

(C-1)

By combining this with eq. (3-2b), the facet radius and crystal height can be determined, and then the shape is given by the Pakrovsky-Talapov form. For the metastable structures, one can solve the differential equation for the shape numerically, and then determine the volume as a function of the facet radius and shape parameter. We have shown numerically (Figure 2-4) that the physical observables (e.g. crystal height, interface radius, etc), collapse to a universal curve with appropriate scaling. They can thus be used to determine the facet radius for any

given shape parameter. As an example, the scaled crystal height at $c_{\max}$ takes a universal value of ~1.75. Given an observed value of z_h, it is then possible to determine the facet radius using the scaling form.

$$1.75 \approx \tilde{z}_{hc\max} = \frac{\beta z_h}{\rho_{c\max} h(2\gamma_o - E_a)} \qquad \text{(C-2)}$$

The scaling for volume presented in the previous paper is approximate, but can be used for estimates. For $c_{\max}$, the scaled volume is ~70, which allows the facet radius to be estimated using:

$$70 \sim \tilde{V}_{c\max} = \frac{\beta V}{\rho_c^3 h(2\gamma_o - E_a)}.$$

The crystal height can then be determined with the second equality of eq. (3-2b)

Appendix D

For scaling we define dimensionless variables similar to those of previous workers [38, 39] and scale out the kinetic parameters and step free energy.

$$\tilde{r}_i = \frac{k_B T r_i}{\Omega\beta}, \quad \tilde{z}_h = \frac{z_h}{h}, \quad \tilde{t} = D_S \Omega c_{eq}^0 \left(\frac{k_B T}{\Omega\beta}\right)^2 t, \; \tilde{d} = \frac{k_B T D_S}{\Omega\beta\kappa}$$

$$\tilde{g} = \frac{g\Omega}{k_B T}\left(\frac{h k_B T}{\Omega\beta}\right)^3, \quad \tilde{\mu}_i = \frac{\mu_i}{k_B T}, \quad \tilde{J}_i = \frac{J_i}{D_S c_{eq}^0},$$

$$\tilde{\gamma}_0 = \frac{\Omega\gamma_0}{k_B T}, \quad \tilde{E}_A = \frac{\Omega(2\gamma_0 - E_A)}{k_B T}, \quad \tilde{F} = \frac{k_B T F}{\Omega\beta^2}, \quad \tilde{V} = \frac{V}{h}\left(\frac{k_B T}{\Omega\beta}\right)^2 . \text{(D-1)}$$

The dimensionless interaction coefficient $\tilde{g}$ for Pb as a function of temperature is shown in Fig. 1 b). The scaling leads to the following results

$$\tilde{\mu} = \frac{1}{\tilde{r}_i} + \frac{\tilde{g}}{2\tilde{r}_i}\left(\frac{3\tilde{r}_{i+1} + \tilde{r}_i}{\tilde{l}_i^{\,3}} - \frac{\tilde{r}_i + 3\tilde{r}_{i-1}}{\tilde{l}_{i-1}^{\,3}}\right) \quad : \tilde{l}_i = \tilde{r}_i - \tilde{r}_{i+1},$$

$$\tilde{J}_i = \frac{\exp(\tilde{\mu}_{i+1}) - \exp(\tilde{\mu}_i)}{\ln\dfrac{\tilde{r}_i}{\tilde{r}_{i+1}} + \tilde{d}\left(\dfrac{1}{\tilde{r}_i} + \dfrac{1}{\tilde{r}_{i+1}}\right)}, \qquad \frac{d\tilde{r}_i}{d\tilde{t}} = \frac{\tilde{J}_i - \tilde{J}_{i-1}}{\tilde{r}_i},$$

$$\tilde{F} = \pi\sum_i^{\tilde{z}h}(\tilde{r}_i^{\,2} - \tilde{r}_{i+1}^{\,2})\left(\tilde{\gamma}_0 + \frac{1}{\tilde{r}_i - \tilde{r}_{i+1}} + \frac{\tilde{g}}{(\tilde{r}_i - \tilde{r}_{i+1})^3}\right), \qquad \tilde{V} = \pi\sum_i^{\tilde{z}h}\tilde{r}_i^{\,2}. \quad \text{(D-2)}$$

Results of $\tilde{r}$ vs. $\tilde{t}$, $\tilde{\mu}$ vs. $\tilde{t}$, $\tilde{z}_h$ vs. $\tilde{t}$ and $\tilde{F}$ vs. $\tilde{t}$ with constant $\tilde{V}$ are shown in Fig. 2. When calculating the final state of the crystallite in eq. (7) c is scaled as in the previous paper [80] giving the following result,

$$\tilde{c} = \frac{cgh}{r_f\beta}, \qquad \therefore \tilde{c} \cong \frac{1}{3}\left(1 - \frac{\tilde{E}_A\tilde{r}_f}{\tilde{z}_h}\right) \quad \text{(D-3)}$$

Appendix E

Python program for nano-crystallite evolution simulations in chapter 5.

```
from math import *
from time import *

def consts():
        global omega, h, boltz, ek, beta0, a, gamma0, A
        gamma0=0.017            #eV/A^2
        ek=42e-3                #eV
        beta0=128e-3            #eV/atom
        omega=10.6              #A^2
        h=2.86                  #A
        a=4.95*(2.)**(1./2.)/2.  #A (nn)
        A=0.05                  #eVA
        boltz = 8.6e-5          #eV/K

def beta(beta0, ek, a, kT):  #hexagonal Ising (eV/A)
      from cmath import *
      w=exp(-ek/kT)
```

```
        beta=abs(2*kT*acosh(-0.5+0.5*(3+(1+3*w**4)/((1-
w)*(1+w)*w**2))**0.5)/a)-2.*ek/a+beta0/a
        return beta

def g(kT, beta, h, omega, A):   #interacting fermion (eV/A^2)
        g0=((pi*kT)**2./(24*beta*h**3))*(1+(1+4*A*beta/(kT**2.))**(1./2.))**2
        g=omega*g0/kT*(h*kT/(omega*beta))**3.
        return g


def mustep(g, R, n, tcount):    #scaled step chemical potential
            mulist=[0.]
            for ncount in range(1,n+1):
                        if rlist[ncount]==0.:
                                    mulist.append(0.)
                        else:
                                    mulist.append(1./rlist[ncount])
            for ncount in range(1,n+1):
                        if rlist[ncount]==0.:
                                    ncount=n
                        else:
                      if ncount==n or rlist[ncount+1]==0:
                        lower=(3*rlist[ncount-1]+rlist[ncount])/(rlist[ncount]*(rlist[ncount-1]-
rlist[ncount])**3)
                        mulist[ncount]=mulist[ncount]+g*lower/2.
                      else:

            upper=(3*rlist[ncount+1]+rlist[ncount])/(rlist[ncount]*(rlist[ncount]-
rlist[ncount+1])**3)
                                    lower=(3*rlist[ncount-
1]+rlist[ncount])/(rlist[ncount]*(rlist[ncount-1]-rlist[ncount])**3)
                                    mulist[ncount]=mulist[ncount]-g*(upper-lower)/2.
        return mulist

def jstep(kT, a, beta, omega, n, d, pi, tcount):    #scaled adatom flux
    j=[0.]
    for ncount in range(1,n):
        if rlist[ncount+1]<=a*kT/(omega*beta):
            j.append(0.)
        else:
            diff=log(rlist[ncount]/rlist[ncount+1])
            ad=d*(1./rlist[ncount]+1./rlist[ncount+1])
            jn=exp(mu[ncount+1])-exp(mu[ncount])
            j.append(jn/(diff+ad))
    j.append(0.)
    return j
```

```
def deltaR(kT, a, beta, omega, pi, tcount):    #scaled step motion
   check=[0.]
   delr=[0.]
   for ncount in range(1,n+1):
      if rlist[ncount]<=a*kT/(omega*beta):
         dr=0.
         R[ncount][tcount]=0.
      else:
         dr=1./rlist[ncount]
      delr.append(dr*(j[ncount]-j[ncount-1])*dt)
      if rlist[ncount]==0.:
         pass
      else:
         check.append(abs(delr[ncount]/(rlist[2]-rlist[1])))
   checkmax=max(check)
   delt=dt
   if checkmax>0.1:
      for ncount in range(1,n+1):
         delr[ncount]=delr[ncount]/(10.*checkmax)**2
         delt=dt/(10.*checkmax)**2
   return delr, delt

def tfree(gamma, g, R, n, tcount):    #scaled free energy
   if rlist[n]==0:
      tfree=0.
   else:
      tfree=pi*(gamma+1./rlist[n]+g*(1./rlist[n])**3.)*rlist[n]**2.
   for ncount in range(1,n):
      if rlist[ncount]==rlist[ncount+1]:
         freed=0.
      else:
         freed=gamma+1./(rlist[ncount]-rlist[ncount+1])+g*(1./(rlist[ncount]-
rlist[ncount+1]))**3.
         tfree=tfree+pi*(rlist[ncount]**2.-rlist[ncount+1]**2.)*freed
   tfree=tfree+pi*(gamma-AE)*rlist[1]**2
   return tfree

#initial settings
consts()
t=0.
tmax=1
dt=1.0e-3
print "\n"
print "\n                Welcome to the step kinetics program\n"
T= input("\nEnter the temperature in K  (enter number):")
```

```
kT= boltz*T
gamma=omega*gamma0/kT
beta=beta(beta0, ek, a, kT)
g=g(kT, beta, h, omega, A)
d= input("Enter the ratio D/kappa in nm(enter number):")*10*kT/(omega*beta)
AE= input("Enter the ratio AE/gamma (enter number):")*gamma
print " \n scaled surface tention is %5.5f" %gamma
print " scaled interaction coefficiant is %5.8f" %g
print " scaled ratio D/k is %5.5f" %d

R=[[0]]

#initial configuration
filename=raw_input("\nEnter the name of input file :")
infile=open(filename,"r")
n=infile.readline()
n=int(n)
dlx=infile.readline()
dx=float(dlx)*10*kT/(omega*beta)
print "\n initial scaled step position"
for ncount in range(1,n+1):
   rad=infile.readline()
   R.append([float(rad)*10*kT/(omega*beta)])
   for x in R[ncount]: print "% 5.3f" %(x),
infile.close()

#initial condition
z=n
M=(g*(3.*R[2][0]+R[1][0])*z+2.*((R[2][0]-R[1][0])**3.)*(z-2.*(2.*gamma-
AE)*R[1][0]))/(z*g*(R[1][0]-R[2][0])**3.)
dx=(1.+(2.*R[1][0]*(M**(1./2.))+(-
1.+4.*M*(R[1][0]**2.))**(1./2.))**(2./3.))/((M**(1./2.))*(2.*R[1][0]*(M**(1./2.))+(
-1.+4.*M*(R[1][0]**2.))**(1./2.))**(1./3.))
volume=0.
for ncount in range(1,n+1):
   volume=volume+pi*((R[ncount][0])**2.)
rlist=[R[1][0]+dx]
for ncount in range(1,n+1):
   rlist.append(R[ncount][0])
mutest=mustep(g, R, n, 0)
tfetest=tfree(gamma, g, R, n, 0)
print "\n initial scaled chemical potential"
for x in mutest: print " %5.3e" %x,
print "\n"
print " scaled volume of cristallite is %5.2f" %(volume)
print " initial scaled total free energy is %5.2f" %(tfetest)
```

```
print "\n"

#output file for kinetics
filename=raw_input("Enter the name of output file for radii:")
outfile=open(filename,"w")
outfile.write("M.Degawa\n")
outfile.write(strftime("%a, %d %b %Y %H:%M:%S\n",gmtime()))
outfile.write("T=%8dK\n"%T)
outfile.write("A=%8.2feVA\n"%A)
outfile.write("d=%8.2f"%d)
outfile.write("\n time(sec) and step radii(nm) \n")
outfile.write("\t%8.1f"%t)
for ncount in range(1,n+1):
   outfile.write("\t%8.3f"%(R[ncount][0]))
outfile.write("\n")

#output file for chemical potential
filename2=raw_input("Enter the name of output file for chemical potential:")
outfile2=open(filename2,"w")
outfile2.write("M.Degawa\n")
outfile2.write(strftime("%a, %d %b %Y %H:%M:%S\n",gmtime()))
outfile2.write("\n time(sec) and chemical potential(eV) \n")
outfile2.write("\t%8.1f"%t)
for x in mutest: outfile2.write("\t%5.6f"%x)
outfile2.write("\n")

#output file for total free energy
filename3=raw_input("Enter the name of output file for total free energy:")
outfile3=open(filename3,"w")
outfile3.write("M.Degawa\n")
outfile3.write(strftime("%a, %d %b %Y %H:%M:%S\n",gmtime()))
outfile3.write("\n time(sec) and total free energy(eV) \n")
outfile3.write("\t%8.1f"%t)
outfile3.write("\t%5.6f"%tfetest)
outfile3.write("\n")


#step kinetics program
cyclecount=0
cycleinc=int(100./dt)
tmem=1000000
tcount=0
tglobal=0
end=0.1
while tglobal<=tmax:
```

```
    M=(g*(3.*R[2][tcount]+R[1][tcount])*z+2.*((R[2][tcount]-R[1][tcount])**3.)*(z-
2.*(2.*gamma-AE)*R[1][tcount]))/(z*g*(R[1][tcount]-R[2][tcount])**3.)
    dx=(1.+(2.*R[1][tcount]*(M**(1./2.))+(-
1.+4.*M*(R[1][tcount]**2.))**(1./2.))**(2./3.))/((M**(1./2.))*(2.*R[1][tcount]*(M*
*(1./2.))+(-1.+4.*M*(R[1][tcount]**2.))**(1./2.))**(1./3.))
    rlist=[R[1][tcount]+dx]
    for ncount in range(1,n+1):
          rlist.append(R[ncount][tcount])
    if R[ncount][tcount]==0:
       z=rlist.index(0.)-1
    mu=mustep(g,R,n,tcount)
    j=jstep(kT,a,beta,omega,n,d,pi,tcount)
    delr=deltaR(kT,a,beta,omega,pi,tcount)[0]
    delt=deltaR(kT,a,beta,omega,pi,tcount)[1]
    tfe=tfree(gamma,g,R,n,tcount)
    for ncount in range(1,n+1):
       R[ncount].append(R[ncount][tcount]+delr[ncount])
    if tglobal==tmax-1:
       print "\n step #    mu(n)       j(n)     delr(n)     Ro(n)    Rf(n)"
       print "\n"
       for ncount in range(1,n+1):
          print "%5d    %8.3e  %8.4f  %8.2e    %8.3f  %8.3f" %(ncount,
mu[ncount],j[ncount],delr[ncount],R[ncount][tcount],R[ncount][tcount+1])
       print "\n"
       print " total free energy is %5.2f" %(tfe)
    tcount=tcount+1
    tglobal=tglobal+1
    cyclecount=cyclecount+1
    t=t+delt
    R[0].append(t)
    #if abs(delr[1])<=1.0e-011:
       #dt=dt*10
       #print "The present value of dt is %5.2e" %dt
    if cyclecount==cycleinc:
       outfile.write("\t%8.1f"%t)
       for ncount in range(1,n+1):
          outfile.write("\t%8.3f"%(R[ncount][tcount]))
       outfile.write("\n")
       outfile2.write("\t%8.1f"%t)
       for x in mu: outfile2.write("\t%5.6f"%x)
       outfile2.write("\n")
       outfile3.write("\t%8.1f"%t)
       outfile3.write("\t%5.6f"%tfe)
       outfile3.write("\n")
       cyclecount=0
    if tcount==tmem:  #memory save
```

```
        rtemp=[0.]
        for ncount in range(1,n+1):
           rtemp.append(R[ncount][tmem-1])
        tcount=0
        R=[[0]]
        for ncount in range(1,n+1):
           R.append([rtemp[ncount]])
    if tglobal==tmax:  #closing or continue program
        print "\n"
        print "Iteration completed"
        #print "The present value of delt is %5.2e and dt is %5.2e" % (delt,dt)
           tinc= input("How many additional iterations would you like to do?  (enter
integer or end):")
        tmax=tinc
        if tinc==0.1:
           outfile.close()
           print"\n"
           q3=raw_input("Do you want to create an output configuration file?
(yes/no):")
           if q3==('y'or'yes'):
              filename=raw_input("Enter the name of outputfile:")
              configout=open(filename,"w")
              configout.write("%8d\n"%n)
              #configout.write("%8.3f\n"%(dx))
              for ncount in range(1,n+1):
                 configout.write("%8.3f\n"%(R[ncount][tcount]))
              configout.close()
              sys.exit()
           else:
              sys.exit()
        tglobal=0
        #print "What value of dt would you like for the next set of iterations?"
        #dt = input (" (enter decimal value):")
```

Appendix F

C program for facet-edge fluctuation MC simulations in chapter 7.

```
/*  Measures the width of fluctuations of N steps on on a vicinal surface
 * interacting with a A/l^2 type interaction with A tilde=2.0 and T =0.5*
 * Hailu Gebremariam March 2004*/
//modified to use 2 random number generators Ran2 and Ran3
//Hailu Gebremariam Oct 2004
//Modifications: Tim Stasevich Feb 2005
```

```
#include <math.h>
#include <stdio.h>
#include <stdlib.h>

#define Ly 100  /* Length of terrace */
#define N 2    /* Number of steps */
#define Lx 1500         /* Width of terrace */
#define d 4           // average distance between initial steps
#define MCS 3100000   /* Number of Monte carlo step per site */
#define INTERVAL 1
#define NUM_REALIZATIONS 3
#define T 1.0       /* Temperature in units of energy */
#define A 0.0      /* Step-Step repulsion strength */
#define B 0.00      /* Linear potential strength */
#define SAT 3000000       /* Saturation time found from width.c */

#define MBIG 1000000000     //parameters for Ran3
#define MSEED 161803398     //
#define MZ 0                //
#define FAC (1.0/MBIG)      //


#define IM1 2147483563      //parameters for Ran2
#define IM2 2147483399      //
#define AM (1.0/IM1)        //
#define IMM1 (IM1-1)        //
#define IA1 40014           //
#define IA2 40692           //
#define IQ1 53668           //
#define IQ2 52774           //
#define IR1 12211           //
#define IR2 3791            //
#define NTAB 32             //
#define NDIV (1+IMM1/NTAB)  //
#define EPS 1.2e-7          //
#define RNMX (1.0-EPS)      //

void update_lattice(void);
void initialize_lattice(void);
void widthCalc(int);
void printWidth(void);
void spatialCor(void);
void printSpatial(void);
void autoCor(float data[]);
void Cor(void);
float ran3(long *);
```

```
float ran2(long *);

int X[N][Ly];
float Pkink[9],*Pstep, *PstepLin;
float *width,*autoc,*G,*TC;
int **step;            //stores step positions at each time
int nrf;  //number of realizations flag
long r1,r2,r3,r4,r5,r6;

FILE *output;


//MAIN PROGRAM BEGINS
HERE*****************************************************
//*****************************************************************
**********
int main()
{
 int i,j,k,t,p,count,indepc;
 char mainfilename[70];

 //Print out all variables to screen:
 printf("A = %.5f\t B= %.5f\t N = %d\t Ly = %d\t Lx = %d\t MCS %d\t NR = %d\n
T=%.3f\t INT=%d\t sat=%d\t
d=%d\n",A,B,N,Ly,Lx,MCS,NUM_REALIZATIONS,T,INTERVAL,SAT,d);
 printf("max = %d\n",(MCS/INTERVAL));
 printf("Number of indep. calcs= %d\n",((MCS-SAT)/INTERVAL));
 printf("sat = %d\n",SAT);

 indepc=MCS-SAT;
 //  width = (float *)calloc((MCS/INTERVAL), sizeof(float));
 width = malloc((MCS/INTERVAL)*sizeof(float));
 Pstep = (float *)calloc(Lx, sizeof(float));
 PstepLin = (float *)calloc(Lx, sizeof(float));
 autoc=(float*)calloc(indepc, sizeof(float));
 G = (float *)calloc(Ly,sizeof(float));
 TC = (float *)calloc(indepc,sizeof(float));
 step=malloc(Ly*sizeof(int*));
 for(i=0;i<Ly;i++){
  step[i]=malloc(indepc*sizeof(int));
 }

 /* Initialize energy arrays */
 for (i=-4;i<=4;i++)
  Pkink[i+4] = exp(-i/T);
```

```
  Pstep[0] = 0;
  for (i=1;i<Lx;i++)
    Pstep[i] = exp(-A/(T*i*i));   //inverse r^2 potential

  for (i=0;i<Lx;i++)
    PstepLin[i] = exp(-(B*i)/T);   //linear potential

  printf("It starts now...\n");
  printf("are we here yet?...\n");
  for(nrf=0;nrf<NUM_REALIZATIONS;nrf++){

    //Seeds for the random-number generators
    //printf("%d\n",n+1);
    r1 = -1*(nrf+1);r2 =r1 -1000000;r3 =r2 -1000000;
    r4 =r3 -1000000;r5 =r4 -1000000;r6 =r5 -1000000;

    //Initialize and print initial step configuration to a file
    initialize_lattice();
  sprintf(mainfilename, "InitialMCS%dLy%dLx%dN%d-
INT%dA%.3fB%.3fNR%dT%.2fsat%dd%d",MCS,Ly,Lx,N,INTERVAL,A,B,NUM_
REALIZATIONS,T,SAT,d);
  output=fopen(mainfilename,"w");
  //output = fopen("initConfig.dat","w");
    for(i=0; i<N; i++){
      for(j=0; j<Ly; j++){
           fprintf(output,"%d\n",X[i][j]);
      }
    }
    fclose(output);
    //printf("are we here yet?...\n");
    //Start Monte-Carlo steps...
    for(t=0;t<MCS;t++){
          update_lattice();
          //printf("%d\n",t+1);
      if(t%INTERVAL==0){
          //widthCalc(t); //Use to calculate equilibration time
          if(t>=SAT){   //I think there's still a small problem here...if t>SAT t starts
from 0!?
            //for(j=0;j<Ly;j++){
            //autoc[t-SAT][j]=(float)X[N-1][0]; //Use to find correlation time.
            //spatialCor(); //Use to calculate the spatial correlation

            for(i=0;i<Ly;i++){
              step[i][t-SAT]=X[N-1][i];  //Store data into step array for calcs at end
            }
            //printf("%d\n",t);
```

```
          }
      }
    }
    printf("%d\n",nrf+1);
    Cor();  //Calculate spatial and temporal correlation functions at end of run and print.
  }

  //Print out appropriate data:
  //printWidth();   //Use if using widthCalc(t)
  //autoCor(autoc);
  //printSpatial(); //Use if using spatialCorr(t)


  //Print out the final configuration to a file
  sprintf(mainfilename, "FinalMCS%dLy%dLx%dN%d-
INT%dA%.3fB%.3fNR%dT%.2fsat%dd%d",MCS,Ly,Lx,N,INTERVAL,A,B,NUM_
REALIZATIONS,T,SAT,d);
  output=fopen(mainfilename,"w");
  //  output = fopen("finConfig.dat","w");
  for(i=0; i<N; i++){
    for(j=0; j<Ly; j++){
      fprintf(output,"%d\n",X[i][j]);
    }
  }
  fclose(output);

  //Print out to log file:
  output=fopen("logfile.txt","a");
  fprintf(output, "A = %.5f\t B = %.5f\t N = %d\t Ly = %d\t Lx = %d\t MCS %d\t NR
= %d\t T=%.3f\t INT=%d\t
sat=%d\n",A,B,N,Ly,Lx,MCS,NUM_REALIZATIONS,T,INTERVAL,SAT);
  fclose(output);
  return(0);
}

//END
MAIN**********************************************************************
*****
//**********************************************************************
*********

//FUNCTIONS USED IN MAIN

/*initializes the lattice*/
void initialize_lattice(void)
{
```

```
  int i,j;

  //modified to separate the first N-1 rows by Y, and the last row by 5.
  for(i=0;i<N;i++){
    for(j=0;j<Ly;j++){
      //X[i][j]=3.0/2.0*(N-1-pow(N-1,1.0/3.0)*pow(N-1-i,2.0/3.0));
      X[i][j]=d*i;
    }
  }
  return;
}

/*Updates the lattice with Monte carlo moves */
void update_lattice(void)
{
  //int left,right,next,last; distances to nearest neighbors
  int m,i,j,left,right,last,next;
  int i2,j2,left2,right2,last2,next2,dir;
  int dkinke;
  double Pr;
  for(m=1;m<=N*Ly;m++){
    i = (int)((N-1)*ran2(&r1))+1;  //adding +1 to fix the first step and choosing
between 0 and N-1
    j = (int)((Ly)*ran2(&r2));
    //printf("i=%d",i);

  left = X[i][j] - X[i][(j+Ly-1)%Ly];
  right = X[i][j] - X[i];
  next = (X[(i+1)%N][j] - X[i][j]+Lx)%Lx;
  last = (X[i][j] - X[(i+N-1)%N][j]+Lx)%Lx;

  //USE FOR CONSERVED DYNAMICS
    i2=i;
    j2=(j+Ly+1)%Ly;
    //j2= (int)((Ly)*ran2(&r5));

  left2 = X[i2][j2] - X[i2][(j2+Ly-1)%Ly];
  right2 = X[i2][j2] - X[i2][(j2+Ly+1)%Ly];
  next2 = (X[(i2+1)%N][j2] - X[i2][j2]+Lx)%Lx;
  last2 = (X[i2][j2] - X[(i2+N-1)%N][j2]+Lx)%Lx;

  //CALCULATE THE KINK ENERGY:
     dir = (ran2(&r3)<0.5?-1 : 1);
     dkinke= abs(left+dir) + abs(right+dir) - abs(left) - abs(right);

  //USE FOR CONSERVED DYNAMICS
```

```
    dkinke+= abs(left2-2.0*dir) + abs(right2-dir) - abs(left2-dir) - abs(right2); //extra
dir critical for periphery diffusion
    //dkinke+= abs(left2-dir) + abs(right2-dir) - abs(left2) - abs(right2);
  Pr=Pkink[dkinke+4];

  //USE FOR STEP-STEP INTERACTIONS, INCLUDING FERMIONIC
REPULSION:
  Pr=Pr*Pstep[next-dir]*Pstep[last+dir]/Pstep[next]/Pstep[last];

  //USE FOR CONSERVED DYNAMICS
  Pr=Pr*Pstep[next2+dir]*Pstep[last2-dir]/Pstep[next2]/Pstep[last2];

  //USE FOR LINEAR POTENTIAL:
  //Pr=Pr*PstepLin[X[i][j]+dir]/PstepLin[X[i][j]];

  if(Pr>ran2(&r4)){
    //USE FOR CONSERVED DYNAMICS
    //if(X[i][j]+dir != X[i2][j2]-dir){
          X[i][j] = X[i][j]+dir;
          X[i2][j2]=X[i2][j2]-dir;
          //  }
  }
}
}

/*Calculates width to find saturation time*/
void widthCalc(int tdum)
{
  float widtht;
  int sij,sij2,i,j;

  widtht =0.0;
  for (i=N-1;i<N;i++){      //focus on last step only...
    sij=0.0;
    sij2=0.0;
    for(j=0;j<Ly;j++){
      sij2+=(float)X[i][j]*X[i][j];
      sij+=(float)X[i][j];
    }
    widtht+= sqrt((sij2/(float)Ly) - (sij/(float)Ly)*(sij/(float)Ly));
  }
  width[tdum/INTERVAL]=width[tdum/INTERVAL]+widtht;  //only last step->no
division by N
  //printf("%f\n",width[t/INTERVAL]);
}
```

```
/*Prints out width data to file*/
void printWidth(void){
  char filename[70];
  int time;

  //Specify file for output:
  sprintf(filename, "fwMCS%dLy%dLx%dN%d-
INT%dA%.3fB%.3fNR%dT%.2fd%d",MCS,Ly,Lx,N,INTERVAL,A,B,NUM_REA
LIZATIONS,T,d);

  //Printing out the width
  output=fopen(filename,"w");
  //printf("max = %d\n",(MCS/INTERVAL));
  for(time=0;time<(MCS/INTERVAL);time++){
    width[time] = width[time]/NUM_REALIZATIONS;
    fprintf(output,"%f\n",width[time]);
  }
  fclose(output);
}

/*Calculates the spatial & temporal correlation functions of step at the end of the
run*/
void Cor(void){
  int j,k,time,l;
  float g[Ly];
  float temp[MCS-SAT];
  char filename[70];

  //Prepare file for spatial correlation function:
  sprintf(filename, "fsMCS%dLy%dLx%dN%d-
INT%dA%.3fB%.3fNR%dnrf%dT%.2fsat%ddis%d",MCS,Ly,Lx,N,INTERVAL,A,
B,NUM_REALIZATIONS,nrf,T,SAT,d);
  output=fopen(filename,"w");

  //Calculate spatial correlation function G
  for(j=0;j<Ly;j++){
    g[j]=0.0;
    for(time=0;time<(MCS-SAT);time++){
      for(k=0;k<Ly;k++){
          g[j]+=((float)step[(k+j)%Ly][time] -
(float)step[k][time])*((float)step[(k+j)%Ly][time] - (float)step[k][time]);//Ly;
      }
    }
    //G[j]+=g[j]/(MCS-SAT);
    fprintf(output,"%f\n",g[j]/((MCS-SAT)*Ly));
```

```
  }
  fclose(output);

  //Prepare file for temporal correlation function:
  sprintf(filename, "ftMCS%dLy%dLx%dN%d-
INT%dA%.3fB%.3fNR%dnrf%dT%.2fsat%ddis%d",MCS,Ly,Lx,N,INTERVAL,A,
B,NUM_REALIZATIONS,nrf,T,SAT,d);
  output=fopen(filename,"w");

  //Calculate temporal correlation function TC
  for(time=0;time<(MCS-SAT);time++){
    temp[time]=0.0;
    for(j=0;j<Ly;j++){
      for(l=0; l<(MCS-SAT-time); l++){
          temp[time]+=((float)step[j][l+time]-(float)step[j][l])*((float)step[j][l+time]-
(float)step[j][l]);//(MCS-SAT-time);
      }
    }
    //    TC[time]+=temp[time]/Ly;
    fprintf(output,"%f\n",temp[time]/(Ly*(MCS-SAT-time)));

  }
  fclose(output);

}

/*Calculates the spatial correlation function*/
void spatialCor(void){
  int j,k;
  float g[Ly];

  //Begin spatial correlation calculation:
  for (j=0;j<Ly;j++){
    g[j]=0.0;   //this is the spatial correlation function
    for(k=0;k<Ly;k++){
      g[j]+=((float)X[N-1][(k+j)%Ly] - (float)X[N-1][k])*((float)X[N-1][(k+j)%Ly] -
(float)X[N-1][k]);
    }
  }
  //Average together spatial correlations at each time:
  for (j=0; j<Ly; j++){
    G[j] += g[j]/Ly;
  }

}
```

```
/*Prints out the spatial correlation data to a file*/
void printSpatial(void){
  char filename[70];
  int j;

  sprintf(filename, "fsMCS%dLy%dLx%dN%d-
INT%dA%.3fB%.3fNR%dT%.2fsat%d",MCS,Ly,Lx,N,INTERVAL,A,B,NUM_RE
ALIZATIONS,T,SAT);
  output=fopen(filename,"w");

  //Printing out the spatial correlation
  for(j=0;j<Ly;j++){
    G[j] = G[j]*INTERVAL/(MCS-SAT);
    fprintf(output,"%f\n",G[j]);
  }
  fclose(output);
}

/*Performs time-correlation on data to check for correlation time and
  prints out to a file */
void autoCor(float data[])
{
  int i,j,tot;
  float avg1, avg2, cort;
  char filename[70];

  //Print out original data to autoData.dat for external checking:
  sprintf(filename, "fadMCS%dLy%dLx%dN%d-
INT%dA%.3fB%.3fNR%dT%.2f",MCS,Ly,Lx,N,INTERVAL,A,B,NUM_REALIZA
TIONS,T);
  output=fopen(filename,"w");
  for(i=0;i<(MCS-SAT);i++){
    fprintf(output, "%d\t %f\n",i,data[i]);
  }
  fclose(output);

  //Perform time-correlation on data and print to timeCor.dat:
  sprintf(filename, "facMCS%dLy%dLx%dN%d-
INT%dA%.3fB%.3fNR%dT%.2f",MCS,Ly,Lx,N,INTERVAL,A,B,NUM_REALIZA
TIONS,T);
  output=fopen(filename,"w");
   for(i=0; i<(MCS-SAT) ;i++){
    cort=0;
    avg1=0;
    avg2=0;
    tot=MCS-SAT-i;
```

```
    for(j=0; j<tot; j++){
      avg1+=data[j];
      avg2+=data[j+i];
      cort+=data[j]*data[j+i];
    }
    fprintf(output,"%f\n",cort/(tot+1)-avg1/(tot+1)*avg2/(tot+1) );
   }
   fclose(output);
}

/* The random numbers generator from Numerical recipes*/
float ran3(long *idum)
{
  static int inext,inextp;
  static long ma[56];
  static int iff=0;
  long mj,mk;
  int i,ii,k;

  if (*idum < 0 || iff == 0) {
    iff=1;
    mj=MSEED-(*idum < 0 ? -*idum : *idum);
    mj %= MBIG;
    ma[55]=mj;
    mk=1;
    for (i=1;i<=54;i++) {
      ii=(21*i) % 55;
      ma[ii]=mk;
      mk=mj-mk;
      if (mk < MZ) mk += MBIG;
      mj=ma[ii];
    }
    for (k=1;k<=4;k++)
      for (i=1;i<=55;i++) {
          ma[i] -= ma[1+(i+30) % 55];
          if (ma[i] < MZ) ma[i] += MBIG;
      }
    inext=0;
    inextp=31;
    *idum=1;
  }
  if (++inext == 56) inext=1;
  if (++inextp == 56) inextp=1;
  mj=ma[inext]-ma[inextp];
  if (mj < MZ) mj += MBIG;
  ma[inext]=mj;
```

```
  return mj*FAC;
}
#undef MBIG
#undef MSEED
#undef MZ
#undef FAC
/* (C) Copr. 1986-92 Numerical Recipes Software m'5M. */

float ran2(long *idum)
{
  int j;
  long k;
  static long idum2=123456789;
  static long iy=0;
  static long iv[NTAB];
  double temp;

  if(*idum<=0){
    if(-(*idum)<1) *idum=1;
    else *idum=-(*idum);
    idum2=(*idum);
    for(j=NTAB+7;j>=0;j--){
      k=(*idum)/IQ1;
      *idum=IA1*(*idum-k*IQ1)-k*IR1;
      if(*idum<0) *idum+=IM1;
      if(j<NTAB) iv[j]=*idum;
    }
    iy=iv[0];
  }
  k=(*idum)/IQ1;
  *idum=IA1*(*idum-k*IQ1)-k*IR1;
  if(*idum<0) *idum+=IM1;
  k=idum2/IQ2;
  idum2=IA2*(idum2-k*IQ2)-k*IR2;
  if(idum2<0) idum2+=IM2;
  j=iy/NDIV;
  iy=iv[j]-idum2;
  iv[j]=*idum;
  if(iy<1) iy+=IMM1;
  if((temp=AM*iy)>RNMX) return RNMX;
  else return temp;
}
```

References

[1] A. Ramasubramanian and S. B. Shenoy, Journal of Applied Physics **95**, 7813 (2004).

[2] S. J. Prado, C. Trallero-Giner, A. M. Alcalde, et al., Physical Review B **69**, 201310 (2004).

[3] S. Kan, T. Mokari, E. Rothenberg, et al., Nature Materials **2**, 155 (2003).

[4] A. A. Golovin, S. H. Davis, and P. W. Voorhees, Physical Review E **68**, 056203 (2003).

[5] Z. Hens, D. Vanmaekelbergh, E. J. A. J. Stoffels, et al., Physical Review Letters **88**, 236803 (2002).

[6] Z. Gai, B. Wu, J. P. Pierce, et al., Physical Review Letters **89**, 235502 (2002).

[7] R. C. Nelson, T. L. Einstein, S. V. Khare, et al., Surface Science **295**, 462 (1993).

[8] M. Wortis, in *Chemistry and Physics of Solid Surfaces VII*, edited by R. Vanselow and R. F. Howe (Springer Verlag, Berlin, 1988), p. 367.

[9] P. Nozieres, in *Solids far from Equilibrium*, edited by C. Godreche (Cambridge University Press, Cambridge, 1991), p. 1.

[10] H. C. Jeong and E. D. Williams, Surface Science Reports **34**, 175 (1999).

[11] W. W. Mullins, Interface Science **9**, 9 (2001).

[12] B. Krishnamachari, J. McLean, B. Cooper, et al., Physical Review B **54**, 8899 (1996).

[13] J. G. McLean, B. Krishnamachari, D. R. Peale, et al., Abstracts of Papers of the American Chemical Society **213**, 471 (1997).

[14] K. Thurmer, J. E. Reutt-Robey, and E. D. Williams, Surface Science **537**, 123 (2003).

[15] V. L. Pokrovsky and A. L. Talapov, Physical Review Letters **42**, 65 (1979).

[16] M. Uwaha and P. Nozières, in *Morphology and Growth Unit of Crystals*, edited by I. Sunagawa (Terra Scientific Publishing Co., Tokyo, 1989), p. 17.

[17] A. F. Andreev, Zhurnal Eksperimentalnoi I Teoreticheskoi Fiziki **80**, 2042 (1981).

[18] S. V. Khare, S. Kodambaka, D. D. Johnson, et al., Surface Science **522**, 75 (2003).

[19] A. Pimpinelli and J. Villain, *Physics of crystal growth* (Cambridge University Press, Cambridge ; New York, 1998).

[20] M. Uwaha, Journal of the Physical Society of Japan **57**, 1681 (1988).

[21] S. V. Khare and T. L. Einstein, Physical Review B **57**, 4782 (1998).

[22] M. Giesen, Progress in Surface Science **68**, 1 (2001).

[23] N. C. Bartelt, T. L. Einstein, and E. D. Williams, Surface Science **276**, 308 (1992).

[24] A. Pimpinelli, J. Villain, D. E. Wolf, et al., Surface Science **295**, 143 (1993).

[25] O. Pierre-Louis, Surface Science **529**, 114 (2003).

[26] T. Ihle, C. Misbah, and O. Pierre-Louis, Physical Review B **58**, 2289 (1998).

[27] L. Kuipers, M. S. Hoogeman, J. W. M. Frenken, et al., Physical Review B **52**, 11387 (1995).

[28] Z. Toroczkai and E. D. Williams, Physics Today **52**, 24 (1999).

[29] A.-L. Barabási and H. E. Stanley, *Fractal Concepts in Surface Growth* (Cambridge University Press, Cambridge, 1995).

[30] C. Rottman and M. Wortis, Physical Review B **24**, 6274 (1981).

[31] N. Akutsu and Y. Akutsu, Surface Science **376**, 92 (1997).

[32] R. K. P. Zia and J. E. Avron, Physical Review B **25**, 2042 (1982).

[33] Y. Akutsu, N. Akutsu, and T. Yamamoto, Physical Review Letters **61**, 424 (1988).

[34] F. Family, Journal of Physics a-Mathematical and General **19**, L441 (1986).

[35] D. E. Wolf and J. Villain, Europhysics Letters **13**, 389 (1990).

[36] S. Dassarma and P. Tamborenea, Physical Review Letters **66**, 325 (1991).

[37] I. Lyubinetsky, S. Thevuthasan, D. E. McCready, et al., Journal of Applied Physics **94**, 7926 (2003).

[38] M. Uwaha and K. Watanabe, Journal of the Physical Society of Japan **69**, 497 (2000).

[39] N. Israeli and D. Kandel, Physical Review B **60**, 5946 (1999).

[40] A. Ichimiya, K. Hayashi, E. D. Williams, et al., Physical Review Letters **84**, 3662 (2000).

[41] P. Muller and R. Kern, Surface Science **457**, 229 (2000).

[42] B. J. Spencer, Physical Review B **59**, 2011 (1999).

[43] K. H. Hansen, T. Worren, S. Stempel, et al., Physical Review Letters **83**, 4120 (1999).

[44] W. Vervisch, C. Mottet, and J. Goniakowski, European Physical Journal D **24**, 311 (2003).

[45] Winterbo.Wl, Acta Metallurgica **15**, 303 (1967).

[46] C. Herring, Physical Review **82**, 87 (1951).

[47] A. W. Searcy, Journal of Solid State Chemistry **48**, 93 (1983).

[48] C. Jayaprakash, C. Rottman, and W. F. Saam, Physical Review B **30**, 6549 (1984).

[49] C. Rottman and M. Wortis, Physics Reports-Review Section of Physics Letters **103**, 59 (1984).

[50] J. J. Metois and J. C. Heyraud, Surface Science **180**, 647 (1987).

[51] E. D. Williams and N. C. Bartelt, Ultramicroscopy **31**, 36 (1989).

[52] C. Rottman, M. Wortis, J. C. Heyraud, et al., Physical Review Letters **52**, 1009 (1984).

[53] A. Pavlovska, D. Dobrev, and E. Bauer, Surface Science **326**, 101 (1995).

[54] J. M. Bermond, J. J. Metois, J. C. Heyraud, et al., Surface Science **416**, 430 (1998).

[55] J. Tersoff and E. Pehlke, Physical Review B **47**, 4072 (1993).

[56] D. J. Eaglesham, A. E. White, L. C. Feldman, et al., Physical Review Letters **70**, 1643 (1993).

[57] A. Emundts, H. P. Bonzel, P. Wynblatt, et al., Surface Science **481**, 13 (2001).

[58] M. Nowicki, C. Bombis, A. Emundts, et al., New Journal of Physics **4**, 60 (2002).

[59] S. Balibar, H. Alles, and A. Y. Parshin, Reviews of Modern Physics **77**, 317 (2005).

[60] D. J. Eaglesham, F. C. Unterwald, and D. C. Jacobson, Physical Review Letters **70**, 966 (1993).

[61] M. Giesen, C. Steimer, and H. Ibach, Surface Science **471**, 80 (2001).

[62] S. Kodambaka, S. V. Khare, V. Petrova, et al., Surface Science **523**, 316 (2003).

[63] R. Van Moere, H. J. W. Zandvliet, and B. Poelsema, Physical Review B **67**, 193407 (2003).

[64] W. W. Mullins and G. S. Rohrer, Journal of the American Ceramic Society **83**, 214 (2000).

[65] G. S. Rohrer, C. L. Rohrer, and W. W. Mullins, Journal of the American Ceramic Society **84**, 2099 (2001).

[66] N. Combe, P. Jensen, and A. Pimpinelli, Physical Review Letters **85**, 110 (2000).

[67] J. Tersoff, A. W. D. Vandergon, and R. M. Tromp, Physical Review Letters **70**, 1143 (1993).

[68] K. Thurmer, J. E. Reutt-Robey, E. D. Williams, et al., Physical Review Letters **8718**, 186102 (2001).

[69] D. B. Dougherty, K. Thurmer, M. Degawa, et al., Surface Science **554**, 233 (2004).

[70] P. L. Ferrari, M. Prähofer, and H. Spohn, Physical Review E **69**, 035102(R) (2004).

[71] M. Degawa, K. Thurmer, and E. D. Williams, Jpn.J.Appl.Phys. **45** (2005).

[72] P. J. Feibelman, Physical Review B **65**, 129902 (2002).

[73] D. G. Vlachos, L. D. Schmidt, and R. Aris, Physical Review B **47**, 4896 (1993).

[74] V. Johanek, M. Laurin, A. W. Grant, et al., Science **304**, 1639 (2004).

[75] J. Tersoff, C. Teichert, and M. G. Lagally, Physical Review Letters **76**, 1675 (1996).

[76] C. Teichert, M. G. Lagally, L. J. Peticolas, et al., Physical Review B **53**, 16334 (1996).

[77] N. Lopez, J. K. Norskov, T. V. W. Janssens, et al., Journal of Catalysis **225**, 86 (2004).

[78] F. Silly and M. R. Castell, Physical Review Letters **94**, 046103 (2005).

[79] P. L. Hansen, J. B. Wagner, S. Helveg, et al., Science **295**, 2053 (2002).

[80] M. Degawa, F. Szalma, and E. D. Williams, Surface Science **583**, 126 (2005).

[81] W. L. Winterbottom, Acta Metallurgica **15**, 303 (1967).

[82] S. V. Khare and T. L. Einstein, Physical Review B **54**, 11752 (1996).

[83] M. Degawa and E. D. Williams, in preparation (2005).

[84] A. Emundts, M. Nowicki, and H. P. Bonzel, Surface Science **496**, L35 (2002).

[85] M. Degawa and E. D. Williams, Surface Science (2005).

[86] K. Morgenstern, G. Rosenfeld, E. Laegsgaard, et al., Physical Review Letters **80**, 556 (1998).

[87] N. Akutsu and Y. Akutsu, Journal of Physics-Condensed Matter **11**, 6635 (1999).

[88] K. Arenhold, S. Surnev, H. P. Bonzel, et al., Surface Science **424**, 271 (1999).

[89] M. Nowicki, C. Bombis, A. Emundts, et al., Physical Review B **67**, 0754505 (2003).

[90] J. C. Heyraud and J. J. Metois, Surface Science **128**, 334 (1983).

[91] M. Nowicki, C. Bombis, A. Emundts, et al., Europhysics Letters **59**, 239 (2002).

[92] H. P. Bonzel, Physics Reports-Review Section of Physics Letters **385**, 1 (2003).

[93] M. Degawa and E. D. Williams, Surface Science **595**, 87 (2005).

[94] R. J. Needs, M. J. Godfrey, and M. Mansfield, Surface Science **242**, 215 (1991).

[95] P. Muller and R. Kern, Journal of Crystal Growth **193**, 257 (1998).

[96] S. Surnev, K. Arenhold, P. Coenen, et al., Journal of Vacuum Science & Technology A **16**, 1059 (1998).

[97] A. Pimpinelli, M. Degawa, T. L. Einstein, et al., Surface Science Letters **598**, L355 (2005).

[98] I. Lyubinetsky, D. B. Dougherty, T. L. Einstein, et al., Physical Review B **66**, 085327 (2002).

[99] O. Bondarchuk, D. B. Dougherty, M. Degawa, et al., Physical Review B **71**, 045426 (2005).

[100] S. Speller, W. Heiland, A. Biedermann, et al., Surface Science **333**, 1056 (1995).

[101] Z. Kuntova, Z. Chvoj, V. Sima, et al., Physical Review B **71**, 125415 (2005).

[102] H. Gebremariam, C. Dasgupta, and T. L. Einstein, in preparation (2005).

[103] M. Degawa and E. D. Williams, Surface Science **595**, 87 (2005).

[104] C. Bombis, A. Emundts, M. Nowicki, et al., Surface Science **511**, 83 (2002).

[105] M. Ondrejcek, M. Rajappan, W. Swiech, et al., Surface Science **574**, 111 (2005).

[106] M. Ondrejcek, W. Swiech, M. Rajappan, et al., Physical Review B **72** (2005).

[107] C. Tao, T. J. Stasevich, T. L. Einstein, et al., Submitted to Phys. Rev. B (2005).

[108] N. C. Bartelt, J. L. Goldberg, T. L. Einstein, et al., Surface Science **273**, 252 (1992).

[109] T. J. Stasevich, H. Gebremariam, T. L. Einstein, et al., Physical Review B **71**, 245414 (2005).

[110] Y. Kim, S. Y. Yoon, and H. Park, Physical Review E **66**, 040602 (2002).

[111] M. Degawa, T. J. Stasevich, T. L. Einstein, et al., in preparation (2005).

[112] H. G. E. Hentschel and F. Family, Physical Review Letters **66**, 1982 (1991).

[113] H. C. Jeong and J. M. Kim, Physical Review E **66** (2002).